Effect of Porous Structure of Carbon Support on CO Tolerance of PEFC Platinum Alloy Anode Catalysts

PEFC の白金合金 アノード用触媒の CO 耐性への炭素担体の細孔構造の影響に関する研究

DOCTORAL DISSERTATION

Napan Narischat

Division of Molecular Chemistry and Engineering

Graduate School of Chemical Sciences and Engineering

Hokkaido University

Abstract

This thesis investigated how the porous structure of carbon support affected the CO tolerance of PtRu alloy anode catalysts. Various PtRu/C catalysts were prepared, characterized, and tested for their CO tolerance in PEFC single cell. The carbon supports used in this work were prepared using carbonization of resorcinol-formaldehyde gels, which were derived from sol-gel polymerization of resorcinol with formaldehyde in the presence of sodium carbonate. The preparation condition was varied so that carbon supports with different pore structures were obtained. Two commercial carbon supports were used in this work. One was Carbon ECP that was used for comparison. The other was Carbon ECP600JD which was very new in the market. PtRu/C catalysts were prepared using these carbon supports with the rapid quenching method. Usually the preparation was done with a Pt/Ru molar ratio of 1.5. Moreover, in a typical MEA production the weight ratio between Nafion® and catalyst was 5:9. However, in some cases these values were varied. Moreover, in a specific case SnO_2 was doped on a carbon support before it was used for a catalyst preparation. A commercial PtRu/C catalyst from Tanaka Kikinzoku Kogyo K.K., which is known widely to have a very high CO tolerance, was generally used for comparison. We found that the porous carbon supports had a very strong relationship with the CO tolerance of the catalysts. Suitable pore structures led to high CO tolerance (Chapters 2 and 4). A proper carbon support selection also led to a high Pt-Ru surface relative bonding ratio, which is a key factor for obtaining high CO tolerance (Chapter 3). Deposition of SnO_2 on a carbon support before the catalyst preparation helps obtaining high CO tolerance due to the reduction of Pt-CO bond strength (Chapter 5). Moreover, pore volume and pore structure of catalyst could specific the amount of necessary Nafion® in order to obtain high efficiency and high CO tolerance MEAs (Chapter 6).

Table of Contents

List of Figures

List of Table

Chapter 1

General Introduction

1.1 Background of fuel cells

The development of a sustainable energy supply is needed as a solution for the global energy crisis. There are many types of renewable energy technologies which are interesting. The utilization of fuel cells has been recognized in both industry and academic fields as the most effective method for producing energy. The use of fuel cells is also expected to reduce emissions of CO_2, NO_x, SO_x and particulate matter that are generated by fossil fuel engines. Therefore, fuel cells are promising energy sources for the new era because of their high efficiency and low environmental impact.

1.1.1 Fuel cell definition

A fuel cell is a device that can convert fuel to electricity by a chemical reaction between positively charged hydrogen ions and oxygen or other oxidizing agents. A fuel cell is composed of a positive electrode and a negative electrode, which are called a cathode and an anode, respectively. A reaction that produces electricity takes place at these electrodes. Fuel cells also have an ion-conductive electrolyte that carries electrically charged particles from one electrode to the other. Hydrogen is the basic fuel in fuel cells, but oxygen is also required. The biggest benefit of fuel cells is that they generate electricity but discharge only water.

1.1.2 History of fuel cells[1-3]

Hydrogen was discovered by Paracelsus in the sixteenth century. He accidentally dropped iron into condensed sulphuric acid and this combination produced a gas or "air" as he conceived it at the time. The French chemist Nicholas Lemery showed that the gas produced was flammable, but it was Henry Cavendish, a British physicist, who is credited with the discovery of hydrogen in 1766. Another French chemist, Antoine-Laurent Lavoisier (1743-1793), described one of the component elements of water as hydrogen, and he also noted that the only byproduct of burning hydrogen was water itself. Alessandro Volta discovered the battery principle in 1799, and Michael Faraday formulated electrochemical conversion principles (Faraday's law) in 1832. The concept of fuel cells emerged around 1802, when Sir Humphry Davy found that passing an electric current through water caused the water to chemically decompose into

its component elements (electrolysis) of hydrogen and oxygen. This discovery was followed by the pioneering works of Christiam Friedrich Schönbein (1838), who first discovered the fuel cell effect, and Sir William Robert Grove (1839), who presented the first fuel cell power generator. Grove worked on a hydrogen-oxygen cell using liquid sulfuric acid as an electrolyte. However, Grove's apparatus did not generate sufficient electricity. One hundred years later, in 1932, Francis T. Bacon started exploring a novel electrode for fuel cells using a less corrosive alkaline electrolyte and cheaper nickel catalysts instead of expensive platinum electrodes. In the 1960s, alkaline fuel cells were used to provide both electricity and drinking water onboard for more than 65,000 hours in over 87 flights in manned space shuttles during the Gemini and Apollo programs. In the late 1960s, Siemens and Varta constructed converter stations based on alkaline fuel cell technology for television transmitters in the power range of 25-100 W. In 1973, after the energy crisis, the Moonlight Program was started in Japan.

1.1.3 Types of fuel cells

There are various types of fuel cells that are categorized by their electrolytes: alkali, molten carbonate, phosphoric acid, polymer electrolyte and solid oxide.

1.1.3.1 A solution of potassium hydroxide (KOH) is generally used as the electrolyte in alkali fuel cells (AFC)[4]. The ionic species is OH^-. The operating temperature is 60 to 100 °C. The cell output range is from 300 watts to 5000 watts. Electrochemical reactions of an AFC are as follows:

Anode: $H_2 + 2OH^- \rightarrow 2H_2O + 2e^-$ (1.1)

Cathode: $1/2O_2 + H_2O + 2e^- \rightarrow 2OH^-$ (1.2)

1.1.3.2 Compounds of salts (such as lithium, potassium, sodium or magnesium) and carbonates (CO_3) are generally used as the electrolyte in molten carbonate fuel cells (MCFC)[5]. The ionic species is CO_3^{2-}. The operating temperature is in the range of 600-650 °C. The output units are constructed up to 2 megawatts. A nickel electrode catalyst, which is used in this type of fuel cell, is much cheaper than platinum electrode-catalysts used in other types of fuel cell. However, the temperature is probably too high for household applications. Electrochemical reactions of an MCFC are as follows:

Anode: $H_2 + CO_3^{2-} \rightarrow H_2O + CO_2 + 2e^-$ (1.3)

Cathode: $1/2O_2 + CO_2 + 2e^- \rightarrow CO_3^{2-}$ (1.4)

1.1.3.3 An acid solution is used as the electrolyte in phosphoric acid fuel cells (PAFCs)[6]. The operating temperature is about 180-220 °C. The outputs of existing phosphoric acid cells are up to 200 kW, and the units have been tested at 11 MW. A PAFC can tolerate carbon monoxide at a concentration of up to 1.5 percent, and thus the choice of fuels that can be used is broadened. Electrochemical reactions of a PAFC are as follows:

Anode: $H_2 \rightarrow 2H^+ + 2e^-$ (1.5)

Cathode: $1/2O_2 + 2H^+ + 2e^- \rightarrow H_2O$ (1.6)

1.1.3.4 A polymer electrolyte in the form of a thin permeable sheet is used in polymer electrolyte fuel cell (PEFCs)[7]. The operating temperature range is about 60-80 °C. The cell outputs are generally in the range of 50-250 kW. The solid flexible electrolyte results in no leakage and these cells are operated at a low temperature, making them suitable for household and vehicle applications. The main fuel for a PEFC is pure H_2; however, if the fuel is methanol, they are called direct methanol fuel cells (DMFCs). Since a PEFC is the main focus in this work, the full details of a PEFC are given in section 1.2. Electrochemical reactions of a PEFC are as follows:

Anode: $H_2 \rightarrow 2H^+ + 2e^-$ (1.7)

Cathode: $1/2O_2 + 2H^+ + 2e^- \rightarrow H_2O$ (1.8)

1.1.3.5 Ceramic compounds of metal oxides (such as calcium or zirconium) are used as the electrolyte in solid oxide fuel cells (SOFCs)[8, 9]. The operating temperature is about 700-800°C. The cell output is up to 100 kW. At a very high temperature, a reformer is not required for converting the fuel to hydrogen, and the waste heat can be recycled to produce additional electricity. However, the applications of an SOFC are limited by the high temperature, and the units are rather large. Electrochemical reactions of an SOFC are as follows:

Anode: $H_2 + O^{2-} \rightarrow H_2O + 2e^-$ (1.9)

Cathode: $1/2O_2 + 2e^- \rightarrow O^{2-}$ (1.10)

1.2 Polymer electrolyte fuel cells (PEFCs)

Polymer electrolyte fuel cells (PEFCs) or proton exchange membrane fuel cells (PEMFCs) have been operated using hydrogen gas or short-chained alcohols (carbon 1-4 molecules), sodium borohydride, formic and acid as fuels. The proton-transporting polymer electrolyte (ionomer) is utilized in the form of a thin permeable membrane (ca. 25-175 gm) that is commonly composed of a perfluorosulfonic acid compound (e.g., Nafion®). The attachment of the two electrodes (anode and cathode) to the membrane is referred to as a membrane electrode assembly (MEA). Platinum (Pt) catalysts are used on both the anode and cathode. Since a Pt catalyst is sensitive to CO poisoning, the purity of hydrogen used must be high (CO contamination should be less than 10 ppm.). Moreover, a PtRu alloy anode catalyst is frequently used due to its high CO tolerance. More details of PtRu catalysts will be given in section 1.4.

1.2.1 PEFC components and operation

As mentioned above, an MEA consists of an anode, a cathode, and an ionomer. There are some concepts and steps in order to make an MEA and to operate a PEFC single cell. The components of a PEFC are shown in Fig. 1.1.

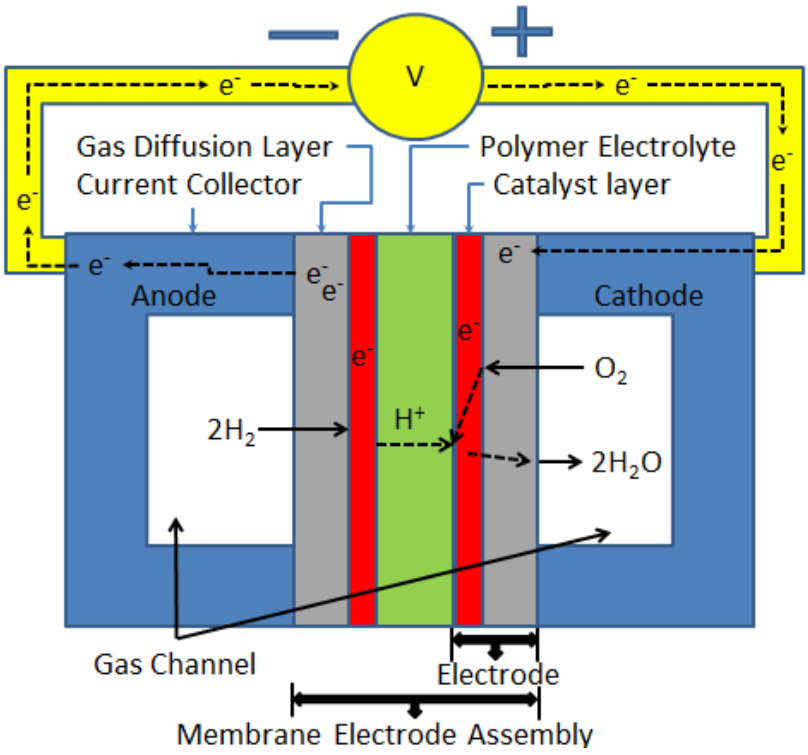

Fig. 1.1 Components of a PEFC.

1.2.1.1 Electrolyte[10, 11]

Nafion® is a perfluorinated sulfonic acid resin (PFSA) developed by Dr. Walther Grot at the E. I. DuPont Company in the late 1960's by modifying Teflon. Due to its chemical stability, superior mechanical properties, high chemical inertness, and proton conductivity, Nafion® is currently used in commercial membranes and catalyst layers of fuel cells. The structure of Nafion® is shown in Fig. 1.2. After fabrication (extrusion and lamination) into the desired shape, the $-SO_2F$ groups are hydrolyzed in a hot solution of NaOH or KOH and optionally converted to the H^+ form using HNO_3.

.

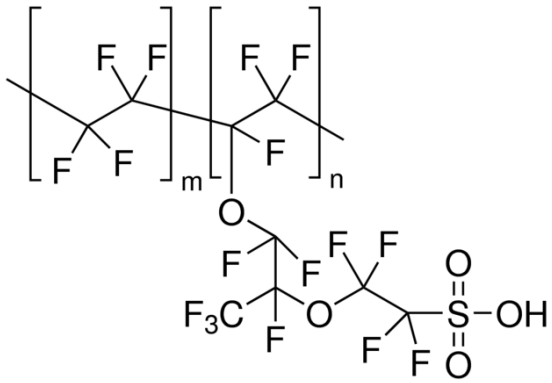

Fig. 1.2 Structure of Nafion®.
(ref:http://www.sigmaaldrich.com/catalog/product/aldrich/274674?lang=en&region=JP)

1.2.1.2 Catalyst ionomer ink and catalyst layer[12, 13]

A catalyst ink or a catalyst ionomer ink is a mixture of a catalyst and an ionomer for paint or spraying to make a catalyst layer on a gas diffusion layer. One of the main resistances in the catalyst layer is contact resistance at the membrane/catalyst layer interface. The content of the ionomer in the catalyst layer is a key parameter for optimizing the MEA structure and performance. With the optimization, a significant reduction of the platinum content from about 4.0 mg cm^{-2} to less than 0.5 mg cm^{-2} has been achieved.

1.2.1.3 Gas diffusion layer

A gas diffusion layer is a porous material composed of a dense array of carbon fibers that functions as a gas diffused pathway from flow channels to the catalyst layers and provides an electrically conductive pathway for current collection. It also aids the removal of by-produced water outside the catalyst layer. This can prevent flooding but still keep some water on the surface and thus maintain conductivity through the

membrane. Ishikawa reported that the water distribution inside an MEA strongly affected current density and O_2 partial pressure in the gas diffusion layer.[14] In addition, a gas diffusion layer can be a medium for heat transfer during cell operation and also provides sufficient mechanical strength to prevent extension of MEA caused by water absorbance. Normally, a gas diffusion layer is coated with polytetrafluoroethylene (PTFE) in order to bind carbon particles with a large surface area. The amount of PTFE loading was reported to influence the performance of the electrode.

1.2.1.4 Electrode and membrane assembly electrode[7]

After the catalyst ink has been painted or sprayed to form a catalyst layer on the PTFE-coated gas diffusion layer, the resulting layer is ready to be assembled to an MEA. In the MEA, the polymer electrolyte membrane is sandwiched with an anode and a cathode. The precise control of charges and of mass and energy transport within the MEA is a key issue for highly efficient PEFCs. The transportation of protons from the membrane into the catalyst layers and the deposited catalysts is very important.

1.2.1.5 Single cells[15]

To create a single PEFC, the MEA must be placed between bipolar plates that provide a gas channel and serve as reactant distributors, current collectors, and heat-transfer elements. The requirements for the bipolar plate are uniform distribution of reactants over the entire electrode surface and effective water removal from the cell. Recent studies have shown that sustained voltage oscillations can occur in PEFCs fed with H_2/CO mixtures. Oscillatory behavior can also result from degradation effects.

1.2.2 PEFC application

A PEFC using hydrogen fuel is a key option for transportation and small-scale power applications in combination with heat (residential units) due to its compactness, high modularity, high conversion efficience and low levels of noise and pollutant emission[16, 17]. The major challenge for the implementation of a hydrogen fueling infrastructure is the storage of hydrogen, which requires high pressure (30 MPa at 298 K), low temperature (-20 K) and the use of weight intensive metal hydrides. Furthermore, a network of fueling stations should be established. The absence of a hydrogen distributing infrastructure and the problem of hydrogen storage have led to the development of hydrogen-rich reformate gas from natural gas and biogas for use in the PEFC system[18-20]. In order to utilize the reformate gas, CO concentration has been

reduced to an acceptable level (10 ppm) for protection against CO poisoning, which will degrade the anode catalyst[21, 22].

Commercialized residential PEFC units have been installed and utilized in Japan since 2009. One residential PEFC co-generation unit, in which natural gas can be used directly, consists of a desulfurizer unit to remove sulfur contamination, a steam reforming unit to convert CH_4 to H_2, a CO shift converter unit to reduce CO contamination to less than 5000 ppm, and a CO preferential oxidizer unit to reduce CO contamination from about 5000 ppm to less than 10 ppm. This results in quite a complicated system. A simple system is needed to accelerate the use of residential fuel cells. CO-insensitive electrocatalysts are therefore needed.

1.3 PEFC catalysis

The major cost of a PEFC is the Pt-based catalysts. Pt-based catalysts for both the anode (H_2 oxidation reaction) and cathode (O_2 reduction reaction) are the most reliable catalysts in terms of catalytic activity and stability.

1.3.1 Oxygen reduction reaction (ORR)

ORR at a cathode is normally a very slow reaction. A cathode ORR catalyst is therefore necessary to speed up the ORR kinetics to usable level. It is well known that Pt-based materials are the most active catalysts. However, Pt-based catalysts are very expensive, and many researches have therefore focused on the development of alternative catalysts.

1.3.1.1 Oxygen reduction reaction (ORR) mechanism on Pt[23, 24]

ORR is a multistep reaction. Dissociative and associative mechanisms have been proposed for a low current density range and high current density range.

Dissociative mechanism:

$$1/2O_2 + * \rightarrow O* \quad (1.11)$$

$$O* + H^+ + e^- \rightarrow OH* \quad (1.12)$$

$$OH* + H^+ + e^- \rightarrow H_2O + * \quad (1.13)$$

* denotes a site on the Pt surface. O_2 adsorbs on the Pt surface, then the O-O bond breaks, resulting in the formation of adsorbed atomic O.

Associative mechanism:

$$O_2 + * \rightarrow O_2* \quad (1.14)$$
$$O_2* + H^+ + e^- \rightarrow HO_2* \quad (1.15)$$
$$HO_2* + H^+ + e^- \rightarrow H_2O + O* \quad (1.16)$$
$$O* + H^+ + e^- \rightarrow OH* \quad (1.17)$$
$$OH* + H^+ + e^- \rightarrow H_2O + * \quad (1.18)$$

Since adsorbed O_2 is present, the O-O bond may not be broken in the following steps, and then H_2O_2 can be formed. The H_2O_2 could be further reduced to H_2O or remain in the H_2O_2 form.

1.3.2 Hydrogen oxidation reaction (HOR)

On the anode side, hydrogen electrooxidation catalysis is a model system for understanding the electrochemical kinetics, electrocatalysis and electrochemical surface science. Moreover, hydrogen evolution/oxidation (HER/HOR) reaction is the most widely studied electrochemical process.

1.3.2.1 HOR mechanism[25]

There are three steps of the HOR. The first step is adsorption. Hydrogen molecules diffuse from the electrolyte to the electrode and then adsorb on the electrode surface to form surface species ($H_{2,\,ads}$):

$$H_2 \rightarrow H_{2,\,solv} \rightarrow H_{2,\,ads} \quad (1.19)$$

The second step is hydration. The adsorbed hydrogen forms adsorbed H atoms (H_{ad}) through the Tafel or Heyrovsky reaction followed by the Volmer reaction.

Tafel reaction: $$H_{2,\,ads} \rightarrow 2H_{ad} \quad (1.20)$$
Heyrovsky reaction: $$H_{2,\,ads} \rightarrow H_{ad}\, H^+ + e^- \rightarrow H_{ad} + H^+ + e^- \quad (1.21)$$
Volmer reaction: $$H_{ad} \rightarrow H^+ + e^- \quad (1.22)$$

The last step is desorption. Products such as H^+ and H_2O are desorbed from the anode catalyst and transported into the electrolyte.

The adsorption of hydrogen is considered to be the rate-determining step in both the Tafel-Volmer and Heyrovsky-Volmer mechanisms. It has been reported that the

Tafel-Volmer mechanism is the rate-determining step at low potential while Heyrovsky-Volmer mechanism is the rate determining step at higher potentials.

1.3.2.2 Thermodynamics

Thermodynamic relations for the HOR (H_2 to proton) are as follows:

$$E_H = -\frac{\Delta G}{F} \quad (1.23)$$

$$\Delta G = -\frac{1}{2}\mu_{H_2} - \mu_{H^+}$$

$$= \left[\frac{1}{2}\mu^0_{H_2} - \mu^0_{H^+}\right] + RT\ln\frac{P^{1/2}_{H_2}}{a_{H^+}} \quad (1.24)$$

$$E_H = E^0_H - \frac{RT}{F}\ln\left[\frac{P^{1/2}_{H_2}}{a_{H^+}}\right] \quad (1.25)$$

where ΔG is Gibbs energy, μ_{H_2} and μ_{H^+} are chemical potentials of H_2 and H^+, respectively, a_{H^+} is the activity of protons, F is the Faraday constant, and a_{H^+} has a practical significance through the definition of pH. E^0_H is defined as the standard hydrogen electrode potential with E^0_H equal to 0 V under the standard condition.

1.4 Mechanisms of CO poisoning and factors enhancing CO tolerance

It is generally accepted that CO adsorbs onto the Pt surface (Eq. (1.26)) at low potentials and is not electrochemically oxidized until the potential reaches about 0.7 V vs. RHE. The concentration of CO at ppm levels causes a high degree of Pt surface coverage:

$$CO + Pt \rightarrow Pt\text{-}CO \quad (1.26)$$

The CO coverage also causes dramatic deactivation of the anode electrocatalyst by hydrogen dissociation and oxidation reactions as shown in Eqs. (1.27) and (1.28), respectively:

$$2Pt + H_2 \rightarrow 2Pt\text{-}H \quad (1.27)$$

$$Pt\text{-}H \rightarrow Pt + H^+ + e^- \quad (1.28)$$

At higher potentials, CO can be removed by the Langmuir-Hinshelwood mechanism as follows:

$$Pt + H_2O \leftrightarrow Pt\text{-}OH + H^+ + e^- \quad (1.29)$$

$$Pt\text{-}CO + Pt\text{-}OH \leftrightarrow CO_2 + 2Pt + H^+ + e^- \quad (1.30)$$

The electrode potential necessary for significant electrochemical CO oxidation on a Pt/C catalyst is too high for practical applications. Therefore, carbon-supported Pt catalysts alloyed with Ru (PtRu/C), which lowers the potential for CO oxidation, are most commonly used. Its mechanism for CO oxidation is shown below:

$$Ru + H_2O \leftrightarrow Ru\text{-}OH + H^+ + e^- \quad (1.31)$$

$$Pt\text{-}CO + Ru\text{-}OH \leftrightarrow CO_2 + Pt + Ru + H^+ + e^- \quad (1.32)$$

It is believed that a Pt-Ru alloy enhances CO tolerance by either of the following two mechanisms. Firstly, Ru forms hydroxide (as described by Eq. (1.31)) for use in CO oxidation (Eq. (1.32)). This mechanism is called a bifunctional mechanism[26]. Secondly, Ru-OH decreases the bond energy of Pt and CO. This mechanism is called the ligand effect[27-29] (or electronic effect). Both mechanisms are shown simply in Fig. 1.3.

There are many factors that can enhance CO tolerance. The most important factors, including as alloying species, Pt-alloying degree and particle sizes as well as catalyst supports, have been reviewed and are described below.

1.4.1 Effect of second element Pt-alloys

In case of pure H_2, the platinum on a carbon-supported (Pt/C) catalyst shows very small polarization loss with respect to hydrogen oxidation in a PEFC. However, when a small amount of CO is present, the potential loss is vital. It has been found that the presence of a second alloy along with Pt such as Ru, Sn, Os, Mo yields significant improvement in CO tolerance compared to that of pure Pt.[27-34] It was discovered for more than 30 years ago that the best catalyst that can endure CO in practical use is a bimetallic Pt-Ru catalyst.[35-37] The function of Ru is generation of an oxygen-containing species or weakening of the bonds of Pt-CO by reducing the d-electron deficiency of Pt atoms.[38-43]

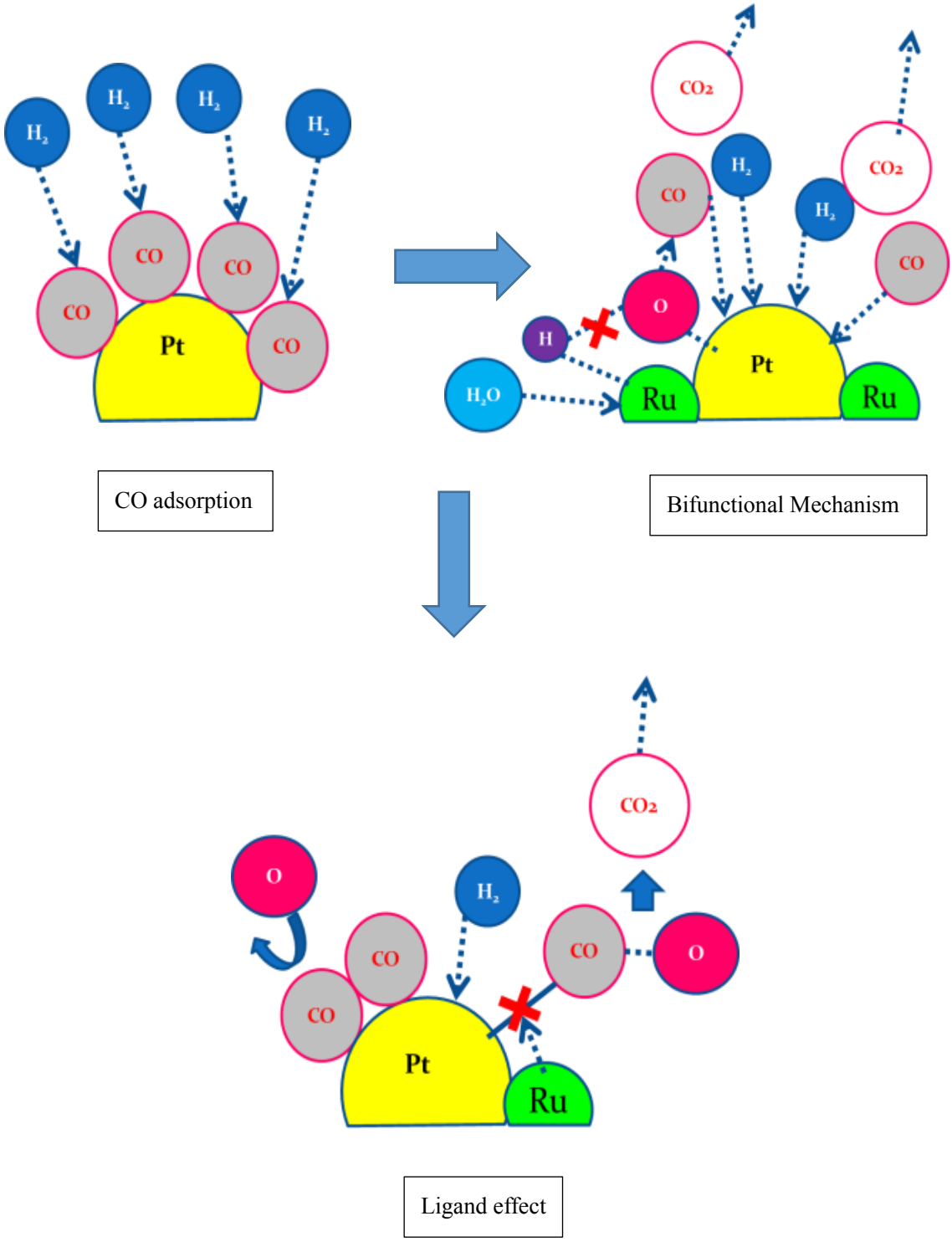

Fig. 1.3 CO adsorption and removal by the bifunctional mechanism and ligand effects.

1.4.2 Effects of alloying degree and particle size

It has been reported that high CO tolerance was achieved when Ru was deposited on a highly dispersed Pt/C catalyst with subsequent annealing to induce alloying between Pt and Ru.[44-49] This PtRu alloy is an important factor for achieving high CO tolerance. However, the alloying process at a high temperature also leads to agglomeration of PtRu particles, resulting in the formation of large PtRu particles. It has therefore been difficult to control the degree of alloying and the degree of dispersion independently. Preparation of highly alloyed and highly dispersed PtRu/C catalysts has been particularly difficult. Information on the effect of particle size on CO tolerance is still lacking. Separate control of alloying degree and dispersion degree (particle size) is needed to obtain such information. However, there is inconsistency in information about PtRu particle size. Some researchers reported that small PtRu particles showed higher activity, whereas other researchers prefer a size of 5 nm (to prevent Ru dissolution after long operations).[50, 51]

1.4.3 Effect of supports

There are many types of supports being used as supports for fuel cell electrode catalysts. Their properties such as type, structure, porosity, and conductivity have been considered to be factors to improve catalyst efficiency and CO tolerance. A metal-support interaction can modify the electronic structure of a metal.[52, 53] The stability of the support in the fuel cell environment is also important because it can affect the durability and stability of catalysts. The presence of water and/or oxygen, high potentials (> 0.6 V vs. RHE), high temperatures (50-90 °C) and low pH (< 1) can cause corrosion on the support. Loss of the support usually leads to the agglomeration of metal particles, resulting in a decrease in the electrochemical surface area. Therefore, the interaction between a metal and carbon support has a strong influence on the physicochemical and electrochemical properties of the catalyst and its performance in fuel cell operations. The various types of supports are explained below.

1.4.3.1 Carbon blacks: Carbon black is widely used as a catalyst support in low temperature fuel cells due to its low cost and high availability. Vulcan XC-72R is commonly used in the preparation of electrocatalysts, especially for a PEFC, because of its high electrical conductivity and high specific surface area. Recently, Ketjen black (highly electro-conductive carbon black) has becoming attractive because of its higher specific surface area and electrical conductivity than those of Vulcan XC72R. However, both Vulcan XC72R and Ketjen black contain a large amount of micropores (less than

2 nm) that are difficult to be fully accessible. To avoid this problem, many types of new carbon materials with a mesoporous (2-50 nm) structure have been tested as supports for fuel cell catalysts.

1.4.3.2 Carbon nanotubes: There have been many studies in which carbon nanotube were used as supports for PtRu/C anode catalysts. They studies showed that a carbon nanotube is a good candidate for supporting materials for a PEFC because very small and uniform PtRu particles can be obtained.[54-58] Neetu et al.[59] reviewed the effect of chemical functionalization on the morphology and physical properties of a single-wall nanotube (SWNT) and suggested that a thin SWNT film based support had superior properties more than conventional supports.

1.4.3.3 Graphene: Graphene has a very high surface area (~2630 $m^2 g^{-1}$), which is higher than that of graphite (~10 $m^2 g^{-1}$) or a carbon nanotube (1300 $m^2 g^{-1}$). Graphene also shows excellent electrical, thermal, mechanical, electronic, and optical properties. It has a high specific surface area, high chemical stability, high optical transmittance, high elasticity, high porosity, biocompatibility, and a tunable band gap. The chemical functionalization actually helps in tuning its properties. All of these remarkable properties make graphene promising for fuel cell applications.[60-63] Novoselov et al.[64] reported an interesting result when using graphene as a support. They found that graphene decreased platinum particle size to a nanometer scale because of strong interaction between platinum atoms and graphene.

1.4.3.4 Mesoporous carbons: Recently, ordered mesoporous carbons have received great attention due to their potential as catalytic supports in fuel cell electrodes. They have high specific surface areas, large pore volumes and controllable pore sizes. Their high specific surface areas enable the preparation of highly dispersed metal particles, whereas their highly interconnected mesopore structures provide an open network around the active sites, facilitating effective diffusion of the reactants and byproducts. The most interesting mesoporous carbon is resorcinol formaldehyde carbon (RFC) gel,[65-67] which is the main support used in this study. Marie et al.[68] investigated many carbon aerogels for cathodes and demonstrated that the texture of the carbon support for cathodes has a significant impact on performance of the MEA because the gas diffusion rate can be significantly improveed. Job et al.[69] reported that carbon xerogels, which are very easy to prepare, could replace carbon aerogels previously used in the same system without decreasing catalytic performance.

In conclusion, carbon supports have a strong influence on particle size and dispersion of metal and provide potential benefits for improvements in both the properties and the stability of electrocatalysts. Moreover, the carbon structure plays an important role in catalyst performance because it affects the access of the reactants on the catalytic sites and the removal of reaction products. Hence, the optimization of carbon supports is very important in the development of PEFC technology.

1.5 RFC synthesis and pore structure adjustment

Pekala[70] reported successful synthesis of carbon aerogels by carbonization of resorcinol-formaldehyde resins. The carbon aerogels are expected to be used for electrochemical applications due to their high surface areas, controllable pore sizes, and low electrical resistance. The structures and properties of carbon aerogel electrodes depend on the synthesis conditions, pyrolysis temperatures, activation procedures, and presence of selected dopants. Tamon et al.[71] reported that the mesoporous structure of aerogels could be controlled by adjusting the molar ratio of resorcinol to the catalyst (Na_2CO_3) used (R/C) and the ratio of resorcinol to distilled water used as the diluent (R/W) in the polycondensation process.

1.5.1 Synthesis conditions[72, 73]

In order to synthesize RFC carbon gel, resorcinol and formaldehyde are first polymerized using a base catalyst. The main reaction is a condensation reaction that leads to the formation of compounds that have methylene bridges and methylene ether bridges. Such oligomers form clusters that agglomerate to colloidal particles. These particles coagulate and form a wet gel (hydrogel). Next, the hydrogel is dried to remove the solvent in its gel structure. Then the dried gel is heat-treated in an inert atmosphere and is transformed to carbon. Finally, the carbon is activated by gases such as steam or CO_2 to increase its pore volume, pore size and surface area. However, a higher carbonization temperature generally leads to lower pore volume. In addition, a change in the R/C molar ratio of the starting solution to be used in the RFC synthesis results in a change in the final carbon microstructure. A lower R/C ratio also results in small polymer particles (3-5 nm) that have a higher density. Polymeric RF gels that are formed by small polymer particles generally have a high surface area and high compressive modulus; however, the gels shrink during the drying process. In the case of synthesis at high R/C ratios and formation by large polymer particles (16-200 nm), the RF gels have low surface areas and low compressive modulus. However, there is no

shrinkage after the drying process.

1.5.2 Solvent exchange process[74, 75]

Kraiwattanawong et al. reported that solvent exchange prior to drying of the hydrogels reduced the pore shrinkage, caused by capillary forces, and enhanced mesoporosity of carbon xerogels.

1.5.3 Heat treatment process[76]

The mesopore volume of an RFC support can be controlled by adjusting the carbonization and activation conditions. In addition, adjustment of the carbonization and activation process can be used for controlling the physical and electrochemical properties.

1.6 Purpose of the research

In order to prepare better CO-tolerant anode catalysts and understand the enhancement mechanism of CO tolerance, several studies have focused on the characteristics of active sites of PtRu structures, the third element to form an alloy, and other issues. However, there has been little investigation of the effects of the support structure and distribution of pore sizes, which can improve both the formation of PtRu particles and transportation of gases. Thus, this work mainly focused on the effect of support on CO tolerance. This thesis consists of 7 chapters. An outline of each chapter is as follows:

Chapter 2: In experiments for which results are shown in Chapter 2, the effects of activation degrees of RFC supports were investigated. After resorcinol formaldehyde carbon gel had been prepared, the activation process with CO_2 was carried out at different specific times to obtain various activation degrees of RFC supports. Then PtRu was deposited on these supports and CO tolerance was evaluated.

Chapter 3: In experiments for which results are shown in Chapter 3, the effect of Ru:Pt ratio on two commercial supports were studied. PtRu/C catalysts with various Ru:Pt ratios were prepared on supports which different surface areas. The obtained catalysts were characterized mainly by XRD and their CO tolerance was evaluated using a PEFC single cell.

Chapter 4: In experiments for which results are shown in Chapter 4, the effect of mesoporous structure on CO tolerance was studied. By changing the resorcinol-to-catalyst (R/C) ratio of the prepared RF carbon gels, the pore structures of obtained RFCs were different. Then PtRu were deposited on these supports, and BET surface area and pore distribution were examined. Finally, MEAs using these catalysts were evaluated for CO tolerance.

Chapter 5: In experiments for which results are shown in Chapter 5, the effect of SnO_2 decorated on a commercial carbon support was studied. A small amount of SnO_2 (2 wt%) was deposited on the carbon support before the PtRu catalyst preparation process. The obtained catalysts were characterized by XRD, FTIR and CO stripping.

Chapter 6: In experiments for which results are shown in Chapter 6, the effect of Nafion® content on CO tolerance of anode catalysts was studied. The prepared Pt_2Ru_3/RFC and commercial Pt_2Ru_3 catalysts were mixed with different amounts of Nafion®. These samples were tested by N_2 adsorption for BET surface area and DH pore distribution. The MEAs using these anode catalysts were evaluated for CO tolerance.

Chapter 7: The results of each chapter are summarized in Chapter 7.

References

1. Sundmacher, K., Fuel Cell Engineering: Toward the Design of Efficient Electrochemical Power Plants. *Ind. Eng. Chem. Res.* **2010**, *49* (21), 10159-10182.
2. Kirubakaran, A.; Jain, S.; Nema, R. K., A Review on Fuel Cell Technologies and Power Electronic Interface. *Renewable Sustainable Energy Rev.* **2009**, *13* (9), 2430-2440.
3. Shripad T.; Revankar P. M.; *Fuel Cells: Principles, Design, and Analysis*; CRC Press: **2014**, pp 1-32.
4. McLean, G. F.; Niet, T.; Prince-Richard, S.; Djilali, N., An Assessment of Alkaline Fuel Cell Technology. *Int. J. Hydrogen Energy* **2002**, *27* (5), 507-526.
5. Mehmeti, A.; Santoni, F.; Della Pietra, M.; McPhail, S. J., Life Cycle Assessment of Molten Carbonate Fuel Cells: State of the Art and Strategies for the Future. *J. Power Sources* **2016**, *308*, 97-108.

6. Song, C., Fuel Processing For Low-Temperature and High-Temperature Fuel Cells: Challenges, and Opportunities for Sustainable Development in The 21st Century. *Catal. Today* **2002**, *77* (1-2), 17-49.
7. Barbir, F.; PEM Fuel Cells. In *Fuel Cell Technology: Reaching Towards Commercialization*; Sammes, N., Ed.; Springer London: London, 2006; pp 27-51.
8. Nishida, R.; Kakinuma, K.; Nishino, H.; Kamino, T.; Yamashita, H.; Watanabe, M.; Uchida, H., Synthesis of Nickel Nanoparticles Supported on Hollow Samaria-Doped Ceria Particles via the Solution-Spray Plasma Technique: Anode Catalysts for SOFCs. *Solid State Ionics* **2009,** *180* (14-16), 968-972.
9. Sammes, N. M.; Bove, R.; Pusz, J., Solid Oxide Fuel Cells. In *Fuel Cell Technology: Reaching Towards Commercialization*, Sammes, N., Ed.; Springer London: London, 2006; pp 1-26.
10. Ito, H.; Maeda, T.; Nakano, A.; Takenaka, H., Properties of Nafion® Membranes under PEM water electrolysis conditions. *Int. J. Hydrogen Energy* **2011,** *36* (17), 10527-10540.
11. Sigma-Aldrich, Chemical structure of Nafion®, Nafion® 117. http://www.Sigmaaldrich.com/catalog/product/aldrich/274674?lang=ja&region=JP (access, October 31, 2015).
12. Passalacqua, E.; Lufrano, F.; Squadrito, G.; Patti, A.; Giorgi, L., Nafion® Content in the Catalyst Layer of Polymer Electrolyte Fuel Cells: Effects on Structure and Performance. *Electrochim. Acta* **2001,** *46* (6), 799-805.
13. Ticianelli, E. A.; Derouin, C. R.; Redondo, A.; Srinivasan, S., Methods to Advance Technology of Proton Exchange Membrane Fuel Cells. *J. Electrochem. Soc.* **1988,** *135* (9), 2209-2214.
14. Ishigami, Y.; Waskitoaji, W.; Yoneda, M.; Takada, K.; Hyakutake, T.; Suga, T.; Uchida, M.; Nagumo, Y.; Inukai, J.; Nishide, H.; Watanabe, M., Oxygen Partial Pressures on Gas-Diffusion Layer Surface and Gas-Flow Channel Wall in Polymer Electrolyte Fuel Cell During Power Generation Studied by Visualization Technique Combined with Numerical Simulation. *J. Power Sources* **2014,** *269*, 556-564.
15. Kulikovsky, A. A.; Scharmann, H.; Wippermann, K., Dynamics of Fuel Cell Performance Degradation. *Electrochem. Commun.* **2004,** *6* (1), 75-82.
16. Heinzel, A.; Vogel, B.; Hübner, P., Reforming of Natural Gas-Hydrogen Generation for Small Scale Stationary Fuel Cell Systems. *J. Power Sources* **2002**, *105*, 202-207.
17. Lee, S.-I.; Mitani, S.; Park, C. W.; Yoon, S.-H.; Korai, Y.; Mochida, I., Electric Double-Layer Capacitance of Microporous Carbon Nano Spheres Prepared

Through Precipitation of Aromatic Resin Pitch. *J. Power Sources* **2005**, *139*, 379-383.

18. Chen, C.-Y.; Chen, C.-C.; Hsu, S.-W.; Lai, M.-P.; Lai, W.-H.; Yang, W.-M., Behavior of a Proton Exchange Membrane Fuel Cell in Reformate Gas. *Energy Procedia* **2012**, *29*, 64-71.
19. Hedström, L.; Tingelöf, T.; Alvfors, P.; Lindbergh, G., Experimental Results from a 5 Kw Pem Fuel Cell Stack Operated on Simulated Reformate from Highly Diluted Hydrocarbon Fuels: Efficiency, Dilution, Fuel Utilisation, CO Poisoning and Design Criteria. *Int. J. Hydrogen Energy* **2009**, *34*, 1508-1514.
20. Ahmed, S.; Krumpelt, M., Hydrogen from Hydrocarbon Fuels for Fuel Cells. *Int. J. Hydrogen Energy* **2001**, *26*, 291-301.
21. Chen, C.-Y.; Lai, W.-H.; Yan, W.-M.; Chen, C.-C.; Hsu, S.-W., Effects of Nitrogen and Carbon Monoxide Concentrations on Performance of Proton Exchange Membrane Fuel Cells With Pt-Ru Anodic Catalyst. *J. Power Sources* **2013**, *243*, 138-146.
22. Zhang, Z.-G.; Xu, G.; Chen, X.; Honda, K.; Yoshida, T., Process Development of Hydrogenous Gas Production for PEFC from Biogas. *Fuel Process. Technol.* **2004**, *85*, 1213-1229.
23 Zhdanov, V. P.; Kasemo, B., Kinetics of Electrochemical O_2 Reduction on Pt. *Electrochem. Commun.* **2006,** *8* (7), 1132-1136;
24 Nørskov, J. K.; Rossmeisl, J.; Logadottir, A.; Lindqvist, L.; Kitchin, J. R.; Bligaard, T.; Jónsson, H., Origin of the overpotential for oxygen reduction at a Fuel-Cell Cathode. *J. Phys. Chem. B* **2004,** *108* (46), 17886-17892.
25 Li, H.; Lee, K.; Zhang, J., Electrocatalytic H_2 Oxidation Reaction. In *PEM Fuel Cell Electrocatalysts and Catalyst Layers: Fundamentals and Applications*, Zhang, J., Ed.; Springer London; London, 2008; pp 135-164.
26. Watanabe, M.; Motoo, S., Electrocatalysis by Ad-Atoms: Part III. Enhancement of Oxidation of Carbonmonoxide on Platinum by Ruthenium Ad-Atoms. *J. Electroanal. Chem.* **1975**, *60*, 275-283.
27. Scott, F. J.; Mukerjee, S.; Ramaker, D. E., Contrast in Metal-Ligand Effects on Pt_nm Electrocatalysts with M Equal Ru vs Mo and Sn As Exhibited by in Situ XANES and EXAFS Measurements in Methanol. *J. Phys. Chem. C* **2010**, *114*, 442-453.
28. Burch, R., Importance of Electronic Ligand Effects in Metal Alloy Catalysts. *Acc. Chem. Res.* **1982**, *15*, 24-31.

29. Koper, M. T. M., Electrocatalysis on Bimetallic and Alloy Surfaces. *Surf. Sci.* **2004**, *548*, 1-3.

30. Pereira, L. G. S.; dos Santos, F. R.; Pereira, M. E.; Paganin, V. A.; Ticianelli, E. A., CO Tolerance Effects of Tungsten-Based PEMFC Anodes. *Electrochim. Acta* **2006**, *51*, 4061-4066.
31. de Bruijn, F. A.; Makkus, R. C.; Mallant, R. K. A. M.; Janssen, G. J. M., Chapter 5: Materials for State-of-the-Art PEM Fuel Cells, and Their Suitability for Operation Above 100 °C. In *Advances in Fuel Cells*, T.S. Zhao, K. D. K.; Trung Van, N., Eds.; Elsevier Science; 2007; pp 235-336.
32. Pereira, L. G. S.; Paganin, V. A.; Ticianelli, E. A., Investigation of the CO Tolerance Mechanism at Several Pt-Based Bimetallic Anode Electrocatalysts in A PEM Fuel Cell. *Electrochim. Acta* **2009**, *54*, 1992-1998.
33. Lopez-Haro, M.; Dubau, L.; Guétaz, L.; Bayle-Guillemaud, P.; Chatenet, M.; André, J.; Caqué, N.; Rossinot, E.; Maillard, F., Atomic-Scale Structure and Composition of Pt_3CO/C Nanocrystallites During Real Pemfc Operation: a Stem-EELs Study. *Appl. Catal. B: Environmental* **2014**, *152–153*, 300-308.
34. Tripkovic, V., First Principles Study of (Cd, Hg, In, Tl, Sn, Pb, As, Sb, Bi, Se) Modified Pt(111), Pt(100) and Pt(211) Electrodes as CO Oxidation Catalysts. *Electrochim. Acta* **2015**, *168*, 370-378.
35. Watanabe, M.; Motoo, S., Electrocatalysis by Ad-Atoms: Part II. Enhancement of Oxidation of Methanol on Platinum by Ruthenium Ad-Atoms. *J Electroanal. Chem.* **1975**, *60*, 267-273.
36. Ross, P. N.; Kinoshita, K.; Scarpellino, A. J.; Stonehart, P., Electrocatalysis on Binary Alloys: Ii. Oxidation of Molecular Hydrogen on Supported Pt + Ru Alloys. *J. Electroanal. Chem. and Interfacial Electrochem.* **1975**, *63*, 97-110.
37. Gasteiger, H. A.; Markovic, N.; Ross Jr, P. N.; Cairns, E. J., CO Electrooxidation on Well-Characterized Pt-Ru Alloys. *J. Phys. Chem.,Us* **1994**, *98*, 617-625.
38. Adams, R. D.; Barnard, T. S., Does a Metal to Metal "Ligand" Effect Influence the Catalytic Activity of Bimetallic Cluster Complexes? Synthesis and Catalytic Activity of $Pt_3Ru_6(Co)_{19}(SMe_2)(\mu_3\text{-}PhC_2Ph)(\mu_3\text{-}H)(\mu\text{-}H)$. *Organometallics* **1998**, *17*, 2885-2890.
39. Balk, R. W.; Stufkens, D. J.; Oskam, A., Characterization of Metal-to-Ligand Charge-Transfer and Intraligand Transitions of Fac-$[Re(Co)_3L(X)]$ Complexes [L = Di-Imine – X = Halide or $Mn(Co)_5$] and Explanation of the Photochemistry of $[Re(Co)_3L\text{-}[Mn(Co)_5]]$ Using the Resonance Raman Effect. *J. Chem. Soc. Dalton*

Trans **1981**, 1124-1133.

40. Davies, J. C.; Bonde, J.; Logadottir, A.; Norskov, J. K.; Chorkendorff, I., The Ligand Effect: CO Desorption from Pt/Ru Catalysts. *Fuel Cells* **2005**, *5*, 429-435.
41. Koper, M. T. M.; Shubina, T. E.; van Santen, R. A., Periodic Density Functional Study of CO and OH Adsorption on Pt-Ru Alloy Surfaces: Implications for CO Tolerant Fuel Cell Catalysts. *J. Phys. Chem. B* **2002**, *106*, 686-692.
42. Chang, S. C.; Weaver, M. J., Coverage-Dependent and Potential-Dependent Binding Geometries of Carbon-Monoxide at Ordered Low-Index Platinum Aqueous and Rhodium Aqueous Interfaces - Comparisons with Adsorption in Corresponding Metal Vacuum Environments. *Surf. Sci.* **1990**, *238*, 142-162.
43. Ianniello, R.; Schmidt, V. M.; Stimming, U.; Stumper, J.; Wallau, A., CO Adsorption and Oxidation on Pt and Pt-Ru Alloys: Dependence on Substrate Composition. *Electrochim. Acta* **1994**, *39*, 1863-1869.
44. Aberdam, D.; Durand, R.; Faure, R.; Gloaguen, F.; Hazemann, J. L.; Herrero, E.; Kabbabi, A.; Ulrich, O., X-Ray Absorption near Edge Structure Study of the Electro-Oxidation Reaction of CO on $Pt_{50}Ru_{50}$ Nanoparticles. *J. Electroanal. Chem.* **1995**, *398*, 43-47.
45. Antolini, E.; Cardellini, F., Formation of Carbon Supported PtRu Alloys: an XRD Analysis. *J Alloy Compd* **2001**, *315*, 118-122.
46. Wang, D.; Zhuang, L.; Lu, J. T., An Alloying-Degree-Controlling Step in the Impregnation Synthesis of PtRu/C Catalysts. *J. Phys. Chem. C* **2007**, *111*, 16416-16422.
47. Chen, Y.; Zhou, Y. M.; Tang, Y. W.; Lu, T. H., Electrocatalytic Properties of Carbon-Supported PtRu Catalysts with the High Alloying Degree for Formic Acid Electrooxidation. *J. Power Sources* **2010**, *195*, 4129-4134.
48. Lee, K. S.; Jeon, T. Y.; Yoo, S. J.; Park, I. S.; Cho, Y. H.; Kang, S. H.; Choi, K. H.; Sung, Y. E., Effect of PtRu Alloying Degree on Electrocatalytic Activities and Stabilities. *Appl. Catal., B* **2011**, *102*, 334-342.
49. Pires, F. I.; Corradini, P. G.; Paganin, V. A.; Antolini, E.; Perez, J., Effect of the Degree of Alloying of PtRu/C (1:1) Catalysts on Ethanol Oxidation. *Ionics* **2013**, *19*, 1037-1045.
50. Yamanaka, T.; Takeguchi, T.; Wang, G.; Muhamad, E. N.; Ueda, W., Particle Size Dependence of CO Tolerance of Anode PtRu Catalysts for Polymer Electrolyte Fuel Cells. *J. Power Sources* **2010**, *195*, 6398-6404.

51. Wang, G.; Takeguchi, T.; Muhamad, E. N.; Yamanaka, T.; Ueda, W., Investigation of Grain Boundary Formation in PtRu/C Catalyst Obtained in a Polyol Process with Post-Treatment. *Int. J. Hydrogen Energy* **2011**, *36*, 3322-3332.
52. Goodenough, J. B.; Hamnett, A.; Kennedy, B. J.; Manoharan, R.; Weeks, S. A., Porous Carbon Anodes for the Direct Methanol Fuel Cell-I: The Role of the Reduction Method for Carbon Supported Platinum Electrodes. *Electrochim. Acta* **1990**, *35*, 199-207
53. Ma, J.; Habrioux, A.; Guignard, N.; Alonso-Vante, N., Functionalizing Effect of Increasingly Graphitic Carbon Supports on Carbon-Supported and TiO_2-Carbon Composite-Supported Pt Nanoparticles. *J. Phys. Chem. C* **2012**, *116*, 21788-21794.
54. Arbizzani, C.; Righi, S.; Soavi, F.; Mastragostino, M., Graphene and Carbon Nanotube Structures Supported on Mesoporous Xerogel Carbon as Catalysts for Oxygen Reduction Reaction in Proton-Exchange-Membrane Fuel Cells. *Int. J. Hydrogen Energy* **2011**, *36*, 5038-5046.
55. Jha, N.; Leela Mohana Reddy, A.; Shaijumon, M. M.; Rajalakshmi, N.; Ramaprabhu, S., PtRu/Multi-Walled Carbon Nanotubes as Electrocatalysts for Direct Methanol Fuel Cell. *Int. J. Hydrogen Energy* **2008**, *33*, 427-433.
56. Kardimi, K.; Tsoufis, T.; Tomou, A.; Kooi, B. J.; Prodromidis, M. I.; Gournis, D., Synthesis and Characterization of Carbon Nanotubes Decorated with Pt and PtRu Nanoparticles and Assessment of Their Electrocatalytic Performance. *Int. J. Hydrogen Energy* **2012**, *37*, 1243-1253.
57. Sieben, J. M.; Duarte, M. M. E., Methanol, Ethanol and Ethylene Glycol Electro-Oxidation at Pt and PtRu Catalysts Electrodeposited over Oxidized Carbon Nanotubes. *Int. J. Hydrogen Energy* **2012**, *37*, 9941-9947.
58. Zhao, Y.; Fan, L.; Ren, J.; Hong, B., Electrodeposition of PtRu and PtRuNi Nanoclusters on Multi-Walled Carbon Nanotubes for Direct Methanol Fuel Cell. *Int. J. Hydrogen Energy* **2014**, *39*, 4544-4557.
59. Jha, N.; Ramesh, P.; Bekyarova, E.; Tian, X.; Wang, F.; Itkis, M. E.; Haddon, R. C., Functionalized Single-Walled Carbon Nanotube-Based Fuel Cell Benchmarked against US DOE 2017 Technical Targets. *Sci. Rep.* **2013**, *3*, 2257.
60. Antolini, E., Graphene as a New Carbon Support for Low-Temperature Fuel Cell Catalysts. *Appl. Catal., B* **2012**, *123–124*, 52-68.
61. Ma, C. A.; Liu, W.; Shi, M.; Lang, X.; Chu, Y.; Chen, Z.; Zhao, D.; Lin, W.; Hardacre, C., Low Loading Platinum Nanoparticles on Reduced Graphene Oxide-Supported Tungsten Carbide Crystallites as a Highly Active Electrocatalyst for

Methanol Oxidation. *Electrochim. Acta* **2013**, *114*, 133-141.
62. Wang, C.; Li, H.; Zhao, J.; Zhu, Y.; Yuan, W. Z.; Zhang, Y., Graphene Nanoribbons as a Novel Support Material for High Performance Fuel Cell Electrocatalysts. *Int. J. Hydrogen Energy* **2013**, *38*, 13230-13237.
63. Julkapli, N. M.; Bagheri, S., Graphene Supported Heterogeneous Catalysts: an Overview. *Int. J. Hydrogen Energy* **2015**, *40*, 948-979.
64. Novoselov, K. S.; Falko, V. I.; Colombo, L.; Gellert, P. R.; Schwab, M. G.; Kim, K., A Roadmap for Graphene. *Nature* **2012**, *490*, 192-200.
65. Alcántara, R.; Lavela, P.; Ortiz, G. F.; Tirado, J. L., Carbon Microspheres Obtained from Resorcinol-Formaldehyde as High-Capacity Electrodes for Sodium-Ion Batteries. *Electrochem. Solid-State Lett.* **2005**, *8*, A222-A225.
66. Landon, J.; Gao, X.; Kulengowski, B.; Neathery, J. K.; Liu, K., Impact of Pore Size Characteristics on the Electrosorption Capacity of Carbon Xerogel Electrodes for Capacitive Deionization. *J. Electrochem. Soc.* **2012**, *159*, A1861-A1866.
67. Sharma, C. S.; Katepalli, H.; Sharma, A.; Teixidor, G. T.; Madou, M., Fabrication of Resorcinol-Formaldehyde Xerogel Based High Aspect Ratio 3-D Hierarchical C-Mems Structures. *ECS Trans.* **2014**, *61*, 45-54.
68. Marie, J.; Berthon-Fabry, S.; Achard, P.; Chatenet, M.; Pradourat, A.; Chainet, E., Highly Dispersed Platinum on Carbon Aerogels as Supported Catalysts for PEM Fuel Cell-Electrodes: Comparison of Two Different Synthesis Paths. *J. Non-Cryst. Solids* **2004**, *350*, 88-96.
69. Job, N.; Marie, J.; Lambert, S.; Berthon-Fabry, S.; Achard, P., Carbon Xerogels as Catalyst Supports for PEM Fuel Cell Cathode. *Energy Convers. Manage.* **2008**, *49*, 2461-2470.
70. Pekala, R. W., Organic Aerogels from the Polycondensation of Resorcinol with Formaldehyde. *J. Mater. Sci.* **1989**, *24*, 3221-3227.
71. Tamon, H.; Ishizaka, H.; Mikami, M.; Okazaki, M., Porous Structure of Organic and Carbon Aerogels Synthesized by Sol-Gel Polycondensation of Resorcinol with Formaldehyde. *Carbon* **1997**, *35*, 791-796.
72. ElKhatat, A. M.; Al-Muhtaseb, S. A., Advances in Tailoring Resorcinol-Formaldehyde Organic and Carbon Gels. *Adv. Mater.* **2011**, *23*, 2887-2903.
73. Al-Muhtaseb, S. A.; Ritter, J. A., Preparation and Properties of Resorcinol-Formaldehyde Organic and Carbon Gels. *Adv. Mater.* **2003**, *15*, 101-114.
74. Kraiwattanawong, K.; Mukai, S. R.; Tamon, H.; Lothongkum, A. W., Improvement of Mesoporosity of Carbon Cryogels by Acid Treatment of Hydrogels. *Microporous Mesoporous Mater.* **2008**, *115*, 432-439.

75. Kraiwattanawong, K.; Tamon, H.; Praserthdam, P., Influence of Solvent Species Used in Solvent Exchange for Preparation of Mesoporous Carbon Xerogels from Resorcinol and Formaldehyde via Subcritical Drying. *Microporous Mesoporous Mater.* **2011**, *138*, 8-16.
76. Narischat, N.; Takeguchi, T.; Tsuchiya, T.; Mori, T.; Ogino, I.; Mukai, S. R.; Ueda, W., Effect of Activation Degree of Resorcinol-Formaldehyde Carbon Gels on Carbon Monoxide Tolerance of Platinum-Ruthenium Polymer Electrolyte Fuel Cell Anode Catalyst. *J. Phys. Chem. C* **2014,** *118* (40), 23003-23010.

Chapter 2

Effect of Activation Degree of Resorcinol-Formaldehyde Carbon Gels on Carbon Monoxide Tolerance of Platinum-Ruthenium Polymer Electrolyte Fuel Cell Anode Catalyst

2.1 Introduction

Polymer electrolyte fuel cell (PEFC) is considered to become promising energy storage devices because of their low operating temperature, high power density and light weight. Key technologies for automotive, stationary and portable applications have been developed in academic, institutional, and industrial sectors[1]. In Japan, residential PEFC systems have been developed rapidly during the last 10 years. Osaka Gas has commercialized a residential gas engine co-generation system, also known as CHP (combined heat and power), in March, 2003. Recently, a 0.7-1.0 kW class PEFC cogeneration system has become available in Japanese residential market.[2] A joint-project led by Panasonic and Tokyo Gas also has reported a significant development in residential PEFC.[3] Many other countries around the world also have been developing this battery system.[4-6]

In order to utilize a PEFC for residential applications, the fuel source is considered the most important factor. Natural gas appears to be the best fuel as it is a hydrogen-rich gas. The primary route for the reforming of natural gas fuel for PEFC applications is steam reforming. However, fuel obtained through this route contains CO, which is an undesired byproduct because it strongly adsorbs onto the Pt surface used in PEFC, and seriously hinders the hydrogen oxidation reaction (HOR) which occurs at the anode Pt catalyst layer.[7, 8] Electrode catalysts insensitive to CO poisoning are thus desired. For more than 30 years since its discovery, the only catalyst that can endure CO for practical uses has been a carbon-supported PtRu bimetallic catalyst. The function of Ru is to generate oxygen containing species, or to weaken Pt-CO bonding by reducing the d-electron deficiency of Pt atoms.[9] Because of the limited availability of Ru, other metals that can substitute Ru have been sought after for more than a decade.[10-12] Although there has been significant effort to develop multi-metallic Pt-based anode electrocatalysts with higher CO tolerance, common use of PtRu bimetallic catalysts for anodes only permit less than 100 ppm CO at the anode inlet.[13]

It was found earlier that, in order to obtain a high CO tolerant PtRu catalyst, its alloying degree should be high, its particle size should be about 3-5 nm, and its Pt:Ru molar ratio should be 2:3 (or 1:1.5). t was also shown that the size and alloying degree can be controlled by adjusting the preparation condition and heat treatment processe.[14-16] Moreover, from the concept of strong metal support interactions (SMSI), structure of the catalyst support could influence physical and electrical properties of the catalyst significantly.[17, 18] To investigate the effect of support, we chose resorcinol-formaldehyde (RF) resin derived carbon gels because we can tailor its surface area and pore structure by adjusting synthesis conditions.

Recently, some researchers reported the effects of carbon support structure on the performance of PtRu anode catalysts. It was found that the surface area, pore volume and accessibility to PtRu particles highly affects the efficiency of electrocatalysts.[19-21] However, how the structure of the carbon support affects the formation of PtRu particles and how it affects the CO tolerance of the resulting catalyst is not understood yet.

The aim of this present chapter is to clarify how the activation degree of the catalyst support affects the performance and CO tolerance of a carbon-gel based PtRu anode catalyst. Single cell analysis was conducted using fuels containing 0-2,000 ppm CO, and the results were compared with a well-known high CO tolerant commercial catalyst.

2.2 Experimental

2.2.1 Resorcinol-formaldehyde carbon gel preparation

Resorcinol-formaldehyde (RF) solutions were prepared from resorcinol (R), formaldehyde (F), sodium carbonate (C), and distilled water (W). The molar ratios of resorcinol to catalyst (R/C), and resorcinol to formaldehyde (R/F), and the mass to volume ratio of resorcinol to water (R/W) were fixed to 1,000 mol/mol, 0.5 mol/mol, and 0.5 g/mL, respectively. The prepared RF solutions were first kept at room temperature until they transformed to gels. Then, the obtained RF hydrogels were aged at 60 °C for 3 days. Solvent was then exchanged by immersing the RF hydrogels in t-butanol kept at 60 °C for 3 days, the solvent was replaced every day. Then, the RF hydrogels were dried at 120 °C for 3 days before being carbonized. Carbonization was conducted in a 100 cm^3-STP min^{-1} (ccm) flow of nitrogen gas. Samples were heated up to 250 °C at a 250 °C/h heating rate, and were kept at this temperature for 2 h. Heating was then continued at a rate of 250 °C/h until the temperature reached 1,000 °C and

the temperature was kept constant for 4 h. Activation was carried out in a 20 ccm CO_2 and 100 ccm N_2 flow at 1,000 °C. Activation degree (or burn-off ratio) was calculated as follows:

activation degree = weight loss after activation*100/weight before activation (2.1)

RF Carbons were named by their R/C ratio and activation degree, for example, RC1000ac0 denotes that the carbon was prepared at an R/C ratio of 1,000 without activation and RC1000ac58 indicates that the carbon was prepared under the same R/C ratio but was activation to a burn-off of 58%.

2.2.2 Preparation of Pt_2Ru_3 anode catalysts

The Pt_2Ru_3 anode catalyst were prepare through a three-step process. In the first step, the preparation of Pt/RC1000ac58, 189.6 mg of $Pt(NH_3)_2(NO_2)_2$ solution (4.554 wt% Pt, Tanaka Kikinzoku Kogyo K.K.) and 283.7 mg of RC1000ac58, 283.7 mg in were mixed with 300 mL distilled water in a three-neck flask at room temperature (20 °C) for 1 h, Pt was then reduced by adding 30 mL of ethanol to the mixture and heating the mixture up to 95 °C followed by holding the mixture at this temperature overnight. After that, the catalysts were filtered out and washed with distilled water. Then the catalysts were dried in air at 80 °C for 10 h. In the second step, for example for the preparation of Pt_2Ru_3/RC1000ac58, 303.8 mg of $RuCl_3 \cdot nH_2O$ (99.9%, Wako) was dissolved in 100 mL distilled water and the obtained solution was mixed with Pt/RC1000ac58 at room temperature for 1 h. Then Ru was reduced by adding 20 mL of methanol to the mixture and heating the mixture up to 70 °C followed by holding the mixture at this temperature overnight. After that, the obtained catalysts were filtered and washed with distilled water. Then the catalysts were dried in N_2 at 80 °C for 10 h. In the final step, the heat treatment process, the catalysts were reduced in H_2/Ar (5 % H_2) at room temperature for 1 h followed by rapid heating in He up to 880 °C within 12 min. The oven was turned off when the temperature reached 880 °C to cool the catalysts immediately. Then, the catalysts were reduced again in H_2/Ar (H_2 5 %) at 150 °C for 2 h. Pt_2Ru_3/RC1000ac0, Pt_2Ru_3/RC1000ac37 and Pt_2Ru_3/RC1000ac88 were also prepared by the same method. A commercial catalyst Pt_2Ru_3/TKK TEC61E54 (Pt 29.6 %, Ru 23.0 %, Tanaka Kikinzoku Kogyo K.K.) was used as received for comparison.

2.2.3 Physical characterization

In order to estimate the PtRu metal crystallite size, XRD patterns of the catalysts were measured using a X-ray diffractometer (RIGAKU, RINT 2000). The tube current used for Cu Kα radiation was 40 mA and the tube voltage was 40 kV. The angular region of the 2θ scan was set between 10 ° and 85 °, and the scan rate was 1 ° min^{-1}. The peak profile of the (220) reflection of Pt fcc structure was fitted with a Gaussian function. The crystallite sizes were evaluated from the position and width of the optimum Gaussian functions. Catalyst morphology was also investigated by using a Hitachi HD-2000 a scanning transmission electron microscope (STEM) instrument with electron energy of 200 kV and a beam current of 30 μA. Transmission electron microscopy (TEM) images were obtained with a JEM-2000FX (JEOL) equipped with LaB6 filament using an accelerating voltage of 200 kV.

2.2.4 MEA preparation and single cell performance testing

For preparation of the membrane electrode assembly (MEA), carbon paper (P50T) was used as the backing layers of the anode and cathode. Anode catalyst inks were prepared by dispersing PtRu/RC1000 catalysts in 4 drops of distilled water and ethanol with Nafion® solution (5 wt% dispersion, Aldrich). Cathode catalyst ink was prepared by dispersing commercial catalyst TEC61E54, 54 wt% PtRu in distilled water and ethanol with Nafion®. In both electrodes, the catalysts were painted onto each electrode at a metal loading of 0.5 mg cm^{-2}, followed by a coating of Nafion® at density of 0.5 mg cm^{-2}. Finally, the anode and cathode (22 mm × 22 mm) were placed onto the two sides of a Nafion® NRE-212 membrane (Aldrich) and hot-pressed at 135 °C and 10 MPa for 20 min to form the MEA.

The MEA was assembled into a single cell with flow field plates made of graphite and copper end plates attached to a heater (FC05-01SP, ElectroChem, Inc.). The single cell was connected to fuel cell test equipment (Chino Corp.). Pure H_2 (or H_2/CO mixture) and O_2 were supplied at flow rates of 80 mL/min to the anode and cathode, respectively, at ambient pressure. During the measurement, the anode and cathode humidifiers were set at 70 °C and 68 °C, respectively, and a single cell was operated at 70 °C.

2.2.5 CO tolerance experiment

The CO tolerance experiments were performed basically under the same conditions as single cell performance tests. But the current density was fixed at (0.2 A cm^{-2}). Experiments were conducted by first providing pure H_2 for one hour and then 100 ppm of CO was introduced in the H_2 flow for 2 hours. Next, the CO concentration was increased to 500 ppm, 1,000 ppm and 2,000 ppm at an interval of 2 h.

2.3 Results and Discussion

2.3.1 Structural characterization-BET

Table 2.1 shows the surface area of RF carbon RC1000 with various activation degrees from ac0 to ac88. As the activation degree was increased, the surface area and average pore diameter increased. Carbon RC1000Ac0 has a surface area of 633 m^2 g^{-1}, which is smaller than that of the carbon support of the commercial catalyst (823 m^2 g^{-1}). With an increase in activation degree from ac37 to ac88, surface areas increased from 1,671 m^2 g^{-1} to 3,429 m^2 g^{-1}.

2.3.2 Structural characterization-XRD

Fig. 2.1 shows the XRD patterns of Pt_2Ru_3/RC1000 with various activation degrees from ac 0 to ac 88 and the Pt_2Ru_3 commercial catalyst. All XRD data were summarized in Table 2.1. The peaks positioned at 2Θ degrees of 39.2 º, 42.9 º and 67.5 º (corresponding d-spacings are 2.30 Å, 2.11 Å and 1.39 Å, respectively), can be respectively assigned to the (111), (200), (220), and (311) planes of the face-centered cubic (fcc) crystal structure. The crystallite sizes were estimated from the (220) plane using the Scherer's equation because there are no interferences from the carbon background. Pure 50 wt% Pt/RC1000ac48 was analyzed as a reference.

Table 2.1 Relation between activation degrees and surface areas.

RF gel RC 1000	Surface area of support (m^2 g^{-1})	AVG pore diameter (nm)
ac0	633	0.52
ac37	1671	0.57
ac58	2775	0.79
ac88	3429	1.22
commercial catalyst	823	-

Table 2.2 XRD peak positions for (220) plane of Pt metal in the supported Pt_2Ru_3 and calculated metal crystal sizes.

Catalyst	Pt (220) peak position (2Θ) (degrees)	Crystallite size (nm)
ac0	68.75	2.48
ac37	69.15	2.86
ac58	69.47	2.81
ac88	69.14	2.94
commercial catalyst	68.83	3.48

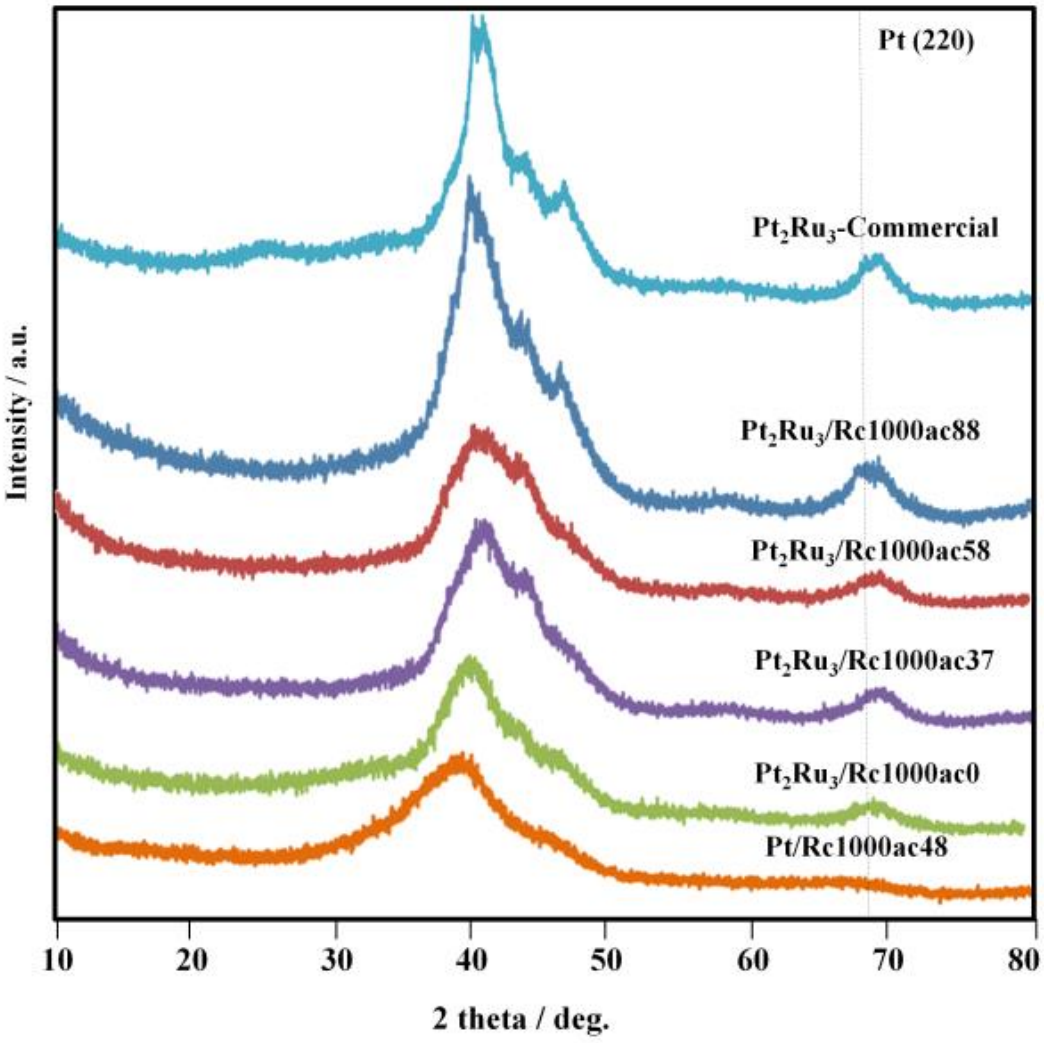

Fig. 2.1 XRD patterns of Pt_2Ru_3-commercial catalyst and prepared catalysts.

All diffractograms show the three peaks. These d-spacings are close to those characteristic of (111), (200) and (220) planes of the face-centered cubic (fcc) crystal structure Pt metal but shifted slightly. Thus, the results indicate all of the samples have a similar degree of alloying of Pt with Ru.

It was found that Pt_2Ru_3 commercial catalyst has the largest PtRu particles (3.48 nm), followed by Pt_2Ru_3/RC1000ac88 and Pt_2Ru_3/RC1000ac37 (2.94 nm and 2.86 nm, respectively). The crystallite size of Pt_2Ru_3/RC1000ac58 was calculated to be 2.81 nm, and that of Pt_2Ru_3/RC1000ac0 was the smallest and was 2.48 nm. In the case of peak position, pure 50 wt% Pt/RC1000ac48 showed the peak of (220) plane at 67.5 º.

A larger surface area was expected to result in a smaller PtRu crystallite size but from BET and XRD data, this was not the case. For example, the crystallite size of Pt_2Ru_3/RC1000ac88 which has the largest surface area but the crystallite size was 2.86 nm, larger than or almost equal to that of Pt_2Ru_3/RC1000ac58 (2.81 nm) which has a much smaller surface area. As another example, the crystallite size of Pt_2Ru_3/RC1000ac0 is smaller than that of the commercial catalyst even though it has the smallest surface area. Therefore, the surface area of the support may not be the major factor which governs the crystallite size.

2.3.3 Structural characterizations-STEM

In order to understand how PtRu particles are formed on the surface of the catalyst support, STEM technique was used. Figs. 2.2 (A)-(F) shows STEM pictures of the Pt_2Ru_3 commercial catalyst, Pt_2Ru_3/RC1000ac0, Pt_2Ru_3/RC1000ac37, Pt_2Ru_3/RC1000ac58 and Pt_2Ru_3/RC1000ac88, respectively. Since only the micropore structure is changed by activation except for Pt_2Ru_3/RC1000ac88 (Figs. 2.2 (E)-(F), 88 % activation degree), macro and mesopore structures are essentially identical. The comparison of the Pt_2Ru_3 commercial catalyst and all prepared catalysts clearly show that the dispersion of metal particles on the surface of prepared catalysts is much better than the commercial one. It should be noted that all catalysts were prepared based on the same metal content of about 53 %.

Figs. 2.2 (B)-(E) showed that the carbon structure of the prepared catalysts were quite the same because all catalysts were prepared from the same RC1000 carbon through the same preparation process. It was observed that the PtRu particle size of Pt_2Ru_3/RC1000ac0 was much larger than other catalysts (different from XRD results).

Unfortunately, in Fig. 2.2 (F) (bright field mode) the existence of agglomerated particles can be confirmed. Many pictures of Pt_2Ru_3/RC1000ac88 showed agglomerated particles located inside the carbon but not on its surface. It is possible that sintering

occurred as the micropores within the carbon are interconnected. Activation degree increases surface area via introduction of additional micropores but it was confirmed by STEM that the basic structure of RF carbons was not changed significantly.

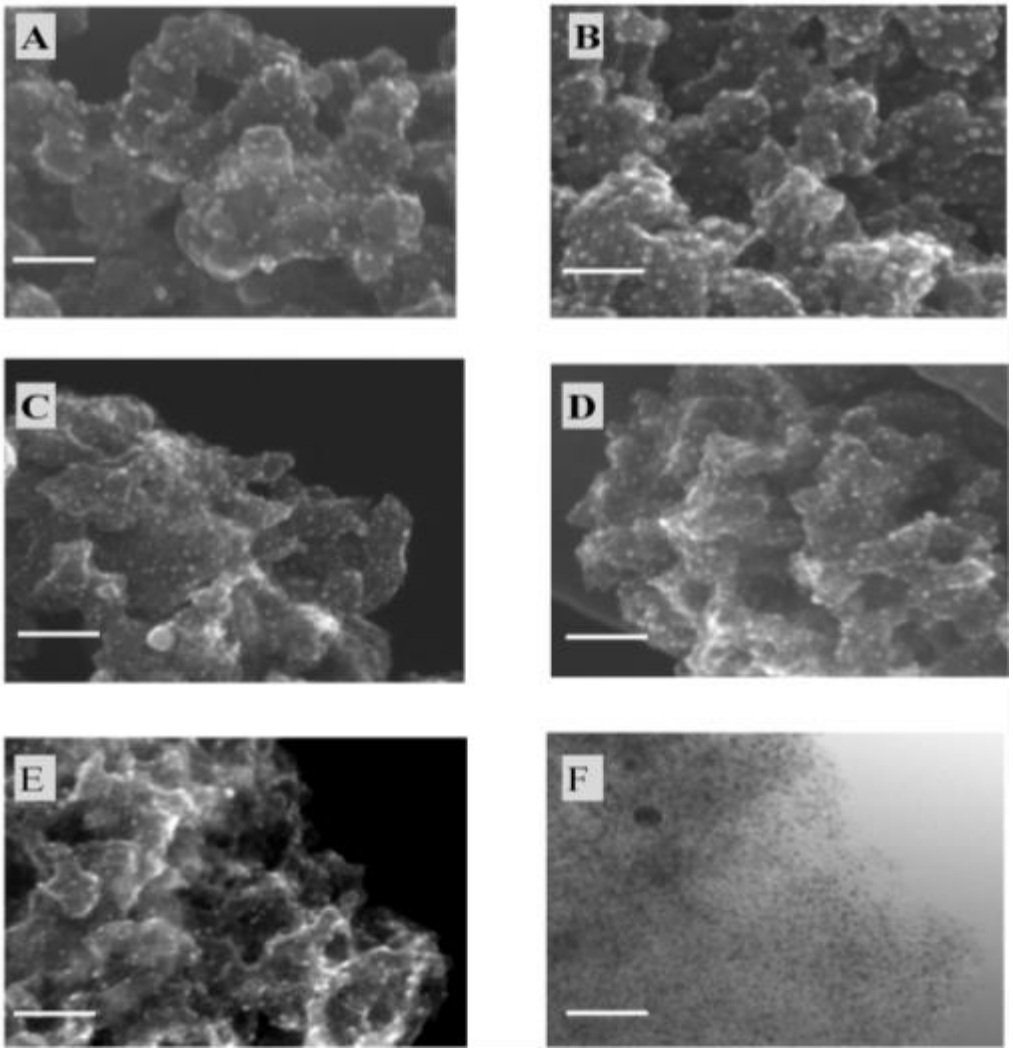

Fig. 2.2 STEM image: (A) commercial Pt_2Ru_3/C, (B) Pt_2Ru_3/RC1000ac0, (C) Pt_2Ru_3/RC1000ac37, (D) Pt_2Ru_3/RC1000ac58, (E) Pt_2Ru_3/RC1000ac88, and (F) transmission mode of Pt_2Ru_3/RC1000ac88 at scale bars = 50 nm.

2.3.4 Structural characterizations-TEM

Fig. 2.3 shows the TEM pictures of the prepared catalysts and the commercial catalyst. Particle size distributions obtained from TEM pictures are also shown. The distributions focus on the range of 1-6 nm, as particles must have sizes in the range

about 3-5 nm to show high catalytic activities 16. About 200 particles per catalyst were measured to obtain these distributions. In Fig. 2.3 (A), TEM picture of the commercial catalyst; large metal particles with sizes around 9 nm can be found. The sizes of the metal particles were not uniform, ranging from 2 nm to 12 nm.

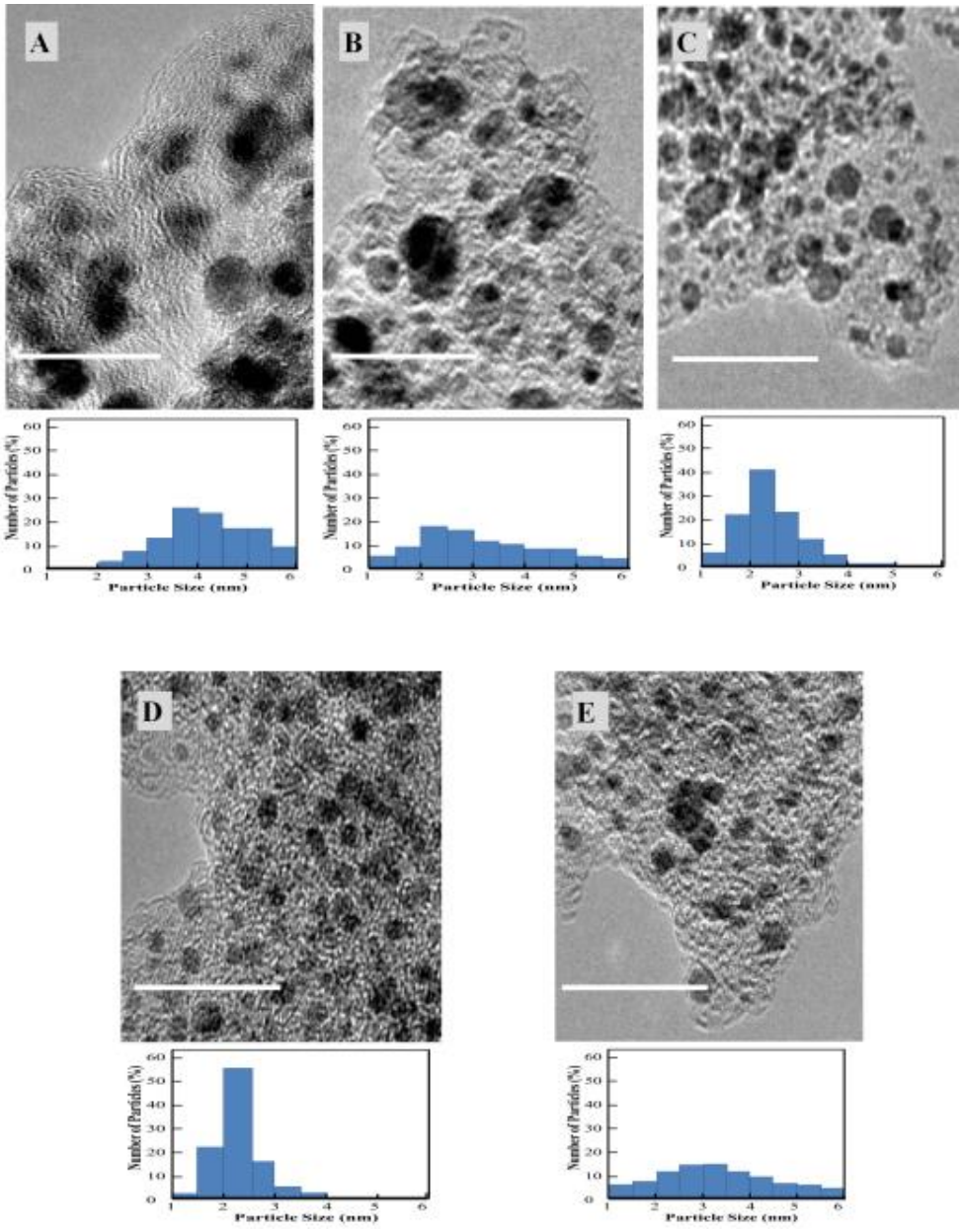

Fig. 2.3 TEM micrograph: (A) Pt_2Ru_3/C commercial catalyst, (B) Pt_2Ru_3/RC1000ac0, (C) Pt_2Ru_3/RC1000ac37, (D) Pt_2Ru_3/RC1000ac58, and (E) Pt_2Ru_3/RC1000ac88 at scale bars = 20 nm.

Fig. 2.3 (B), the TEM picture of Pt_2Ru_3/RC1000ac0, a catalyst with a lower surface area than commercial catalyst, shows that the PtRu particles are not uniform but the sized are a little bit smaller, in the range of 1-10 nm. Fig. 2.3 (C), reveals that the sizes of metal particles in Pt_2Ru_3/RC1000ac37 are much smaller (1-5 nm) and are quite uniform, Fig. 2.3 (D), shows that Pt_2Ru_3/RC1000ac58 has the most uniform sized particles in the range of 1-4 nm. As shown in Fig. 2.3 (E), although Pt_2Ru_3/RC1000ac88 has the largest surface area, the size of its PtRu particles is not as uniform as those of Pt_2Ru_3/RC1000ac58. It was found that the size of the metal particles size between 1 nm and 8 nm and a large particle (30 nm) was also found. This is consistent with Fig. 2.2 (F). These results clearly show that all the prepared catalysts have a narrower PtRu particle size distribution than the commercial catalyst, even RC1000ac0, which surface area is less than that of the commercial catalyst. This strongly suggests that the structure of the carbon support plays a major role in PtRu particle formation, not only its surface area. TEM pictures also show the effect of activation degree. The PtRu particle size distribution basically becomes narrower with the increase in activation degree (from ac0 to ac58), but when the degree becomes too large (ac88), large particles appear, probably due to the sintering through the developed micropore network of the highly activated carbon support.

2.3.5 Performance and CO tolerance examination via single cell analysis

Fig. 2.4 shows the current density-voltage curves and power density curves of electrodes constructed using the catalysts. The metal content in the entire of anode electrodes were 0.5 g cm^{-2}. Fig. 2.4 (a), the power density curve of Pt_2Ru_3/RC1000ac37 shows a maximum power density of 0.73 W cm^{-2} which value is higher than those of Pt_2Ru_3/RC1000ac58 and Pt_2Ru_3 commercial catalysts which are quite similar and are 0.66 W cm^{-2} and 0.67 W cm^{-2}, respectively. On the other hand, the current density of the commercial catalyst at 0.6 V potential is 0.9 A cm^{-2}, lower than those of Pt_2Ru_3/RC1000ac58 and Pt_2Ru_3/RC1000ac37 which are 1.0 A cm^{-2} and 1.1 A cm^{-2}, respectively. If we consider the three potential loss region, all catalysts except Pt_2Ru_3/RC1000ac0 show high activation polarization (reaction rate loss are low) in the first region. In the second region, the region of ohmic polarization (resistance loss), catalyst synthesis using a higher activation degree carbon, such as Pt_2Ru_3/RC1000ac58 and Pt_2Ru_3/RC1000ac88 lose more potential due to their larger surface areas.

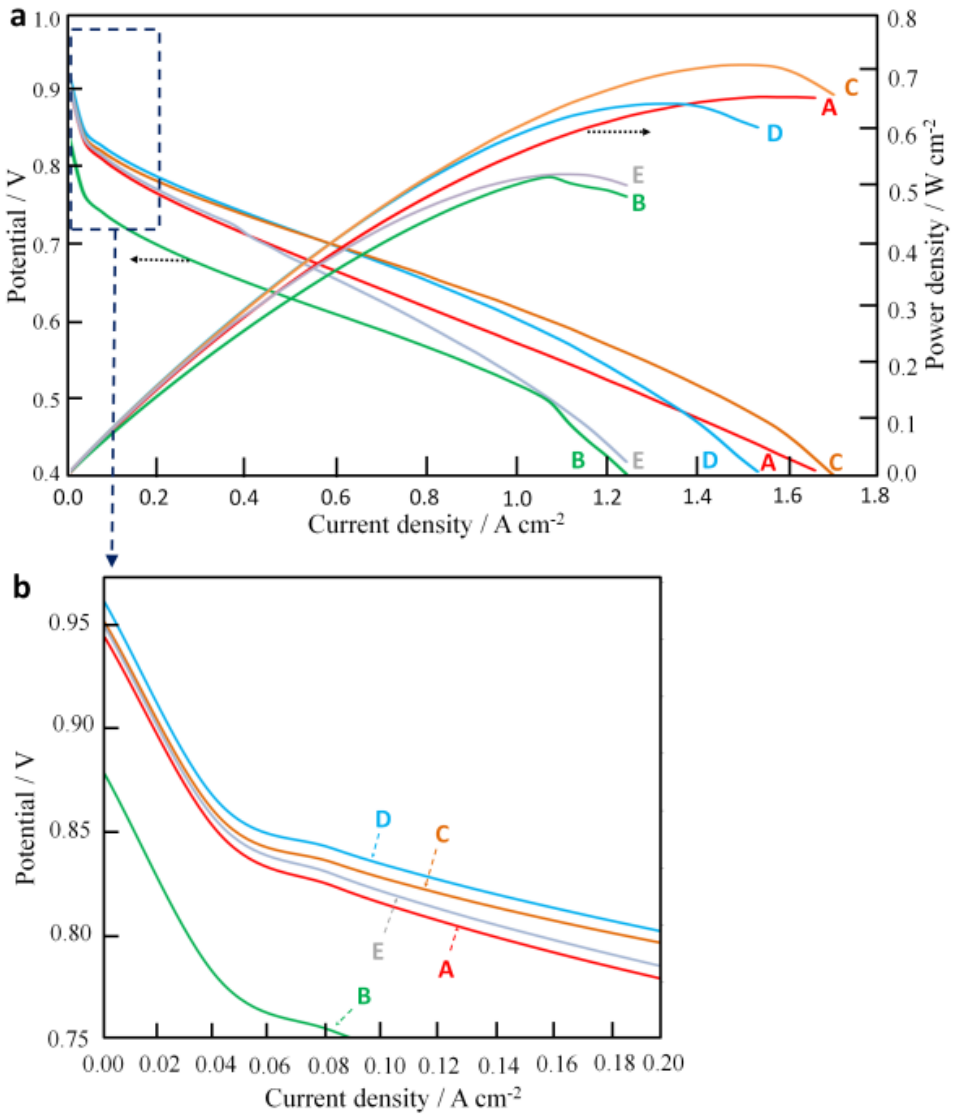

Fig. 2.4 Comparison of unit cell performance between current-voltage curves of electrodes and power density curves of electrodes with prepared and commercial catalysts as respective anode electrocatalyst: (a) full range (b) zoom at activity loss range: (A) Pt_2Ru_3/C commercial catalyst, (B) Pt_2Ru_3/RC1000ac0, (C) Pt_2Ru_3/RC1000ac37, (D) Pt_2Ru_3/RC1000ac58, and (E) Pt_2Ru_3/RC1000ac88.

In the final region, region of concentration polarization (gas transport loss), not only catalysts synthesized using higher activation degree carbons such as Pt_2Ru_3/RC1000ac88 but also those synthesized using lower activation degree carbon such as Pt_2Ru_3/RC1000ac0 show a sharp drop of potential, indicating that optimizing the activation degree of the carbon support may also lead to gas transportation

enhancement. However, Fig. 2.4 (a) showed that Pt_2Ru_3/RC1000ac37 exhibits a better performance than that exhibited by The Pt_2Ru_3 commercial PtRu/C catalyst in a unit cell test. Fig. 2.4 (b), an enlarge portion of Fig. 2.4 (a) reveal that the order of the catalyst are Pt_2Ru_3/RC1000ac58 > Pt_2Ru_3/RC1000ac37 > Pt_2Ru_3/RC1000ac88 > Pt_2Ru_3 commercial catalyst > Pt_2Ru_3/RC1000ac0. Better catalytic activity indicates the possibly of the enhancement of CO oxidation reaction, resulting in the enhancement of CO removal process.

Therefore, we checked the CO tolerance of the catalysts Fig. 2.5 (a) shows the relation between cell efficiency and CO contamination. At the beginning, pure H_2 was fed to the anode side, and it was found that Pt_2Ru_3/RC1000ac58 showed the highest cell voltage of 0.787 V after the current density was fixed to 0.2 A cm^{-2} for 1 h, followed by 0.767 V of Pt_2Ru_3/RC1000ac37. Pt_2Ru_3/RC1000ac88 and the Pt_2Ru_3 commercial catalyst showed cell voltages of 0.755 V and 0.748 V, respectively. Pt_2Ru_3/RC1000ac0 showed a cell voltage of 0.745 V for a few seconds but the voltage suddenly dropped to 0.667 V. Then, 100 ppm CO was mixed with the H_2 and fed to the anode side of the cells. Pt_2Ru_3/RC1000ac58 still showed the highest performance although the cell voltage slightly decreased to 0.758 V after the current density was fixed at 0.2 A cm^{-2}. The cell voltage of Pt_2Ru_3/RC1000ac37 decreased to 0.736 V, and that of Pt_2Ru_3/RC1000ac88 to 0.722 V. The Pt_2Ru_3 commercial catalyst showed a cell voltage of 0.719 V. That of Pt_2Ru_3/RC1000 ac0 was 0.635 V indicating that this catalyst still shows the lowest efficiency.

The critical level of CO contamination is 500 ppm, which is thought to be the actual possible CO concentration in H_2 from refineries and also from CO shift converters in residential gas systems. All of the reported catalysts including the Pt_2Ru_3 commercial catalyst, which is well known as the best CO tolerant catalyst, cannot tolerate this level. After 2 h at a fixed current density of 0.2 A cm^{-2}, the cell voltage of the Pt_2Ru_3 commercial catalyst dropped to 0.567 V, which indicates 24.2 % efficiency decrease. Surprisingly, all prepared catalysts, including Pt_2Ru_3/RC1000ac0 showed higher performances at this CO level. Pt_2Ru_3/RC1000ac58 still showed the highest cell voltage of at 0.72 V, which dropped by only 8.5% from when compared with the voltage of starting period. Cell voltage of Pt_2Ru_3/RC1000ac37, Pt_2Ru_3/RC1000ac88, and Pt_2Ru_3/RC1000ac0 were 0.704 V, 0.669 V and 0.593 V, respectively.

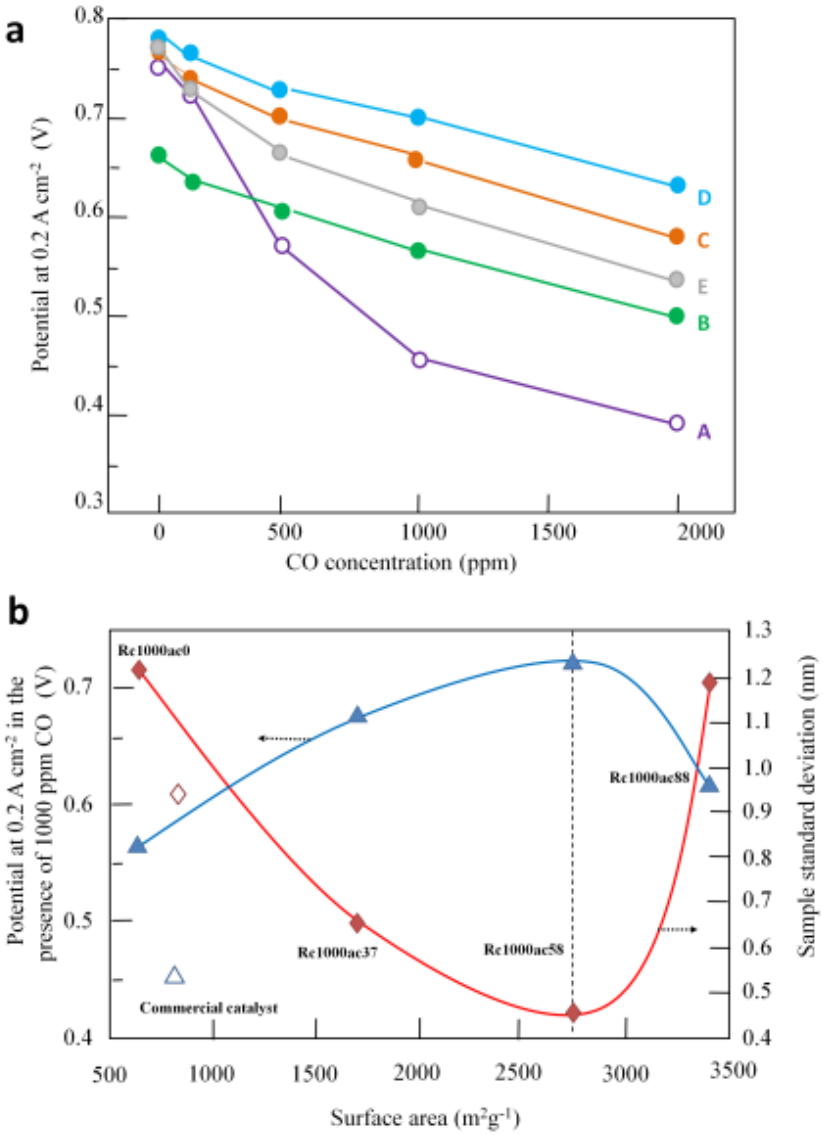

Fig. 2.5 (a) Effect of CO concentration on potential at 0.2 A cm^{-2}. cell temp.: 70 ^{o}C; electrolyte: Nafion® NRE 212; cathode: Pt/C (0.5 mg cm^{-2}); O_2 humidified at 68 ^{o}C; flow rate: 80 mL min^{-1}; anode: Pt_2Ru_3/C (0.5 mg-PtRu cm^{-2}); H_2 containing 0 ppm, 100 ppm, 500 ppm and 2,000 ppm CO humidified at 70 ^{o}C; flow rate: 80 mL min^{-1}: (A) Pt_2Ru_3/C commercial catalyst, (B) Pt_2Ru_3/RC1000ac0, (C) Pt_2Ru_3/RC1000ac37, (D) Pt_2Ru_3/RC1000ac58, and (E) Pt_2Ru_3/RC1000ac88,
(b) Comparison of surface area (m^2 g^{-1}) and potential at 0.2 A cm^{-2} in the presence of CO 1,000 ppm (V) contamination by single cell performance and the second axis presenting the sample standard deviation (SSD) of PtRu particle dispersion as observed by TEM.

CO tolerance analysis at 2,000 ppm confirmed that all of the prepared catalysts show a better CO tolerance than the commercial catalyst. The catalyst showing the highest performance and the order among the catalysts did not change. Pt_2Ru_3/RC1000ac58 showed a cell voltage of 0.655 V (0.132 V or only 16.8 % overvoltage). The cell voltages of Pt_2Ru_3/RC1000ac37, Pt_2Ru_3/RC1000ac88, and Pt_2Ru_3/RC1000ac0 were 0.556 V, 0.583 V and 0.514 V, respectively. On the other hand, the Pt_2Ru_3 commercial catalyst generated only 0.394 V, 0.354 V or 47.3 % overvoltage.

The commercial catalyst is well known for its high CO tolerance, but this investigation reveals that Pt_2Ru_3/RC1000ac37, Pt_2Ru_3/RC1000ac58, and Pt_2Ru_3/RC1000ac88 anode catalysts show higher performance than the Pt_2Ru_3 commercial catalyst in the CO concentration rage from 500 ppm to 2,000 ppm. Even PtRu/RC1000ac0, the catalyst showing the lowest performance, showed a higher efficiency than the commercial catalyst. Especially the over potential of Pt_2Ru_3/RC1000ac58 at 2,000 ppm, CO contamination was 0.132 V (16.8 %) which is much lower than that of the commercial catalyst (0.354 V, 47.3 %). Activation degree of the support highly affects the CO tolerance of the resulting catalyst. Fig. 2.5 (b) shows the relation between the potential at 0.2 A cm^{-2} in the presence of 1,000 ppm CO and the surface area of the catalyst support, it can be seen that an optimum surface area which the highest potential exits. Moreover, the standard deviation of PtRu particle size observed by TEM confirmed the higher uniformity of particle size. Adjusting the activation degree of the catalyst support is thought to have led to the optimization of micropore structure, resulting in the uniform dispersion of catalyst particles.

2.4 Conclusion

Resorcinol-formaldehyde carbon gels with various volumes of micropores were prepared by changing the degree of CO_2 activation from 0 % to 88 %. Pt and Ru nanoparticles were dispersed on these carbons by a rapid quenching method. The crystallite sizes of the PtRu particles within the prepared catalysts were smaller than those in a typical commercial catalyst. STEM pictures show that increasing the degree of activation, leads to a better distribution of PtRu particles on the surface of carbon. TEM pictures also showed the same trend that a higher degree of activation, leads to smaller PtRu particles, but when the degree becomes too large (Pt_2Ru_3/RC1000ac88), large particle tend to be formed inside the carbon. Micorpores play an important role to stabilized PtRu particles on the support surface but too high

volume of micropore increase the electrical resistance of the cell. Finally, single cell experiments were performed. With pure H_2, cell voltage of all anode catalysts at a constant current of 0.2 A cm^{-2} was in the range of 0.759-0.795 V, except that of Pt_2Ru_3/RC1000ac0 (0.66 V). After CO was introduced to H_2 from 100 ppm to 2000 ppm, the decrease in the cell voltage of the prepared showed was much smaller than that commercial catalyst showed. When the contamination level reached 500 ppm even Pt_2Ru_3/RC1000ac0 generated a higher potential than the commercial catalyst. Pt_2Ru_3/RC1000ac58, which is thought to be prepared with the carbon support having the optimum degree of activation, showed the best performance due to its proper carbon micropore structure which allows the uniform dispersion of PtRu particles. From this study, it was shown that adjusting the degree of activation of the carbon support leads to the efficient loading of PtRu particles, both in terms of particle size and distribution resulting in a higher performance and higher CO tolerance.

References

1. Rabis, A.; Rodriguez, P.; Schmidt, T. Electrocatalysis for Polymer Electrolyte Fuel Cells: Recent Achievements and Future Challenges. *ACS Catal.* **2012**, *2*, 864-890.
2. Rena, H. ; Gaoa, W; Ruanb, Y. Optimal Sizing for Residential CHP System. *Appl. Therm. Eng.* **2008**, *28*, 514-523.
3. Kani, Y. IPHE: International Partnership for Hydrogen and Fuel Cells in the Economy; Statements from Panasonic on Residential Fuel Cell m-CHP, Nov, 17, Berlin, 2008
4. Aliabadi, A.; Thomson M.; Wallace J. Efficiency Analysis of Natural Gas Residential Micro-cogeneration Systems. *Energy Fuels.* **2010**, *24*, 1704-1710.
5. Bendaikhaa, W.; Larbib, S.; Mahmaha, B. Hydrogen Energy System Analysis for Residential Applications in the Southern Region of Algeria. *Int. J. Hydrogen Energy* **2011**, *36*, 8159-8166.
6. Schmersahl, R.; Mumme, J.; Scholz, V. Farm-Based Biogas Production, Processing, and Use in Polymer Electrolyte Membrane (PEM) Fuel Cells. *Ind. Eng. Chem. Res.* **2007**, *46*, 8946-8950.
7. Igarashi, H.; Fujino, T.; Watanabe, M. Hydrogen Electro-Oxidation on Platinum Catalysts in the Presence of Trace Carbon Monoxide. *J. Electroanal. Chem*. **1995**, *391*, 119-123.

8. Wakisaka, M.; Mitsui, S.; Hirose, Y.; Kawashima, K.; Uchida, H.; Watanabe, M. Electronic Structures of Pt-Co and PtRu Alloys for CO-Tolerant Anode Catalysts in Polymer Electrolyte Fuel Cells Studied by EC-XPS. *J. Phys. Chem. B* **2006**, *110*, 23489-23496.
9. Dhar, H.; Christner, L.; Kush, A. Nature of CO Adsorption during H_2 Oxidation in Relation to Modeling for CO Poisoning of a Fuel Cell Anode. *J. Electrochem. Soc.* **1987**, *134*, 3021-3026.
10. Scott, F. J.; Mukerjee S.; Ramaker, D. E. Contrast in Metal-Ligand Effects on Pt_nM Electrocatalysts with M Equal Ru vs Mo and Sn as Exhibited by in Situ XANES and EXAFS Measurements in Methanol. *J. Phys. Chem. C* **2010**, *114*, 442-453.
11. Leng, Y.; Wang, X.; Hsing, I. Assessment of CO-Tolerance for Different Pt-Alloy Anode Catalysts in a Polymer Electrolyte Fuel Cell Using AC Impedance Spectroscopy. *J. Electroanal. Chem.* **2002**, *528*, 145-152.
12. Xu, L.; Wu, Z.; Zhang, Y.; Chen, B.; Jiang, Z.; Ma, Y.; Huang, W. Hydroxyls-Involved Interfacial CO Oxidation Catalyzed by FeO_x(111) Monolayer Islands Supported on Pt(111) and the Unique Role of Oxygen Vacancy. *J. Phys. Chem. C* **2011**, *115*, 14290-14299.
13. Yano, H.; Ono, C.; Shiroishi, H.; Saito, M.; Uchimoto , Y.; Okada, T. High CO Tolerance of N,N-Ethylenebis(salicylideneaminato)oxovanadium (IV) as a Cocatalyst to Pt for the Anode of Reformate Fuel Cells. *Chem. Mater*. **2006**, *18*, 4505-4512.
14. Takeguchi, T.; Yamanaka, T.; Asakura, K.; Muhamad, E. N.; Uosaki, K.; Ueda, W. Evidence of Nonelectrochemical Shift Reaction on a CO-Tolerant High-Entropy State PtRu Anode Catalyst for Reliable and Efficient Residential Fuel Cell Systems. *J. Am. Chem. Soc*. **2012**, *134*, 14508-14512.
15. Yamanaka, T.; Takeguchi, T.; Wang, G.; Muhamad, E. N.; Ueda, W. Particle Size Dependence of CO Tolerance of Anode PtRu Catalysts for Polymer Electrolyte Fuel Cells. *J. Power Sources* **2010**, *195*, 6398-6404.
16. Wang, G.; Takeguchi, T.; Muhamad, E. N.; Yamanaka, T.; Ueda, W. Investigation of Grain Boundary Formation in PtRu/C Catalyst Obtained in a Polyol Process with Post-Treatment. *Int. J. Hydrogen Energy* **2011**, *36*, 3322-3332.
17. Matsui, T.; Okanishi, T.; Fujiwara, K.; Tsutsui, K.; Kikuchi, R.; Takeguchi, T.; Eguchi, K. Effect of Reduction-Oxidation Treatment on the Catalytic Activity over Tin Oxide Supported Platinum Catalysts. *Sci. Technol. Adv. Mater*. **2006**, *7*, 524-530.

18. Wang, Q.; Wang, G.; Sasaki, K.; Takeguchi, T.; Yamanaka, T.; Sadakane, M.; Ueda, W. Structure and Electrochemical Activity of WO_x-Supported PtRu Catalyst Using Three-Dimensionally Ordered Macroporous WO_3 as the Template. *J. Power Sources* **2013**, *241*, 728-735.
19. Chai, G.; Yoon, S.; Yu, J.; Choi, J.; Sung, Y. Ordered Porous Carbons with Tunable Pore Sizes as Catalyst Supports in Direct Methanol Fuel Cell. *J. Phys. Chem. B* **2004**, *108*, 7074-7079.
20. Lin, M.; Huang, C.; Lo, M.; Mou, C. Well-Ordered Mesoporous Carbon Thin Film with Perpendicular Channels: Application to Direct Methanol Fuel Cell. *J. Phys. Chem. C* **2008**, *112*, 867-873.
21. Wang, Z.; Zhao, C.; Shi, P.; Yang, Y.; Yu, Z.; Wang, W.; Yin, G. Effect of a Carbon Support Containing Large Mesopores on the Performance of a PtRuNi/C Catalyst for Direct Methanol Fuel Cells, *J. Phys. Chem. C* **2010**, *114*, 672-677.

Chapter 3

Effect of Carbon Supports on Alloying Degree: CO Tolerance of PtRu/C PEFC Anode Catalysts Study

3.1 Introduction

Commercialization of residential polymer electrolyte fuel cells (PEFCs) is hindered by the severe damage of anode catalysts caused by CO contamination. There have been many reports on enhancement of CO tolerance.[1-3] The most widely used method for achieving CO tolerance enhancement is by alloying Pt with other metal elements such as Ru, Mo, and Sn.[4-7] Ru was found to be the best second metal element for increasing the CO tolerance of Pt catalysts.[8-12] There are two theories regarding the role of Ru as second metal element. One theory is the bifunctional mechanism, by which Ru helps Pt to maintain its catalytic activity by activating a CO water-gas shift reaction.[13, 14] The other theory is the ligand effect, by which Ru reduces the bond energy of Pt-CO so that the electronical CO oxidation ability is increased.[15-17] Regarding the ligand effect, it would be interesting to investigate how the nanostructure of Ru incorporated with Pt in PtRu particles affects the catalytic activity of the PtRu/C anode catalyst. Many efforts have been made to develop new synthetic routes in order to fabricate a highly catalytic and highly CO-tolerant PtRu nanostructure. There have been reports on PtRu prepared by an impregnation method, colloidal method, nanocapsule method and rapid quenching method (our laboratory method).[18, 19] The resulted PtRu alloy nanoparticles obtained by using these methods have various nanostructures and degrees of alloying. The degree of alloying is defined as the ratio of the amount of alloyed Ru (Ru_{al}) to the total amount of Ru (Ru_{tot}), which is given by

$$X_{Ru} = \left[\frac{Ru_{al}}{Pt+Ru_{al}}\right] \tag{3.1}$$

$$\frac{Ru_{al}}{Ru_{tot}} = \frac{\frac{Ru_{al}}{Pt}}{\frac{Ru_{tot}}{Pt}} = \frac{X_{Ru}}{(1-X_{Ru})\times\frac{Ru_{tot}}{Pt}} \tag{3.2}$$

where Ru_{tot} is the Ru atomic content in the Pt-Ru alloy catalyst and X_{Ru} is the Ru atomic fraction. The degree of alloying can be determined by changing the lattice parameter. The Ru atomic fraction (X_{Ru}) is estimated by Vegard's law:

$$x_{Ru} = \left[\frac{a_{ul} - a_0}{a_s - a_0}\right] \quad (3.3)$$

where a_{ul} is the lattice parameter obtained from a Pt peak of an X-ray diffraction pattern, and a_0 and a_s are lattice parameters of bulk Pt and PtRu, respectively.

In this work, PtRu/C catalysts with different degrees of alloying were prepared by changing the Ru:Pt molar ratio and carbon support. The two commercial carbon supports used have different BET surface areas. One of them, Ketjenbalck (KB) 300J, also known as E support in Japan, has a low BET surface area and has been widely used for the preparation of PEFC catalysts. The other, Ketjenblack (KB) 600JD, has a large BET surface area and is relatively new in the market.[20] Investigation of the CO tolerance of PtRu/C catalysts prepared using KB600JD would therefore be interesting.

3.2 Experimental

3.2.1 Catalysts synthetic procedures materials and methods

Eight PtRu/C catalysts were prepared in this work. Four of the catalysts were prepared with different nominal Ru:Pt molar ratios, 1.0, 1.3, 1.5 and 2.0 using commercial KB300J (carbon ECP300J of LION Corporation) as a support. The other four catalysts were prepared in the same manner but using KB600JD carbon (carbon ECP600JD of LION Corporation) as a support. The PtRu/C catalysts that were prepared are denoted as Ex or JDx, where E and JD stand for KB300J and KB600JD, respectively, while x is the nominal molar ratio between Ru and Pt. For example, E1.0 refers to the catalyst prepared from KB300J carbon with a nominal Ru:Pt molar ratio of 1.0, while JD2.0 refers to the catalysts prepared from KB600JD carbon with a nominal Ru:Pt molar ratio of 2.0. Note that E1.3, E1.5, JD1.3, and JD1.5 will be test for all experiments.

For preparation of the E1.0 catalyst, 0.57 g of carbon ECP and 8.31 g of 4.571% $Pt(C_2H_5)_2(NH_2)_2$ aqueous solution (4.554 wt% Pt, Tanaka Kikinzoku Kogyo Corporation) were mixed thoroughly with an appropriate amount of distilled water and 30 mL of ethanol and then the solution was stirred and heated at 95 °C overnight. The obtained Pt/C powder containing 40% of Pt was washed, filtrated, and dried at 80 °C in an N_2 flow for 10 h. then 0.67 g of the 40% Pt/C and 0.33 g of 85% $RuCl_3$

were mixed thoroughly with an appropriate amount of distilled water and 10 mL of methanol and the solution was stirred and heated at 70 °C overnight. The obtained powder was washed, filtrated, and dried at 80 °C in an N_2 flow for 10 h and then reduced by 5% H_2/Ar mixture gas at room temperature for 1 h. After the remaining H_2 had been completely purged He, the temperature was increased as rapidly as possible. When the temperature reached 880 °C, the heating process was immediately stopped. After cooling to room temperature, the catalyst was reduced again at 150 °C for 2 h. In this way we could prepare PtRu/C catalysts having Pt and Ru dispersed atomically. PtRu/C catalysts prepared with a Ru:Pt molar ratio of 1.5 were found to have higher CO tolerance than that of a commercial catalyst having the same Ru:Pt molar ratio.[21, 22]

E1.3, E1.5 and E2.0 catalysts were prepared in the same manner except that the amount of $RuCl_3$ were changed, and by changed the carbon support to KB600JD, JDx catalysts were prepared. A commercial catalyst Pt_2Ru_3/TKK TEC61E54 (Pt 29.6 %, Ru 23.0 %, Tanaka Kikinzoku Kogyo K.K.) or TKK1.5 was used as received for comparison.

3.2.1 Physical characterization

Nitrogen adsorption isotherms of all of the samples were measured at -196.15 °C using an adsorption apparatus (BELSORP-mini, BEL Japan). The specific surface areas were calculated from BET plots, and pore size distribution and mesopore volume were calculated from Dollimore–Heal (DH) plots. Mesopores were defined as pores with diameters between 2 and 100 nm.

3.2.2 X-ray diffraction (XRD)

XRD measurement was performed using RINT2000 (RIGAKU Corp.). The X-ray used was Kα operated at 40 kV and 20 mA. Each measurement was performed in the range of 2θ between 60 ° and 80 °. Data were obtained every 0.02 ° with a scan speed of 0.2 step s^{-1}. In each XRD pattern, the peak of platinum at 2θ equaled to 67.5 ° could be assigned to Pt (220) and was selected for metal particle size calculation because it was not interfered by any other peaks. Metal particle size was calculated by using Scherrer equation. The lattice parameter was also calculated from the position of the Pt (220) peak. The obtained lattice parameter was used for the calculation of the alloying degree of the catalyst.[23, 24]

3.2.3 Transmission electron microscopy (TEM)

The structures of catalysts were investigated using a Hitachi HD-2000 scanning transmission electron microscope (STEM) with electron energy of 200 kV and a beam current of 30 μA. For each sample, at least 200 PtRu particles were counted to obtain the precise PtRu particle distribution.

3.2.4 PEFC single cell performance and CO tolerance test

The PtRu/C catalysts that were prepared were tested for their CO tolerance when used as anodes in PEFCs. The anode was made by painting previously prepared carbon paper with catalyst ink. To prepare the carbon paper, carbon slurry was made by mixing ca. 11% of PTFE dispersion mixture (Aldrich) with XC72R carbon powder (Vulcan) so that the weight ratio between PTFE and carbon was 2:3. Then P50T carbon paper (AvCarb) was painted with the slurry. After being dried and calcined at 350 °C for 1 h, the carbon paper was ready to accommodate anode and cathode catalysts. For making the anode, the carbon paper was painted with the prepared catalysts so that the metal in the catalysts was loaded on the carbon paper at a density of 0.5 mg cm^{-2}. The cathode was made in the same manner, but a Pt/C commercial catalyst (46 wt%, TKK TEC10E50) was used instead. The catalyst ink, for painting the carbon paper, was made by mixing a catalyst with 5% of Nafion® dispersion mixture (Aldrich) at the catalyst:Nafion® weight ratio of 9:1.

After an anode and a cathode had been made, each was cut to the size of 2.2 cm x 2.2 cm size and placed on both sides of a 4.0 cm x 4.0 cm Nafion® membrane with the catalyst surface facing the membrane. Then this set was pressed using a 10 kN force at 128 °C for 20 min so that a membrane electrode assembly (MEA) could be obtained. The MEA was set in a PEFC single cell connected with a fuel cell testing system FC5100 Series (Chino) and potentiostat-galvanostat Metrohm Autolab B.V. PGSTAT302N (Autolab) coupled with an Autolab 10 A current booster BSTR 10A (Eco Chemie). Then I-V curves were obtained at 70 °C with H_2 gas (anode side) and O_2 gas (cathode side) flow rates of 80 mL min^{-1} and cell voltage of 0.2 A cm^{-2}. After the system reached a steady state, CO tolerance was tested by measuring the cell voltage at a constant current density of 0.2 A cm^{-2} for 9 h. First, pure H_2 was fed to the cell for 1 h (recorded as cell voltage at 0 ppm CO) and then 100 ppm of CO with H_2 was introduced to the cell for 2 h. The concentration of CO was increased to 500 ppm, 1,000 ppm and finally 2000 ppm for every 2 h.

3.2.5 CO stripping measurement

The catalyst ink was prepared by mixing 6.0 mg of a catalyst with 2 mL of water, 3 mL of ethanol, and 50 μL of 5% Nafion® mixture. Then a glassy carbon electronde was coated with 30 μL of the resulting catalyst ink. After driing in an 80 °C vacuum oven for 30 min, the electrode was set as a working electrode in a glass vessel containing 0.10 M of $HClO_4$ solution and connected to a Solartron Analytical 1280C Electrochemical Test System. A Pt wire was used as a counter electrode, and an Ag/AgCl electrode was used as a reference electrode. Before CO gas was introduced into the system, oxygen dissolved in the $HClO_4$ solution was removed by an Ar flow for 15 min and then the working electrode was cleaned by performing cyclic voltammogram for 10 cycles with a scan speed of 50 mV s^{-1}. The voltage range used was the same as that for CO stripping to be performed later, i.e., 0.05 V to 1.2 V vs RHE. Then CO gas was introduced into the system for 10 min to let CO adsorb on the catalyst on the working electrode, and the solution was purged with Ar gas for 15 min. The potential during CO adsorption and Ar purging was kept constant at 0.1 V vs RHE. In all cases, the gas flow rate was 200 mL min^{-1}. After Ar purging, CO stripping was performed with a scan speed of 10 mV s^{-1}.

3.3 Results and Discussion

3.3.1 Surface area and pore distribution

Nitrogen gas adsorption properties are summarized in Table 3.1. The BET surface area of KB600JD (1,627 m^2g^{-1}) was about two-times larger than that of KB300J (789 m^2g^{-1}). The pore size distribution derived by using the DH method is shown in Fig. 3.1. The mesopore volume of KB600JD was also significantly larger than that of KB300J. The mode average (most frequently occurring number) of pore diameters of both supports was 3.8 nm.

Table 3.1 BET surface areas and pore volumes of carbon supports.

Carbon support	**BET surface area(m^2 g^{-1})**	**Average pore diameter (nm)**	**Mesopore volume (cm^3 g^{-1})**
KB300J	789	5.44	0.96
KB600JD	1627	6.28	2.4

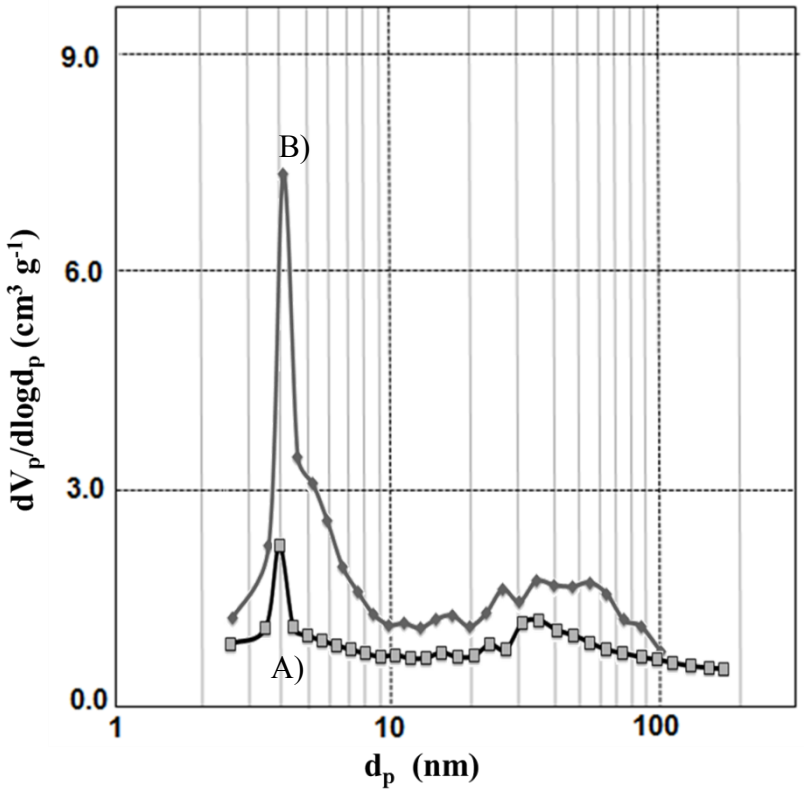

Fig. 3.1 Pore size distribution of A) ECP300J and B) ECP600JD.

3.3.2 X-ray diffraction (XRD)

XRD measurements were performed, and the metal particle sizes and alloying degrees of the prepared catalysts were calculated, and the effects of particle size and alloying degree on CO tolerance of the catalysts were examined. Fig. 3.2 shows XRD patterns of the prepared E1.3, E1.5, JD1.3 and JD1.5 catalysts. The Pt (220) peak positions and the data calculated from XRD patterns of the E1.3, E1.5, JD1.3 and JD1.5 catalysts are shown in Table 3.2. It can be seen that the XRD peaks of JDx catalysts were broader than those of Ex catalysts. Therefore, smaller PtRu metal particles could be obtained. The pore distribution data showed that KB600JD had a large volume of micropores and small mesopores. These pores can improve the anchoring size and dispersion of nanoparticles[21]. However, the good anchoring support might prevent good alloying of Pt and Ru. The catalysts using KB 300J supports (E1.3 and E1.5) had higher degrees of alloying (about 80%) than those of JD1.3 and JD1.5 (50-70%). Therefore, it can be seen that the carbon support had an impact on alloying degree of the resulted catalysts.

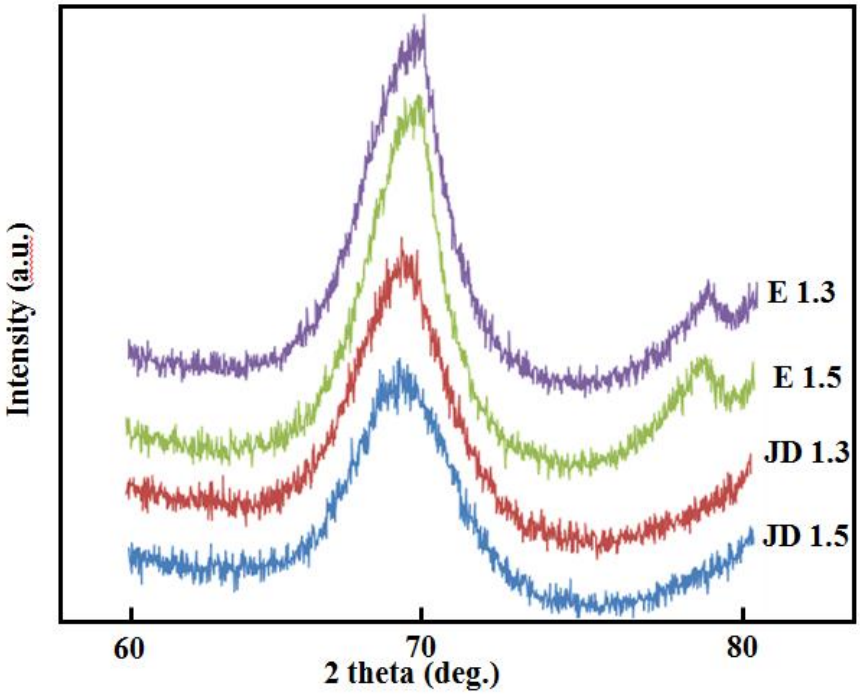

Fig. 3.2 XRD patterns of E1.3, E1.5, JD1.3 and JD1.5 catalysts.

Table 3.2 Structural parameters of the prepared PtRu/C catalysts obtained and calculated from XRD patterns.

Catalyst	Pt (220) position (degree)	Crystallite size (nm)	Lattice constant (nm)	Ru atomic fraction in PtRu (-)	Alloying degree of PtRu (%)
E1.3	68.89	2.0	0.3852	0.51	80
E1.5	68.99	2.3	0.3848	0.55	80
JD1.3	68.79	1.4	0.3857	0.47	68
JD1.5	68.73	1.4	0.3860	0.44	53

3.3.3 Transmission electron microscopy (TEM)

Fig. 3.3 shows TEM images of E1.3, JD1.3, and TKK1.5 catalysts. It can be seen that PtRu particles in TKK1.5 and E1.3 catalysts were not uniformly dispersed and their sizes varied from 1 nm to more than 10 nm. On the other hand, in the case of JD1.3, the sizes of PtRu particles were quite uniform in the range of 1-6 nm (mostly in the rage of 2.5-3.0 nm). Moreover, the average PtRu particle sizes of TKK1.5 (4.2 nm) and E1.3 (3.0 nm) were slightly larger than that of JD1.3 (2.7 nm). Although the average particle sizes obtained by TEM are larger than those obtained from XRD, the trends of the particle sizes in the catalysts are similar.

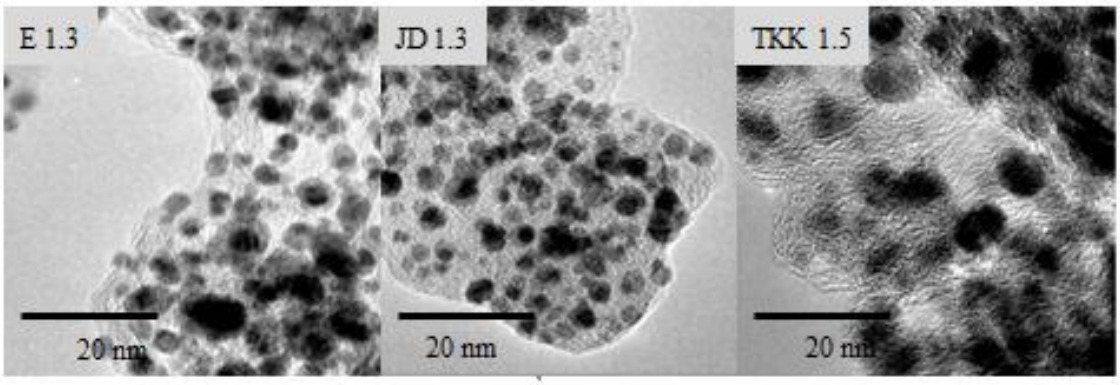

Fig. 3.3 TEM images of E1.3, JD1.3 and TKK1.5 catalysts.

3.3.4 Performance and CO tolerance

The cell voltages at 0.2 A cm^{-2} at different CO concentrations in the anode gas when PtRu/C catalysts prepared in this work were used at the anode are shown in Table 3.3. Before CO gas was introduced into the system, the cell voltages were about 0.75-0.76 V. When the concentration of CO was increased, the cell voltage dropped step by step. However, in all cases even at a CO concentration of 2,000 ppm the cell voltages were higher than 0.3 V. Table 3.3 showed also the result of TKK1.5, a commercial PtRu/C catalyst, for comparison. This TKK1.5 catalyst (Tanaka Kikinzoku Kokyu) having a Ru:Pt molar ratio of 1.5, is known to be a very high CO-tolerant catalyst. We then use the data in Table 3.3 to plot graphs to see more clearly how the type of carbon support and the Ru:Pt molar ratio affected the CO tolerance of the prepared PtRu/C catalysts.

Fig. 3.4 shows how different Ru:Pt molar ratios in the Ex catalysts affected the CO tolerance of anode catalyst. At CO concentrations up to 100 ppm, change in the Ru:Pt molar ratio had almost no effect on CO tolerance for any of the prepared PtRu/C catalysts. The results in Fig. 3.4 also suggest that the best Ru:Pt ratio for improving the CO tolerance of Ex catalysts used at the anode is 1.3. Fig. 3.5 shows how different Ru:Pt molar ratios in JDx catalysts affected CO tolerance of anode catalysts. Even when the carbon support was changed to KB600JD, the best Ru:Pt molar ratio for improving CO tolerance of the catalysts was still 1.3.

Table 3.3 Cell voltages at 0.2 A cm^{-2} at different CO concentrations in anode gas when PtRu/C catalysts prepared in this work were used at the anode.[a)]

Ru:Pt molar ratio	Catalyst name	CO concentration (ppm)				
		0	100	500	1000	2000
1.0	E1.0	0.76	0.72	0.54	0.40	0.34
	JD1.0	0.75	0.71	0.60	0.47	0.36
1.3	E1.3	0.75	0.72	0.66	0.57	0.40
	JD1.3	0.75	0.72	0.67	0.63	0.47
1.5	E1.5	0.74	0.72	0.65	0.52	0.39
	JD1.5	0.75	0.70	0.62	0.48	0.40
	TKK1.5	0.74	0.69	0.57	0.44	0.39
2.0	E2.0	0.75	0.71	0.51	0.41	0.33
	JD2.0	0.74	0.70	0.58	0.47	0.38

[a)] Cell temperature: 70 °C, electrolyte: Nafion® NRE 212, cathode: Pt/C (0.5 mg cm^{-2}), O_2 humidified at 68 °C, flow rate: 80 mL min^{-1}, anode: Ex, JDx and TKK1.5 catalysts, H_2 containing 0 ppm, 100 ppm, 500 ppm, 1,000 ppm, and 2,000 ppm CO humidified at 70 °C, flow rate: 80 mL min^{-1}.

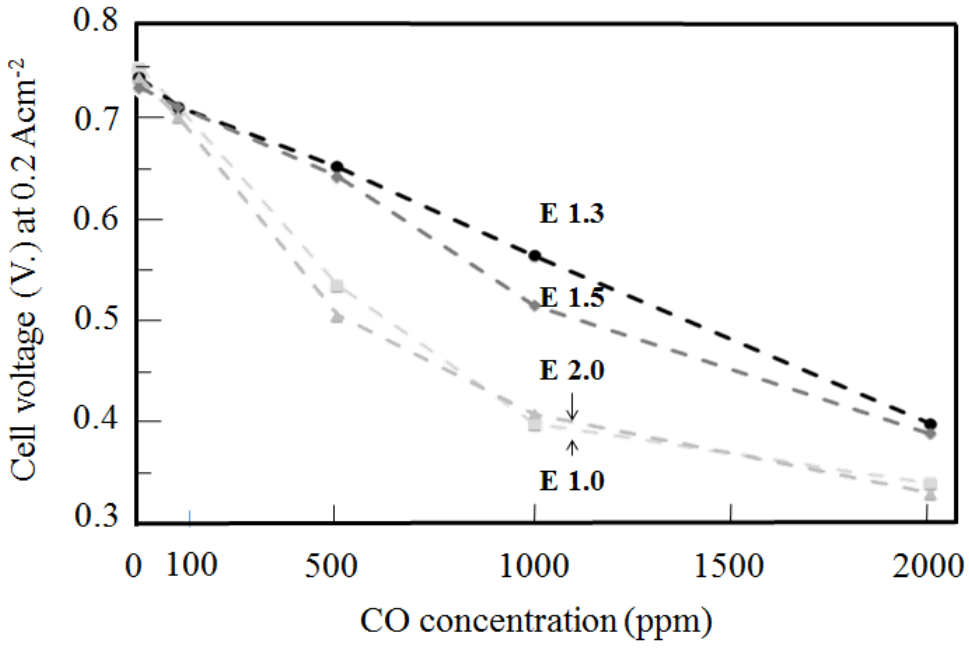

Fig. 3.4 Effect of CO concentration on cell voltage at 0.2 A cm^{-2}. Cell temp.: 70 °C, electrolyte: Nafion® NRE 212, cathode: Pt/C (0.5 mg-Pt cm^{-2}), O_2 humidified at 68 °C, flow rate: 80 mL min^{-1}, Anode: Ex catalysts (0.5 mg-PtRu cm^{-2}), H_2 containing 0 ppm, 100 ppm, 500 ppm , and 2,000 ppm CO humidified at 70 °C, Flow rate: 80 mL min^{-1}.

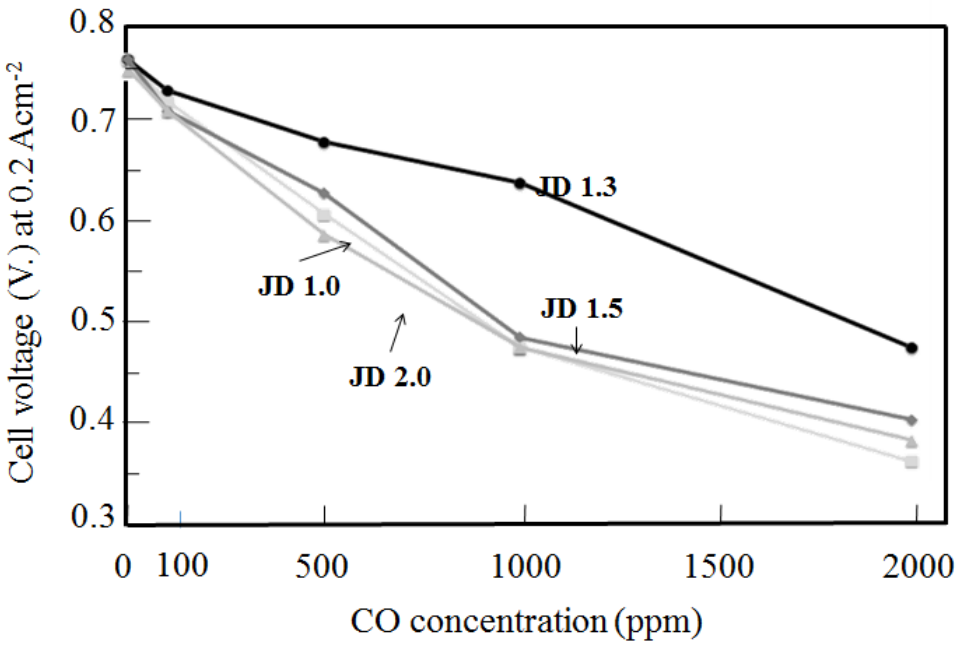

Fig. 3.5 Effect of CO concentration on cell voltage at 0.2 A cm^{-2}. Cell temp.: 70 ^{o}C, electrolyte: Nafion® NRE 212, cathode: Pt/C (0.5 mg-Pt cm^{-2}), O_2 humidified at 68 ^{o}C, flow rate: 80 mL min^{-1}, anode: JDx (0.5 mg-PtRu cm^{-2}), H_2 containing 0 ppm, 100 ppm, 500 ppm, and 2,000 ppm CO humidified at 70 ^{o}C, flow rate: 80 mL min^{-1}.

In order to make a detailed comparison, only four catalysts (E1.3, E1.5, JD1.3 and JD1.5) were focused and compared with the commercial catalyst as shown in Fig. 3.6. It can be seen that JD1.3 exhibited the highest CO tolerance. This result suggests that different carbon supports can assist the addition of Ru for improvement of Pt catalysts differently, and if the carbon support can provide good assistance, a PtRu/C catalyst can maintain its CO-tolerant ability even at high levels of CO concentrations. It is well known that the best Ru:Pt molar ratio for CO tolerant PtRu anode catalyst is 1.5.[25] However, from the results in this work, it can be concluded that an Ru:Pt ratio of 1.3, having a smaller amount of Ru, could be used to achieve the same and even higher level of CO tolerance when carbon KB300J or KB600JD was used as a the carbon support.

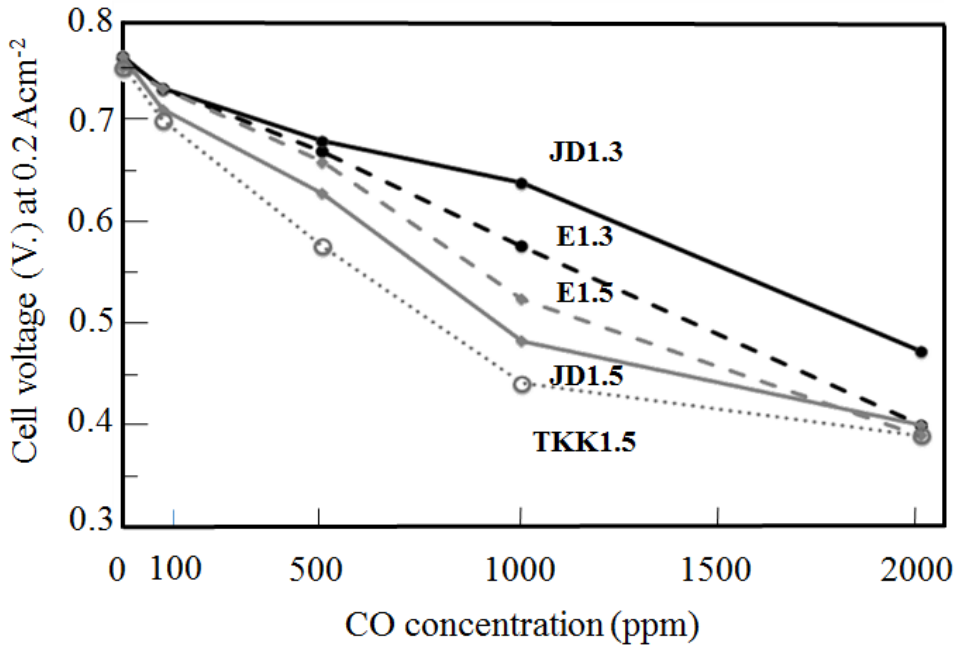

Fig. 3.6 Effect of CO concentration on potential at 0.2 A cm^{-2}. Cell temp.: 70 ^{o}C, electrolyte: Nafion® NRE 212, cathode: Pt/C (0.5 mg-Pt cm^{-2}), O_2 humidified at 68 ^{o}C, flow rate: 80 mL min^{-1}, anode: E1.3, E1.5, JD1.3, JD1.5, and TKK1.5 (0.5 mg-PtRu cm^{-2}), H_2 containing 0 ppm, 100 ppm, 500 ppm, and 2,000 ppm CO humidified at 70 ^{o}C, flow rate: 80 mL min^{-1}.

3.3.5 CO stripping

A CO stripping experiment was performed to determine the relationship between electrooxidation activity of the catalysts and CO tolerance of the catalysts. Fig. 3.7 shows the results of CO stripping measurements of E1.3, E1.5, JD1.3, and JD1.5 catalysts. For all catalysts, the onset position or potential used to start CO oxidation are similar because they all are PtRu alloyed catalysts. From the area of each CO stripping peak, the energy involved in the CO oxidation process was calculated. This energy reflects the amount of adsorbed CO, which reflects the amount of adsorption sites. At higher Ru content, the number of charge coverage (CO adsorption sites) decreased. This should be due to the fact that Ru (non-alloyed) atoms covered some of the Pt adsorption sites.

It can be seen that not only the degree of alloying but also the charge coverage has a significant impact on CO tolerance. JD1.3, which had the highest CO tolerance

catalyst, had an alloying degree lower than those of the E catalysts but had the largest charge coverage. The E1.3 catalyst, the second-best CO-tolerant catalyst in this work, has both a high alloying degree and large charge coverage. The E1.5 catalyst had a slightly lower charge coverage than that of JD1.5. However, its alloying degree was much higher than that of JD1.5. This could sufficiently enhance the CO tolerance of E1.5 to overcome that of JD1.5. In case of the support with lower surface area, the KB 300J carbon, it is thought that Ru can easily reach Pt particles, resulting in the formation of PtRu particles with high alloying degrees. However, the sizes of PtRu particles will be large due to the ease in sintering, which causes a decrease in charge coverage. This should be the reason why the alloying degrees of E1.3 and E1.5 were higher than those of JD1.3 and JD1.5. On the other hand, a larger surface area of the carbon support provides more space for the formation of smaller PtRu particles as shown by XRD results and TEM images. Their alloying degrees are, however, lower because of difficult accessibility of Ru to Pt molecules and the size limit of the small PtRu particles.

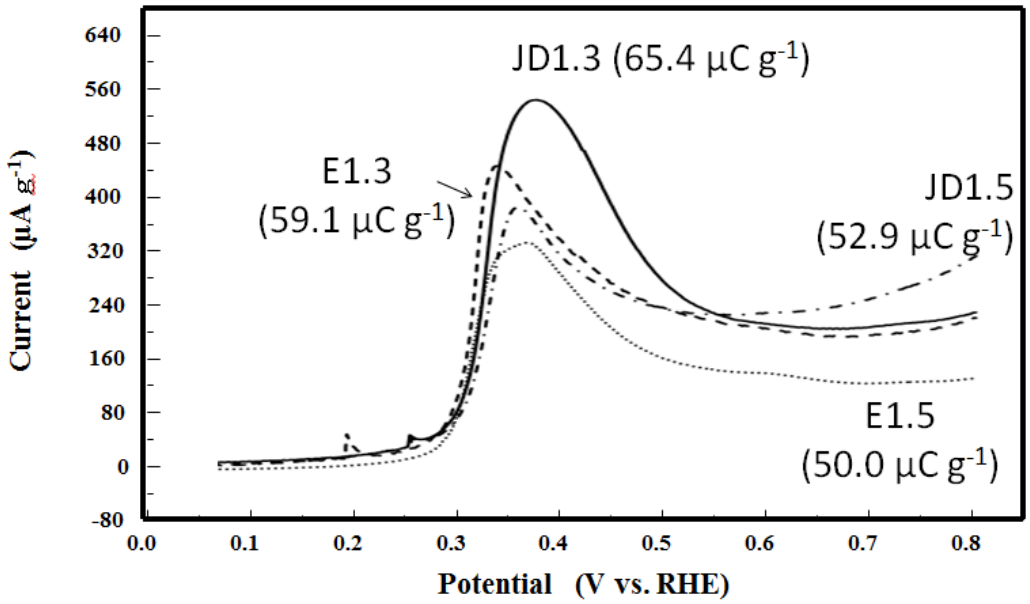

Fig. 3.7 CO stripping results for E1.3, E1.5, JD1.3 and JD1.5 catalysts recorded during potential cycling with 10 mV s^{-1} from 0.05 V to 1.2 V vs RHE in 75 mL of 0.1 M $HClO_4$ at 25 ^{o}C. Prior to the measurement, $HClO_4$ solution was cleaned by Ar gas flow for 15 min and then CV measurement between the above-mentioned potentials was performed for 10 cycles with a scan speed of 50 mV s^{-1}. Then CO gas was introduced into the system for 10 min to let CO adsorb on the catalysts and then the solution was purged with Ar gas for 15 min. The potential during CO adsorption and Ar purging was kept constant at 0.1 V vs RHE. In all cases the gas flow rates were 200 mL min^{-1}.

In the CO tolerance mechanism, Ru-Pt bonding contributes to CO oxidation, but Ru-Ru bonding does not. Therefore, the Ru atomic fraction in PtRu was used together with the charge coverage to estimate CO tolerance property. A new parameter called the "Ru-Pt surface relative bonding ratio" was obtain by multiplying the Ru atomic fraction in PtRu by charge coverage, and the results of calculation are shown in Table 3.4. It can be seen that the Ru-Pt surface relative bonding ratio (JD1.3 > E1.3 > E1.5 > JD1.5 > TKK1.5) agree well with the sequence of the cell voltage at 1,000 ppm CO.

Table 3.4 Ru-Pt surface relative bonding ratios of the prepared PtRu/C E1.3, E1.5, JD1.3, JD1.5, and TKK1.5 catalysts obtained from the Ru atomic fraction in PtRu and charge coverage.

Catalyst	Ru atomic fraction in PtRu (-)	Charge coverage ($\mu C\ g_{PtRu}^{-1}$)	Surface relative ratio of PtRu bonding ($\mu C\ g_{PtRu}^{-1}$)	Cell voltage at 1,000 ppm CO contamination (V)
E1.3	0.509	59.1	30.1	0.57
E1.5	0.549	50.0	27.5	0.52
JD1.3	0.469	65.4	30.7	0.63
JD1.5	0.444	52.9	23.5	0.48
TKK1.5	0.500	45.1	22.5	0.44

3.4 Conclusion

By using different nominal Ru:Pt molar ratios and carbon supports with different BET surface areas, we prepared PtRu/C anode catalysts with various degrees of alloying. In case of KB300J (E series), a support with a relatively small surface area, was employed, Ru could easily mix and form a good alloy with Pt and consequently the Ru atomic fraction and alloying degree were high. Not only the alloying degree but also the charge coverage was found to be a key factor. The catalysts prepared using KB600JD (JD series), which had a larger surface area, had smaller PtRu nanoparticles and thus a larger number of CO oxidation active sites, which led to enhancement of CO tolerance. Ru-Pt bonding does contribute to CO oxidation, but Ru-Ru bonding does not, suggesting that the Ru atomic fraction in PtRu is a major factor together with charge coverage contributing to the improvement of CO tolerance. A new parameter, Ru-Pt surface relative bonding ratio, was obtained by multiplying the Ru atomic fraction in PtRu by the charge coverage, and it was found to agree well with the CO tolerance of PtRu catalysts. This parameter could be optimized by a proper selection of the carbon support.

References

1. Liu, H.; Song, C.; Zhang, L.; Zhang, J.; Wang, H.; Wilkinson, D. P. A Review of Anode Catalysis in the Direct Methanol Fuel Cell. *J. Power Sources* **2006**, *155*, 95-110.
2. Cheng, X.; Shi, Z.; Glass, N.; Zhang, L.; Zhang, J.; Song, D.; Liu, Z.-S.; Wang, H.; Shen, J. A Review of PEM Hydrogen Fuel Cell Contamination: Impacts, Mechanisms, and Mitigation. *J. Power Sources* **2007**, *165*, 739-756.
3. Ehteshami, S. M. M.; Chan, S. H. A Review of Electrocatalysts with Enhanced CO Tolerance and Stability for Polymer Electrolyte Membarane Fuel Cells. *Electrochim. Acta* **2013**, *93*, 334-345.
4. Liu, Z.; Reed, D.; Kwon, G.; Shamsuzzoha, M.; Nikles, D. E. Pt_3Sn Nanoparticles with Controlled Size: High-Temperature Synthesis and Room-Temperature Catalytic Activation for Electrochemical Methanol Oxidation. *J. Phys. Chem. C* **2007**, *111*, 14223-14229.
5. Scott, F. J.; Roth, C.; Ramaker, D. E. Kinetics of CO Poisoning in Simulated Reformate and Effect of Ru Island Morphology on PtRu Fuel Cell Catalysts as Determined by Operando X-Ray Absorption near Edge Spectroscopy. *J. Phys. Chem. C* **2007**, *111*, 11403-11413.
6. Mukerjee, S.; Urian, R. C.; Lee, S. J.; Ticianelli, E. A.; McBreen, J. Electrocatalysis of CO Tolerance by Carbon-Supported PtMo Electrocatalysts in PEMFCs. *J. Electrochem. Soc.* **2004**, *151*, A1094-A1103.
7. Ioroi, T.; Akita, T.; Yamazaki, S.-i.; Siroma, Z.; Fujiwara, N.; Yasuda, K. Comparative Study of Carbon-Supported Pt/Mo-Oxide and PtRu for Use as CO-Tolerant Anode Catalysts. *Electrochim. Acta* **2006**, *52*, 491-498.
8. Watanabe, M.; Uchida, M.; Motoo, S. Preparation of Highly Dispersed Pt + Ru Alloy Clusters and the Activity for the Electrooxidation of Methanol. *J. Electroanal. Chem. Interfacial Electrochem.* **1987**, *229*, 395-406.
9. Lee, S. J.; Mukerjee, S.; Ticianelli, E. A.; McBreen, J. Electrocatalysis of CO Tolerance in Hydrogen Oxidation Reaction in PEM Fuel Cells. *Electrochim. Acta* **1999**, *44*, 3283-3293.
10. Giorgi, L.; Pozio, A.; Bracchini, C.; Giorgi, R.; Turtù, S. H_2 and $H/_2CO$ Oxidation Mechanism on Pt/C, Ru/C and PtRu/C Electrocatalysts. *J. Appl. Electrochem.* **2001**, *31*, 325-334.
11. Maillard, F.; Bonnefont, A.; Chatenet, M.; Guétaz, L.; Doisneau-Cottignies, B.; Roussel, H.; Stimming, U. Effect of the Structure of PtRu/C Particles on CO_{ad}

Monolayer Vibrational Properties and Electrooxidation Kinetics. *Electrochim. Acta* **2007**, *53*, 811-822.

12. Kaiser, J.; Colmenares, L.; Jusys, Z.; Mörtel, R.; Bönnemann, H.; Köhl, G.; Modrow, H.; Hormes, J.; Behm, R. J. On the Role of Reactant Transport and (Surface) Alloy Formation for the CO Tolerance of Carbon Supported PtRu Polymer Electrolyte Fuel Cell Catalysts. *Fuel Cells* **2006**, *6*, 190-202.
13. Watanabe, M.; Motoo, S. Electrocatalysis by Ad-Atom: Part III. Enhancement of Oxidation of Carbon-Monoxide on Platinum by Ruthenium Ad-Atoms. *J. Electroanal. Chem.* **1975**, *60*, 275-283.
14. Frelink, T.; Visscher, W.; van Veen, J. A. R. On the Role of Ru and Sn as Promotors of Methanol Electro-Oxidation over Pt. *Surf. Sci.* **1995**, *335*, 353-360.
15. Adams, R. D.; Barnard, T. S. Does a Metal to Metal "Ligand" Effect Influence the Catalytic Activity of Bimetallic Cluster Complexes? Synthesis and Catalytic Activity of $Pt_3Ru_6(CO)_{19}(SMe_2)(\mu_3\text{-}PhC_2Ph)(\mu_3\text{-}H)(\mu\text{-}H)$. *Organometallics* **1998**, *17*, 2885-2890.
16. Balk, R. W.; Stufkens, D. J.; Oskam, A. Characterization of Metal-to-ligand Charge-transfer and Intraligand Transitions of fac-$[Re(CO)_3L(X)]$ Complexes [L = di-imine; X = Halide or $Mn(CO)_5$] and Explanation of the Photochemistry of $[Re(CO)_3L\{Mn(CO)_5\}]$ Using the Resonance Raman Effect. *J. Chem. Soc., Dalton Trans.* **1981**, 1124-1133.
17. Koper, M. T. M.; Shubina, T. E.; van Santen, R. A. Periodic Density Functional Study of CO and OH Adsorption on Pt-Ru Alloy Surfaces: Implications for CO Tolerant Fuel Cell Catalysts. *J. Phys. Chem. B* **2002**, *106*, 686-692.
18. Takeguchi, T.; Yamanaka, T.; Asakura, K.; Muhamad, E. N.; Uosaki, K.; Ueda, W. Evidence of Nonelectrochemical Shift Reaction on a CO Tolerant High-Entropy State PtRu Anode Catalyst for Reliable and Efficient Residential Fuel Cell Systems. *J. Am. Chem. Soc.* **2012**, *134*, 14508-14512.
19. Yamanaka, T.; Takeguchi, T.; Wang, G.; Muhamad, E. N.; Ueda, W. Particle Size Dependence of CO Tolerance of Anode PtRu Catalysts for Polymer Electrolyte Fuel Cells. *J. Power Sources* **2010**, *195*, 6398-6404.
20. Ketjenblack Highly Electro-Conductive Carbon Black , Lion Specialty Chemicals Co., Ltd. https://www.lion-specialty-chem.co.jp/en/product/carbon/carbon01.htm. (March, 31, 2015)
21. Narischat, N.; Takeguchi, T.; Tsuchiya, T.; Mori, T.; Ogino, I.; Mukai, S. R.; Ueda, W. Effect of Activation Degree of Resorcinol-Formaldehyde Carbon Gels on Carbon Monoxide Tolerance of Platinum-Ruthenium Polymer Electrolyte Fuel Cell

Anode Catalyst. *J. Phys. Chem. C* **2014**, *118*, 23003-23010.
22. Yamanaka, T.; Takeguchi, T.; Wang, G. X.; Muhamad, E. N.; Ueda, W. Particle Size Dependence of CO Tolerance of Anode PtRu Catalysts for Polymer Electrolyte Fuel Cells. *J. Power Sources* **2010**, *195*, 6398-6404.
23. Antolini, E.; Cardellini, F. Formation of Carbon Supported PtRu Alloys: An XRD Analysis. *J. Alloys Compd.* **2001**, *315*, 118-122.
24. Radmilovic, V.; Gasteiger, H. A.; Ross, P. N., Structure and Chemical Composition of a Supported Pt-Ru Electrocatalyst for Methanol Oxidation. *J. Catal.* **1995**, *154*, 98-106.
25. Okaya, K.; Yano, H.; Uchida, H.; Watanabe, M. Control of Particle Size of Pt and Pt Alloy Electrocatalysts Supported on Carbon Black by the Nanocapsule Method. *ACS Appl. Mater. Interfaces* **2010**, *2*, 888-895.

Chapter 4

Effect of the Mesopores of Carbon Supports on the CO Tolerance of Pt_2Ru_3 PEFC Anode Catalysts

4.1 Introduction

As mentioned in the previous chapter, Pt-Ru alloy can enhance the CO tolerance of Pt-Ru catalysts presumably by the bifuctional mechanism[1] and/or ligand effect.[2] Moreover, results from chapters 2 and 3 reveal that carbon support plays a major role in enhancing CO tolerance of PtRu anode catalysts. Many studies report that the CO acceptant limit is lower than 100 ppm[3-6] while in chapter 2, we reported that the cell voltage drop at 1,000 ppm CO contamination for Pt_2Ru_3/RC1000ac58 catalyst was less than 10 %. Although the effect of the support remains unclear, many studies have been focusing on its porous structure. The effects of porous structure of many carbon supports on cell voltage have been investigated and the porous structure of the support found to significantly affect the efficiency of the electrocatalyst and their CO tolerance.[7-14]

In order to understand the effect of porous structure, the pore adjustable carbon is necessary. The resorcinol-formaldehyde carbon gels (RFC) is the one of the most interesting materials to be used as a support. Their surface area, pore diameter, and structure are tunable by varying synthesis condition. Two simple ways to control the porous structure of RFCs are to adjust the ratio of resorcinol to catalyst (R/C) of its starting solution and to adjust its activation degree (as in chapter 2). In addition, there are some studies using RFC as a support for electrode catalysts of cathodes[15, 16] as well as anodes.[17] The effect of activation degree has already been reported.[18]

To synthesize RFC, first resorcinol and formaldehyde are polymerized using a base catalyst. The main reaction is a condensation reaction which leads to the formation of compounds that have methylene and methylene ether bridge. Such oligomers form clusters that agglomerate to colloidal particles. These particles coagulate and form a wet gel (hydrogel). Next the hydrogel is dried so that the solvent trapped in its structure is removed. Then the dried gel is heat-treated in an inert atmosphere and is transformed to carbon. Generally a higher carbonization temperature leads to a lower pore volume of the resulting carbon. Finally the carbon is activated by gases such as steam or CO_2 to increase its pore volume, pore size and surface area.[19-22] By changing the R/C molar ratio in the starting solution used for RFC synthesis, the microstructure of the final

carbons can be varied.[21, 23] A lower R/C ratio results in small polymer particles (3-5 nm) which have a higher density. Polymeric RF gels, formed by small-sized polymer particles, generally have a high surface area and high compressive modulus. However, the gels tend to shrink when dried. Whereas RF gels synthesized at high R/C ratios, which are formed by large polymer particles (16-200 nm) and have low surface area and low compressive modulus, are hardly shrink when dried.

In this study, we focused on porous structure and investigated the effect of R/C ratio of the starting solution on electrochemical performance of the resulting catalysts. As the R/C ratio hardly affects the surface area of the resulting RFC, the direct effect of pore structure on electrochemical property could be clarified.

4.2 Experimental

4.2.1 Resorcinol-formaldehyde carbon gel (RFC) preparation

A resorcinol-formaldehyde (RF) solution was prepared from resorcinol (R), formaldehyde (F), sodium carbonate (C), and distilled water (W). The molar ratios of resorcinol to formaldehyde (R/F) and the mass-to-volume ratio of resorcinol to water (R/W) were fixed to 0.5 mol/mol and 0.5 g/mL, respectively. The molar ratios of resorcinol to catalyst (R/C) were varied as 200, 800, and 1000. The prepared RF solutions were first aged and were transformed to hydrogels at room temperature. After that, RF hydrogels were aged at 60 °C for another 3 days. The water in the hydrogels was then exchanged to t-butanol by immersing the hydrogels in containers including this alcohol and placing the containers in a shaking water bath kept at 50 °C for 3 days. The t-butanol in the containers was replaced every day. Then, RF hydrogels were dried at 120 °C for 3 days before being carbonized. Carbonization was conducted in a 100 cm^3min^{-1} (ccm) flow of nitrogen gas. Samples were heated up from 25 °C to 250 °C within 1 h, and were maintained at this temperature for 2 h. The temperature was then increased to 1,000 °C at a ramp rate of 250 °C h^{-1} and then the temperature was maintained at 1,000 °C for 4 h. Activation was carried out under 20 ccm CO_2 and 100 ccm N_2 flow at 1,000 °C. Activation degree (or burn off ratio) was calculated as follows:

activation degree = weight loss after activation*100/weight before activation (4.1)

RFC samples RC200ac58, RC800ac62 and RC1000ac58 were prepared. The number following RC (200, 800, and 1,000) indicates the R/C ratio at which the samples were prepared, and that following ac (58 and 62) indicates the activation degree.

4.2.2 Preparation of Pt_2Ru_3 anode catalysts

Firstly, Pt/RC1000ac58 (40 wt% Pt/C) was prepared by mixing RC1000ac58 with $Pt(NH_3)_2(NO_2)_2$ (4.554 wt% Pt, Tanaka Kikinzoku Kogyo K.K.), and distilled water in a three-neck flask and stirring vigorously at room temperature (20 °C) for 1 h. Pt was then reduced by ethanol and kept at 95 °C overnight. After that, the catalyst was filtered and washed with distilled water, followed by drying in air at 80 °C for 10 h. Secondly, $RuCl_3 \cdot nH_2O$ (99.9 %, Wako) was dissolved in distilled water and RC1000ac58 supporting Pt was added. The Pt:Ru molar ratio of was adjusted to 2:3. The mixture was kept at room temperature for 1 h. Then the Ru in the catalyst was reduced by keeping the catalyst overnight in methanol maintained at 70 °C. After that, the obtained catalyst was, again, filtered and washed with distilled water. Then the catalyst was dried in N_2 at 80 °C for 10 h. At last, the catalyst was reduced in a H_2/Ar (H_2 5 %) flow at room temperature for 1 h, followed by rapid heating to 880 °C within 12 min in He. The oven was turned off once the temperature reached 880 °C in order to allow the catalyst to cool down immediately. The catalyst was heated again at 150 °C for 2 h in a H_2/Ar (H_2 5 %) flow. Other samples (i.e., Pt_2Ru_3/RC200ac58 and Pt_2Ru_3/RC800ac62) were prepared by the same method. Commercial catalyst, Pt_2Ru_3/TKK TEC61E54 (Pt 29.6 %, Ru 23.0 %, Tanaka Kikinzoku Kogyo K.K.), was used as a reference.

4.2.3 Physical characterization

Nitrogen adsorption isotherms of all of the samples were measured at -196.15 °C using an adsorption apparatus (BELSORP-mini II surface area and pore size analyzer, BEL Japan). Specific surface area was calculated from BET plots. Pore size distributions and mesopore volumes were calculated using the Dollimore-Heal (DH) method[24]. Here mesopores are defined as pores with a diameter between 2 nm and 50 nm. XRD patterns of PtRu metal crystallites within the catalyst were obtained by a X-ray diffractometer (XRD; RIGAKU, RINT 2000). The tube current used for Cu Kα radiation was 40 mA and the tube voltage was 40 kV. The angular region of the 2θ scan was set between 10 ° and 85 °, and the scan rate was 1 ° min^{-1}. The crystallite sizes were evaluated from the Scherrer equation using the peak of the (220) reflection of Pt fcc structure. Catalyst structure was investigated by using

a Hitachi HD-2000 scanning transmission electron microscope (STEM) instrument with electron energy of 200 kV and a beam current of 30 μA.

4.2.4 MEA preparation

In the membrane electrode assembly (MEA) preparation process, carbon paper (P50T) was used as the backing layers of the anode and the cathode. Anode catalyst inks were prepared by dispersing PtRu/RFCs catalysts in distilled water and ethanol mixed with Nafion® solution (5 wt% dispersion, Aldrich). Cathode catalyst ink was prepared by dissolving commercial Pt/C (46 wt%, TKK TEC10E50) in distilled water and ethanol including Nafion®. In both electrodes, the catalyst ink was painted to achieve a metal loading of 0.5 mg cm^{-2} followed by a coating of 0.5 mg cm^{-2} Nafion®. Finally, the anode and cathode (22 mm × 22 mm) were placed onto the two sides of a Nafion® NRE-212 membrane (Aldrich) and hot-pressed at 135 °C and 10 MPa for 20 min to form the MEA.

4.2.5 Single cell performance testing and CO tolerance experiment

The MEA was assembled into a single cell (FC05-01SP, ElectroChem, Inc.) having flow field plates made of graphite and end plates made of copper. The end plates of the cell were attached to a heater. The single cell was connected to a fuel cell test apparatus (Chino Corp.). Pure H_2 (or H_2/CO mixture) and O_2 were supplied at flow rates of 80 mL min^{-1} to the anode and cathode, respectively, at ambient pressure. During measurements, the anode and cathode humidifiers were set at 70 °C and 68 °C, respectively, and the single cell was maintained at 70 °C.

CO tolerance experiments were performed under the same conditions as single cell performance tests. The current density was set to 0.2 A cm^{-2}. First, pure H_2 was fed to the cell for 1 h and then 100 ppm of CO was mixed to H_2. The concentration of CO was increased every 2 h to 500 ppm, 1,000 ppm, and finally 2,000 ppm.

4.3 Results and discussion

4.3.1 Characterization of textural properties of synthesized carbon gels and supported Pt_2Ru_3 catalysts

Nitrogen gas adsorption data are summarized in Table 4.1. The synthesized RFC samples have similar BET surface areas ranging from 2,140 m^2 g^{-1} to 2,490 m^2 g^{-1}, larger than the commercial catalyst (823 m^2 g^{-1}). Although the activation degree and the surface area of the samples are similar, the pore size distribution derived using

the DH method differed significantly. RC800 had the largest mesopore volume among the prepared carbon supports.

Table 4.1 Physical properties of carbon supports and crystallite sizes of PtRu alloy.

RFC	Surface area of carbon gel support ($m^2 g^{-1}$)	Volume of mesopore of carbon gel support ($cm^3 g^{-1}$)	Crystallite size of alloy (nm) (As-synthesized catalyst)
RC200Ac58	2180	0.76	2.7
RC800Ac62	2470	2.29	1.9
RC1000Ac58	2140	2.08	2.3
Commercial catalyst	820	N/A	3.4

4.3.2 XRD and STEM characterization of supported Pt_2Ru_3 catalysts

Fig. 4.1 shows the XRD (X-ray diffractometer) patterns of Pt_2Ru_3/RFC catalysts with various R/C ratios ranging from 200 to 1,000 and the commercial Pt_2Ru_3 catalyst. Diffraction peaks corresponding to the (220) plane were used to calculate PtRu crystallite sizes because there was no interference of peaks arising from the structure of carbon. The pattern of a reference platinum metal shows a peak at 2Θ equaled to 67.5 º that is ascribed to the (220) plane of the face-centered cubic (fcc) crystal structure of the Pt metal. In contrast, the data for Pt_2Ru_3/RFC catalysts and the commercial catalyst how peaks at 69.2 º Thus, the results indicate all of the samples have a similar degree of alloying of Pt with Ru. The PtRu crystallite size was calculated by using the Scherrer equation (Table 4.1). The commercial catalyst has an average PtRu crystallite size of 3.4 nm. The average PtRu crystallite sizes of the synthesized Pt_2Ru_3/RFC samples are slightly smaller than that of the commercial catalyst.

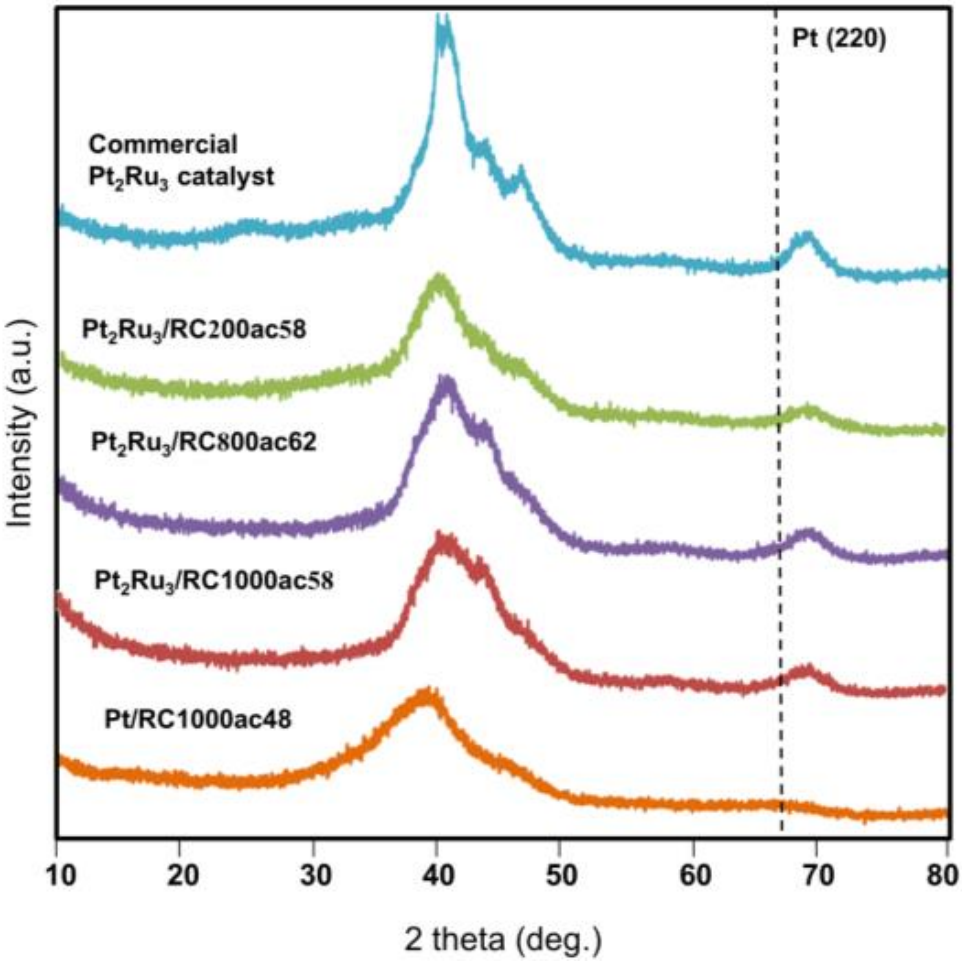

Fig. 4.1 XRD patterns of commercial Pt_2Ru_3 catalyst and prepared catalysts.

Fig. 4.2 shows STEM images of commercial and prepared catalysts. The average PtRu particle size of Pt_2Ru_3/RC200ac58 (Fig. 4.2 (B)) is larger than that of the commercial catalyst (Fig. 4.2 (A)) and larger than the crystallite size calculated from XRD data. On the other hand, the average PtRu particle size of Pt_2Ru_3/RC800ac62 (Fig. 4.2 (C)) and Pt_2Ru_3/RC1000ac58 (Fig. 4.2 (E)) are not much different from that of the commercial catalyst.

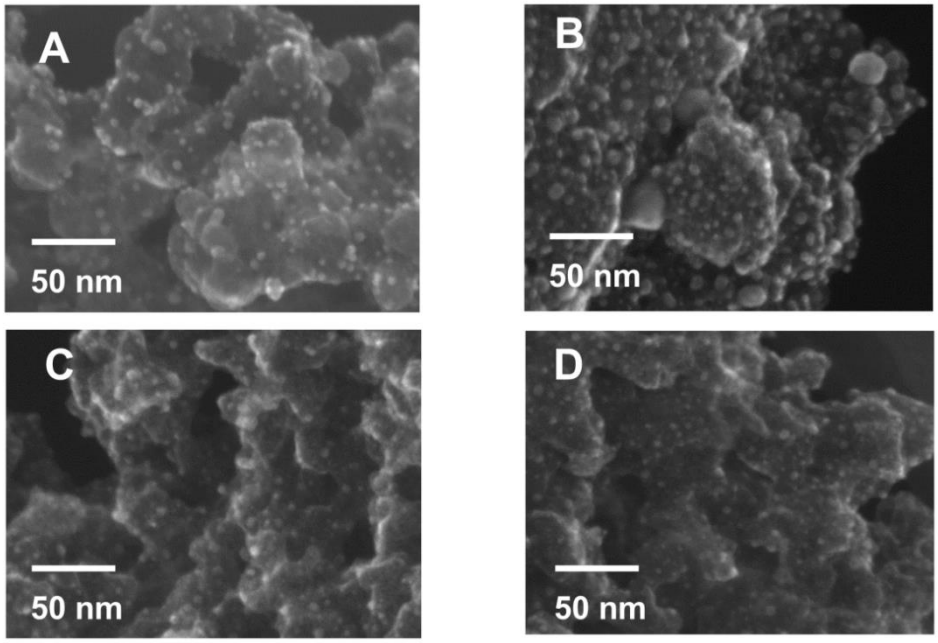

Fig. 4.2 STEM images: (A) commercial Pt_2Ru_3/C, (B) Pt_2Ru_3/RC200ac58, (C) Pt_2Ru_3/RC800ac62, and (D) Pt_2Ru_3/RC1000ac58.

4.3.3 Single cell test and CO tolerance

Fig. 4.3 shows the performance of commercial and prepared catalysts. All catalysts were prepared under the same conditions except for the R/C ratios the carbon support of them were prepared, and the metal loading on the anode for MEA was fixed to 0.5 mg cm^{-2}.

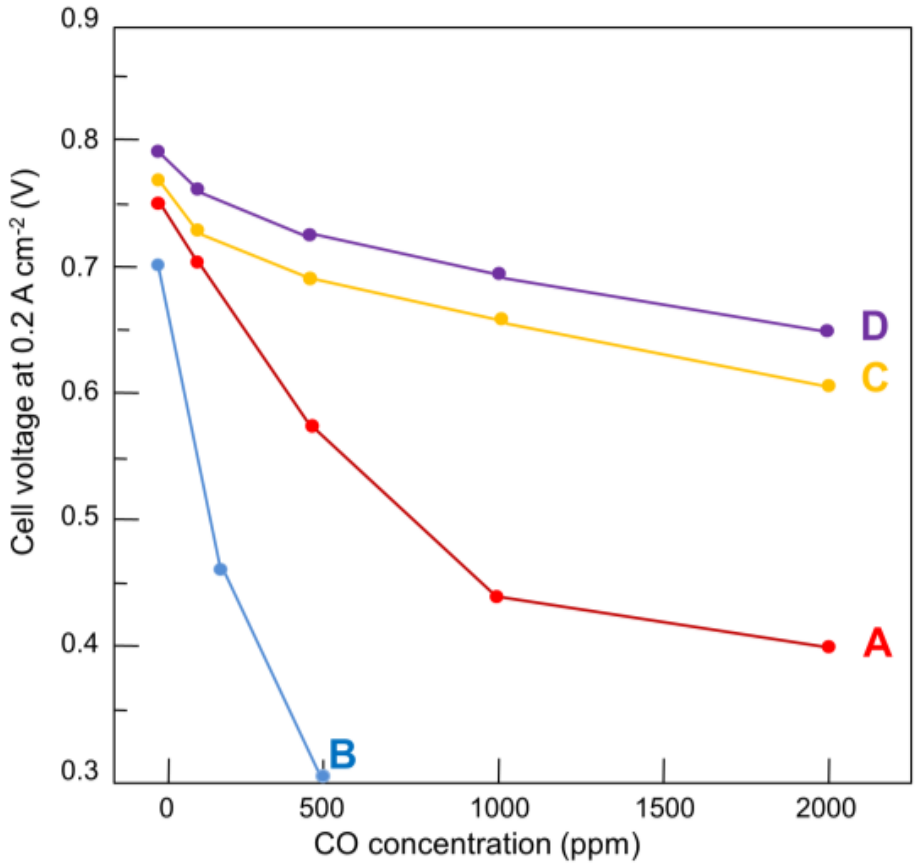

Fig. 4.3 Effect of CO concentration on cell voltage at 0.2 A cm^{-2}. Cell temp.: 70 ^{o}C; electrolyte: Nafion® NRE 212; cathode: Pt/C (0.5 mg cm^{-2}); O_2 humidified at 68 ^{o}C; flow rate: 80 mL/min; anode: Pt_2Ru_3/C (0.5 mg-PtRu cm^{-2}); H_2 containing 0 ppm, 100 ppm, 500 ppm, and 2,000 ppm CO humidified at 70 ^{o}C; flow rate: 80 mL/min.: (A) Pt_2Ru_3/C commercial catalyst, (B) Pt_2Ru_3/RC200ac58, (C) Pt_2Ru_3/RC800ac58, and (D) Pt_2Ru_3/RC1000ac58.

First, pure H_2 is fed to the anode side at 80 mL/min, and the current density was set to 0.2 A cm^{-2}. After feeding pure H_2 for 1 h, the cell using Pt_2Ru_3/RC1000ac58 generated the highest voltage of 0.787 V. The order of the cell voltage is as follows:

0.787 V (Pt_2Ru_3/RC1000ac58) > 0.775 V (Pt_2Ru_3/RC800ac62) > 0.748 V (commercial catalyst) > 0.666 V (Pt_2Ru_3/RC200ac58)

The cell using Pt_2Ru_3/RC200ac58 generated the lowest cell voltage among the catalysts tested. Then, 100 ppm CO was mixed with the H_2 flow. The cell voltage of Pt_2Ru_3/RC1000ac58 slightly decreased by 4 %, from 0.787 V to 0.758 V, after 2 h.

The cell voltage of Pt_2Ru_3/RC800ac62 also slightly decreased by 8 %, from 0.775 V to 0.721 V, after 2 h. The cell voltages of the commercial Pt_2Ru_3 catalyst and Pt_2Ru_3/RC200ac58 were, respectively, 0.719 V and 0.287 V in the presence of 100 ppm CO.

The cell voltage of the commercial catalyst significantly decreased when the CO concentration was increased to 500 ppm. Constant current density was kept at 0.2 A cm^{-2} with feeding H_2 contaminated with 500 ppm CO for 2 h. The voltage decreased by 24 % from 0.748 V in pure H_2 to 0.567 V. Interestingly, the cell voltages of Pt_2Ru_3/RC1000ac58 and Pt_2Ru_3/RC800ac62 slightly decreased by 8 % and 11 %, respectively, to 0.726 V and 0.721 V. On the other hand, the cell voltage of Pt_2Ru_3/RC200ac58 drastically decreased.

Finally, H_2 contaminated with 2,000 ppm CO was fed. The cell using Pt_2Ru_3/RC1000ac58 showed the highest CO tolerance; the cell voltage decreased by 16 %, from 0.787 V in pure H_2 to 0.655 V. The cell voltage of Pt_2Ru_3/RC800ac62 decreased from by 21 %, 0.775 V to 0.615 V, while the cell voltage for the commercial catalyst significantly decreases by 47.3 % from 0.748 V to 0.394 V.

The cell voltages of Pt_2Ru_3/RC1000ac58 and Pt_2Ru_3/RC800ac62 catalysts are higher than that of the commercial catalyst at all levels of CO contamination. Especially, in the presence of 2000 ppm CO, the voltage of Pt_2Ru_3/RC800ac62 is about 0.22 V higher than that of the commercial catalyst.

4.3.4 Effect of PtRu loading and Nafion® mixing on pore volume.

As the results showed above, there were no significant differences in crystallite size, alloying degree, and surface area among the catalysts, but their CO tolerance was significantly different. In order to explain this difference, the pore volume of the samples at each preparation step (carbon support, after PtRu loading and after mixing with Nafion®) was measured.

As shown in Table 4.2, the mesopore volumes of all RFCs (calculated by DH plot) decreased by 50-60 % after PtRu loading. The volume of mesopores after PtRu loading of commercial Pt_2Ru_3 catalyst (0.77 $cm^3\ g^{-1}$) is larger than that of Pt_2Ru_3/RC200ac58 (0.34 $cm^3\ g^{-1}$). The pore size distribution is shown in Fig. 4.4. All samples were mixed with Nafion®. The mesopore volume of both the commercial Pt_2Ru_3 catalyst and Pt_2Ru_3/RC200ac58 decreased drastically, by 94 % and 68 %, respectively. On the other hand, the mesopore volumes of Pt_2Ru_3/RC800ac62 and Pt_2Ru_3/RC1000ac58 decreased by 49 % and 50 % after mixing with Nafion®, respectively. The mesopore volumes of Pt_2Ru_3/RC800ac62 and Pt_2Ru_3/RC1000ac58 are about 5 times larger than that of

Pt_2Ru_3/RC200ac58 at this stage. Fig. 4.5 shows that Pt_2Ru_3/RC800ac62 and Pt_2Ru_3/RC1000ac58 still have a large volume of mesopores after mixing with Nafion®. By contrast, the mesopore volume of the commercial catalyst after mixing with Nafion® is very low. Pt_2Ru_3/RC200ac58 contains only small mesopores (smaller than 10 nm).

Table 4.2 Mesopore volumes of the catalysts at different synthesis stages.

		Mesopore Volume			
RFC	**Carbon support ($cm^3\ g^{-1}$)**	**After PtRu loading ($cm^3\ g^{-1}$)**	**Decrease (%)**	**After Nafion® mixing ($cm^3\ g^{-1}$)**	**Decrease (%)**
Pt_2Ru_3/RC200ac58	0.76	0.34	55	0.11	68
Pt_2Ru_3/RC800ac62	2.29	0.92	60	0.47	49
Pt_2Ru_3/RC1000ac58	2.08	1.02	51	0.51	50
Commercial Pt_2Ru_3 Catalyst	N/A	0.77	N/A	0.05	94

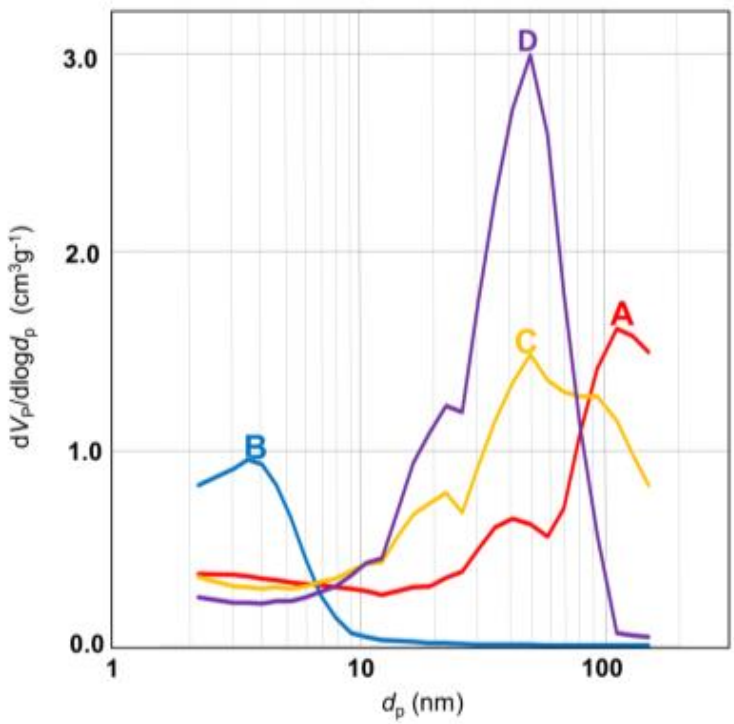

Fig. 4.4 Pore size distribution of all Pt_2Ru_3 catalysts after deposition of PtRu: (A) Pt_2Ru_3/C commercial catalyst, (B) Pt_2Ru_3/RC200ac58, (C) Pt_2Ru_3/RC800ac58, and (D) Pt_2Ru_3/RC1000ac58.

4.3.5 Diffusivity

As explained in the previous section, catalysts on synthesized using carbons with larger mesopore volumes exhibited a higher CO tolerance. It remains elusive why the catalysts having large mesopore volume exhibit a higher CO tolerance. However, because mass transfer within mesopores is generally dictated by Knudsen diffusion, which is proportional to the diameter of mesopores, faster mass transfer of reactants and products may account for it.

Fig. 4.6 shows the effect of mesopore volume on CO tolerance and diffusivity for all samples after Nafion® mixing. The diffusivity shown here is calculated using Knudsen's equation based on the modal size of the meropores of the catalyst after Nafion® mixing. Diffusivity of CO within Pt_2Ru_3/RC1000ac58 and Pt_2Ru_3/RC800ac62 are much higher (D = 0.056 cm^2 s^{-1}) than that within Pt_2Ru_3/RC200ac58 (D = 0.007 cm^2 s^{-1}) and the commercial catalyst (D = 0.014 cm^2 s^{-1}).

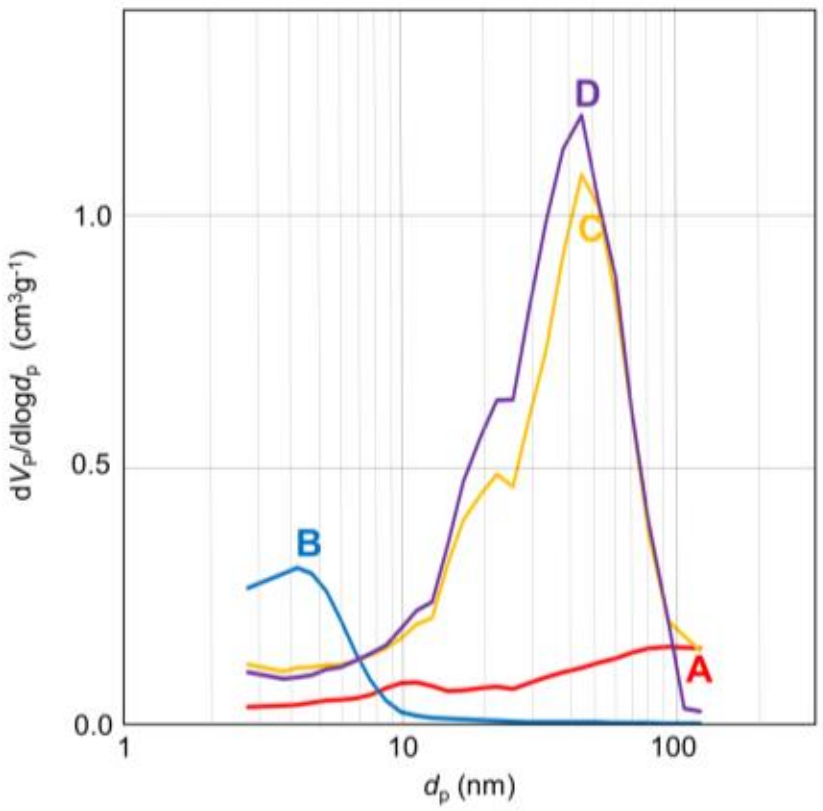

Fig. 4.5 Pore size distribution of all Pt_2Ru_3 catalysts after mixing of Nafion®: (A) Pt_2Ru_3/C commercial catalyst, (B) Pt_2Ru_3/RC200ac58, (C) Pt_2Ru_3/RC800ac58, and (D) Pt_2Ru_3/RC1000ac58.

It is clear that high-CO tolerant Pt_2Ru_3/RC1000ac58 and Pt_2Ru_3/RC800ac62 have larger mesopores. The larger size of mesopores enables faster diffusion of all gases when compared with the mesopores in Pt_2Ru_3/RC200ac58 and the commercial catalyst. The commercial catalyst has a bimodal pore distribution, meaning it has two representative diffusion parameters, but we will focus only on that of its mesopores since macropores are not related to the diffusion near the active sites. Consider the water gas shift reaction (WGSR);

$$CO + H_2O \quad \leftrightarrow \quad CO_2 + H_2 \tag{4.2}$$

By nature of exothermic reactions, the WGSR equilibrium largely shifts to the right side at low temperature of 70 °C. Moreover, the modal size and volume of mesopores of Pt_2Ru_3/RC1000ac58 and Pt_2Ru_3/RC800ac62 are much larger than those of others, resulting in a higher diffusivity of CO. Therefore, rate of water-gas shift reaction was enhanced. Since CO was effectively oxidized by this reaction, HOR progressed effectively even in the presence of high-concentration CO.

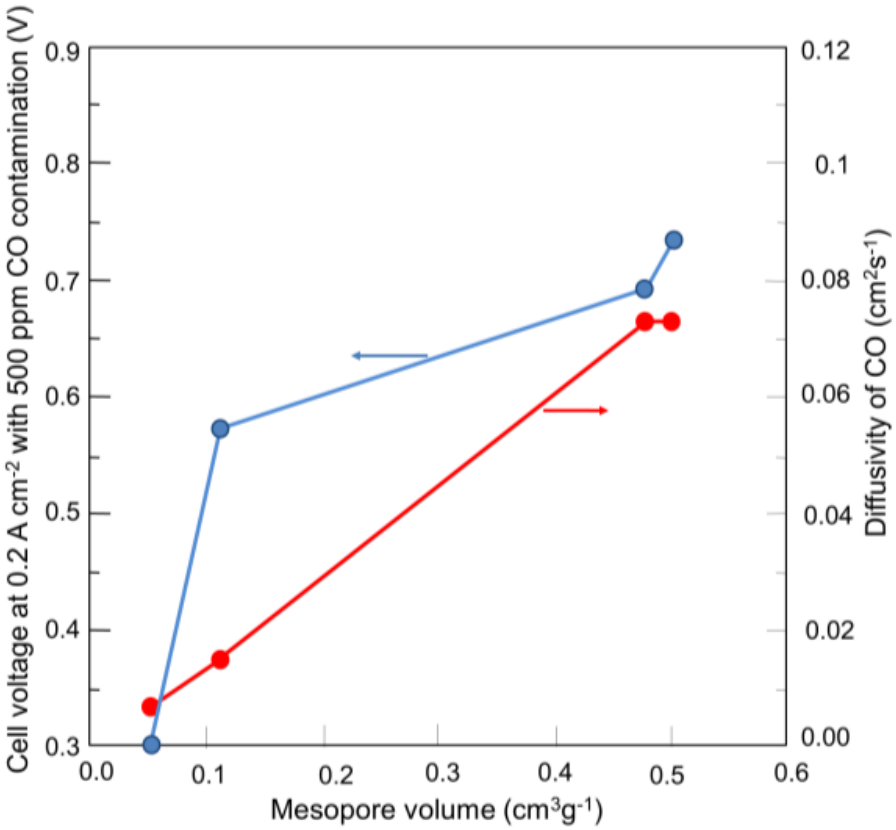

Fig. 4.6 Relation between R/C ratio and diffusivity of CO after mixing of Nafion®.

4.4 Conclusion

Pt_2Ru_3 anode catalysts were prepared using RFCs prepared at various R/C ratios (i.e., 200, 800 and 1,000). The prepared catalysts have similar physical properties such as alloying degree, PtRu size and BET surface area, but the catalysts exhibited significantly different CO tolerances. In addition, the catalysts, which have large volumes of mesopores with modal size as large as 50 nm after Nafion® mixing, exhibited higher CO tolerance, suggesting the importance of these mesopores for CO tolerance. Effective CO removal due to the high diffusivity in large mesopores enhances the CO tolerance of the MEA.

References

1. Watanabe, M.; Motoo, S. Electrocatalysis by Ad-Atoms: Part III. Enhancement of Oxidation of the Carbon Monoxide on Platinum by Ruthenium Ad-Atoms. *J. Electroanal. Chem.* **1975**, *60*, 275-283.
2. Scott, F. J.; Mukerjee, S.; Ramaker, D. E. Contrast in Metal-Ligand Effects on Pt_nM Electrocatalysts with M Equal Ru Vs Mo and Sn as Exhibited by in Situ XANES and EXAFS Measurements in Methanol. *J. Phys. Chem. C* **2010**, *114*, 442-453.
3. Amphlett, J. C.; Mann, R. F.; Peppley, B. A. On Board Hydrogen Purification for Steam Reformation/PEM Fuel Cell Vehicle Power Plants. *Int. J. Hydrogen Energy* **1996**, *21*, 673-678.
4. Starz, K. A.; Auer, E.; Lehmann, T.; Zuber, R. Characteristics of Platinum-Based Electrocatalysts for Mobile PEMFC Applications. *J. Power Sources* **1999**, *84*, 167-172.
5. Lopes, P.; Freitas, K.; Ticianelli, E. CO Tolerance of PEMFC Anodes: Mechanisms and Electrode Designs. *Electrocatalysis* **2010**, *1*, 200-212.
6. Igarashi, H.; Fujino, T.; Watanabe, M. Hydrogen Electro-Oxidation on Platinum Catalysts in the Presence of Trace Carbon Monoxide. *J. Electroanal. Chem.* **1995**, *391*, 119-123.
7. Cui, X.; Guo, L.; Cui, F.; He, Q.; Shi, J. Electrocatalytic Activity and CO Tolerance Properties of Mesostructured Pt/WO_3 Composite as an Anode Catalyst for PEMFCs. *J. Phys. Chem. C* **2009**, *113*, 4134-4138.

8. Han, J.-H.; Lee, E.; Park, S.; Chang, R.; Chung, T. D. Effect of Nanoporous Structure on Enhanced Electrochemical Reaction. *J. Phys. Chem. C* **2010**, *114*, 9546-9553.
9. Hayashi, A.; Kimijima, K. I.; Miyamoto, J.; Yagi, I. Oxygen Transfer and Storage Processes Inside the Mesopores of Platinum-Deposited Mesoporous Carbon Catalyst Thin-Layer Electrode. *J. Phys. Chem. C* **2009**, *113*, 12149-12153.
10. Saleh, M. M. On the Effectiveness Factor of Flow-Through Porous Electrodes. *J. Phys. Chem. B* **2004**, *108*, 13419-13426.
11. Soderberg, J. N.; Co, A. C.; Sirk, A. H. C.; Birss, V. I. Impact of Porous Electrode Properties on the Electrochemical Transfer Coefficient. *J. Phys. Chem. B* **2006**, *110*, 10401-10410.
12. Chai, G. S.; Yoon, S. B.; Yu, J.-S.; Choi, J.-H.; Sung, Y.-E. Ordered Porous Carbons with Tunable Pore Sizes as Catalyst Supports in Direct Methanol Fuel Cell. *J. Phys. Chem. B* **2004**, *108*, 7074-7079.
13. Kumar, K. V.; Müller, E. A.; Rodríguez-Reinoso, F. Effect of Pore Morphology on the Adsorption of Methane/Hydrogen Mixtures on Carbon Micropores. *J. Phys. Chem. C* **2012**, *116*, 11820-11829.
14. Lin, M.-L.; Huang, C.-C.; Lo, M.-Y.; Mou, C.-Y. Well-Ordered Mesoporous Carbon Thin Film with Perpendicular Channels: Application to Direct Methanol Fuel Cell. *J. Phys. Chem. C* **2008**, *112*, 867-873.
15. Marie, J.; Berthon-Fabry, S.; Achard, P.; Chatenet, M.; Pradourat, A.; Chainet, E. Highly Dispersed Platinum on Carbon Aerogels as Supported Catalysts for PEM Fuel Cell-Electrodes: Comparison of Two Different Synthesis Paths. *J. Non-Cryst. Solids* **2004**, *350*, 88-96.
16. Wang, Z.-B.; Zhao, C.-R.; Shi, P.-F.; Yang, Y.-S.; Yu, Z.-B.; Wang, W.-K.; Yin, G.-P. Effect of a Carbon Support Containing Large Mesopores on the Performance of a PtRuNi/C Catalyst for Direct Methanol Fuel Cells. *J. Phys. Chem. C* **2010**, *114*, 672-677.
17. Job, N.; Marie, J.; Lambert, S.; Berthon-Fabry, S.; Achard, P. Carbon Xerogels as Catalyst Supports for PEM Fuel Cell Cathode. *Energy Convers. Manage.* **2008**, *49*, 2461-2470.
18. Alegre, C.; Gálvez, M. E.; Baquedano, E.; Moliner, R.; Pastor, E.; Lázaro, M. J. Oxygen-Functionalized Highly Mesoporous Carbon Xerogel Based Catalysts for Direct Methanol Fuel Cell Anodes. *J. Phys. Chem. C* **2013**, *117*, 13045-13058.
19. Al-Muhtaseb, S. A.; Ritter, J. A. Preparation and Properties of Resorcinol-Formaldehyde Organic and Carbon Gels. *Adv. Mater.* **2003**, *15*, 101-114.

20. Narischat, N.; Takeguchi, T.; Tsuchiya, T.; Mori, T.; Ogino, I.; Mukai, S. R.; Ueda, W. Effect of Activation Degree of Resorcinol-Formaldehyde Carbon Gels on Carbon Monoxide Tolerance of Platinum-Ruthenium Polymer Electrolyte Fuel Cell Anode Catalyst. *J. Phys. Chem. C* **2014**, *118*, 23003-23010.
21. Petričević, R.; Reichenauer, G.; Bock, V.; Emmerling, A.; Fricke, J. Structure of Carbon Aerogels near the Gelation Limit of the Resorcinol-Formaldehyde Precursor. *J. Non-Cryst. Solids* **1998**, *225*, 41-45.
22. Saliger, R.; Bock, V.; Petricevic, R.; Tillotson, T.; Geis, S.; Fricke, J. Carbon Aerogels from Dilute Catalysis of Resorcinol with Formaldehyde. *J. Non-Cryst. Solids* **1997**, *221*, 144-150.
23. Tamon, H.; Ishizaka, H.; Mikami, M.; Okazaki, M. Porous Structure of Organic and Carbon Aerogels Synthesized by Sol-Gel Polycondensation of Resorcinol with Formaldehyde. *Carbon* **1997**, *35*, 791-796.
24. Gregg, S.J.; Sing, K.S.W.; Adsorption, Surface Area and Porosity; Academic Press: London and New York, **1982**.

Chapter 5

Ligand Effect of SnO_2 on PtRu Catalysts and Relation between Pt-CO Bond Strength and CO Tolerance

5.1 Introduction

It was reported that various Pt alloy catalysts, such as Pt-Sn, Pt-Fe, and Pt-Co alloy catalysts showed high CO tolerance.[1-7] Mukerjee et al.[8] reported that a Pt-Mo alloy catalyst (Pt:Mo = 5:1) showed high performance. For metal oxide-modified systems, it was reported that the addition of SnO_2, TiO_2, and NbO_x enhanced CO tolerance.[9-11] Ioroi et al.[12] reported that Pt/MO_x/C catalysts showed higher CO tolerance than Pt-Ru ones. The unoccupied orbital of transition metal suppress the back-donation of Pt 5d electrons to CO, resulting in the weak bond strength of Pt-CO (ligand effect).[13] Not only Pt-alloys but also supports can affect Pt electronic structure. Nakamura et al. reported the evidence that support has an interaction with Pt, resulting in Pt electronic structure modification which lowers adsorption energy of CO.[14-17]

The PtMo/C[6, 18-20] and $PtSnO_x$[21-24] catalysts are investigated for H_2/CO electrochemical oxidation, and the promotional effect of Mo and SnO_x on CO tolerance was observed. Compared with that of the Pt-Ru/C catalyst, lower onset potentials of electrochemical CO oxidation[2, 25, 26] are obtained in the PtMo/C and $PtSnO_x$ catalysts. Electrochemical oxidation of CO does not significantly contribute to CO tolerance. Weakening of Pt-CO bond strength caused by ligand effect contributes to CO tolerance; however, it is hard to evaluate Pt-CO bond strength quantitatively in situ. Weakening of Pt-CO bond strength often decreases HOR activity[27-29] in membrane electrode assembly (MEA) and CO tolerance was not improved in these cases.

In this study, we aimed quantitative evaluation of Pt-CO bond strength, electrochemical CO oxidation, and HOR activity in MEA. Pt-Ru/SnO_2/C catalysts were prepared by rapid quenching method.[30, 31] The structure and morphology of PtRu particles in PtRu/SnO_2/C are controlled. The preparation condition was varied so that PtRu/SnO_2/C catalysts with the same structure and morphology of PtRu particles were obtained. The activities for electrochemical CO oxidation were evaluated by CO stripping voltammetry and in situ infrared reflection-absorption spectroscopy (IRRAS).[32-34] The Pt-CO bond strengths were evaluated by SEIRAS.[3, 35] The HOR activities were evaluated by single cell in the absence/presence of CO.

5.2 Experimental

5.2.1 Catalyst synthetic procedures materials and methods

$SnCl_2$ and ethylene glycol were mixed and stirred in a glass bottle at 190 °C for 0.5 h to form SnO_2 colloid. After cooling to the room temperature, carbon black, E-type carbon from Tanaka Kikinzoku Kogyo K.K., was added to the mixed solution, which was stirred at 190 °C overnight. SnO_2/C sample obtained were filtered and washed with hot distilled water. Then the samples were dried in 60 mL/min stream of N_2 at 80 °C overnight to form 4 wt% SnO_2/C.

Secondly, 40 wt% Pt/SnO_2/C was prepared. SnO_2/C, a solution of $Pt(NO_2)_2(NH_2)_2$ (4.597 wt% as Pt) from Tanaka Kikinzoku Kogyo K.K., ethanol, and distilled water were mixed at 95 ^oC overnight. 40 wt% Pt/SnO_2/C catalyst obtained were filtered and washed with hot distilled water. Then the samples were dried in 60 mL/min stream of N_2 at 80 °C overnight to form 40 wt% Pt/SnO_2/C.

Next, PtRu/SnO_2/C catalysts of Pt:Ru = 2:3 were prepared. 40 wt% Pt/SnO_2/C, $RuCl_3 \cdot nH_2O$, methanol, and distilled water were mixed and stirred in a glass bottle at 70 °C. During this process, Ru was reduced by methanol and adhered to Pt/C. The molar ratio of Pt:Ru in the catalysts a were 2:3. After 12 h of stirring, the catalysts obtained were filtered and washed with hot distilled water. Then the catalysts were dried in 60 mL/min stream of N_2 at 80 °C overnight.

Finally, the catalysts were treated with He for 0.5 h, H_2/Ar (5 % H_2) for 1 h, followed by for He for 1 h at the room temperature. Then, catalysts were treated with He during rapid heating to 900 °C within 10 min. The oven was turned off immediately when the temperature had reached 900 °C to rapidly cool the catalyst. The temperature decreased from 900 °C to 500 °C in 18 min and decreased from 500 °C to room temperature in about 50 min, followed by reduction in H_2/Ar (5 % H_2) for 2 h at 150 °C. Commercial catalyst, Pt_2Ru_3/TKK TEC61E54 (Pt 29.6 %, Ru 23.0 %, Tanaka Kikinzoku Kogyo K.K.), was used as a reference.

5.2.2 Physical characterization

XRD patterns of the Pt-Ru/SnO_2/C catalysts were recorded with a x-ray diffractometer (RIGAKU, RINT 2000) using Cu Ka radiation with a Ni filter. The tube current was 20 mA with a tube voltage of 40 kV. The 2θ angular regions between 10 and 85 ^{o} were explored at a scan rate of 5 ° min^{-1}. The morphology of the PtRu/SnO_2/C catalysts was investigated by using a STEM (Hitachi HD-2000) at 200 kV and 30 mA.

CO stripping voltammetry was carried out in a 250 mL three-electrode cell (HR200, Hokuto Denko Corp.) at 25 °C. A commercial glassy carbon (GC) electrode (HR2-D1-GC-5, 5 mm in diameter, Hokuto Denko Corp.), a Pt-wire electrode (0.3 mm in diameter, Hokuto Denko Corp.) and a saturated calomel electrode (Hokuto Denko Corp.) were used as a working electrode, counter electrode, and reference electrode, respectively. The potential of the working electrode was controlled by an Iviumstat Electrochemical Interface System (Ivium Technologies B.V.). 6 mg of the catalyst was dispersed in a mixture of 2 mL water, 3 mL ethanol, and 50 μL Nafion® solution (5 wt%, Aldrich) with ultrasonic stirring to form a homogeneous catalyst ink. The catalyst layer was prepared by dropping 10 μL of the catalyst ink (PtRu ≈ 6.4 μg) onto a GC disk electrode by a microsyringe and drying at room temperature. All potential values in this paper are referred to a reversible hydrogen electrode. Pure CO was supplied into the electrolyte solution (0.1 M $HClO_4$) for 20 min at a fixed potential of 0.05 V at 60 °C and then high-purity Ar (99.99 %) was bubbled for 30 min to remove the CO dissolved in the electrolyte solution. Current-potential cycles were obtained from 0.05 V to 1.2 V at a scan rate of 10 mV/s.

In situ IRRAS measurements were carried out in a homemade PTFE cell with a CaF_2 optical window using a JASCO FT/IR-6100 spectrometer equipped with a TGS detector.[21, 36] A gold disk (10 mm in diameter) was used as an electrode substrate for IRRAS measurements. The catalyst layers were deposited on the gold electrode surface by the same method as described for the CO stripping voltammetry experiments. Adsorption of CO was conducted first by bubbling CO into the cell for 20 min under potential control at 0 V, and then high-purity Ar was bubbled for 35 min to remove the CO dissolved in the electrolyte solution. Then the electrode was pushed onto the CaF_2 prism window with the thin-layer geometry to reduce the IR absorption by aqueous solution. The in situ IR spectra were recorded with a scan rate of 0.25 mV s^{-1}, and 25 interferograms were co-added to each spectrum. The recorded spectrum at the potential, that adsorbed CO was completely oxidized, was used a reference spectrum of adsorbed CO. The spectrum recorded at 0 V was used as a reference spectrum of the production of CO_2.

The SEIRAS experiments were carried out using a vertical spectro-electrochemical cell in Kretschmann ATR configuration as shown in Fig. 5.1. The working electrode was an Au thin film prepared by electroless deposition onto the hemicylindrical Si prism (Pier optics).[37] A thin gold foil was used for the electrical contact with the Au thin film. Pt wire and Ag/AgCl (sat. NaCl) were used as counter and reference electrodes, respectively. Electrode potential was controlled by a potentiostat (Hokuto Denko,

HA-151B) and a function generator (Hokuto Denko, HB-111). 0.5 M H_2SO_4 solution was used as an electrolyte solution. After CO gas was introduced in to the spectro-electrochemical cell at -150 mV, CO remaining in the solution was removed by bubbling Ar gas through the electrolyte solution for 30 min. Consequently, CO should exist only on the Pt-Ru surface at the initial stage of the experiments. The spectra were collected with p-polarized light and the spectral resolution was 2 cm^{-1}. All the measurements were carried out at room temperature.

5.2.3 Fuel cell test

For preparation of MEA, carbon paper was used as the backing layers of the anode and cathode. Anode catalysts, Pt-Ru/C and Pt-Ru/SnO_2/C, and Nafion® solution were ultrasonically suspended in water. The carbon paper was painted with the catalyst ink. The loading of Pt-Ru in the anode catalyst layer was 0.5 mg cm^{-2}. In all cases, an identical cathode catalyst layer was prepared by the same procedure. A commercial Pt/C cathode catalyst (40 wt% Pt) was used instead of PtRu/C catalysts, and the loadings of Pt in the cathode layer were 0.5 mg cm^{-2}. Finally, the anode and cathode (22 mm × 22 mm) were placed onto the two sides of a Nafion® NRE-212 membrane (Aldrich) and hot-pressed at 135 °C and 4 MPa for 10 min to form the MEA. The MEA was assembled into a single cell with flow field plates made of graphite and copper end plates attached to a heater (FC05-01SP, ElectroChem, Inc.).

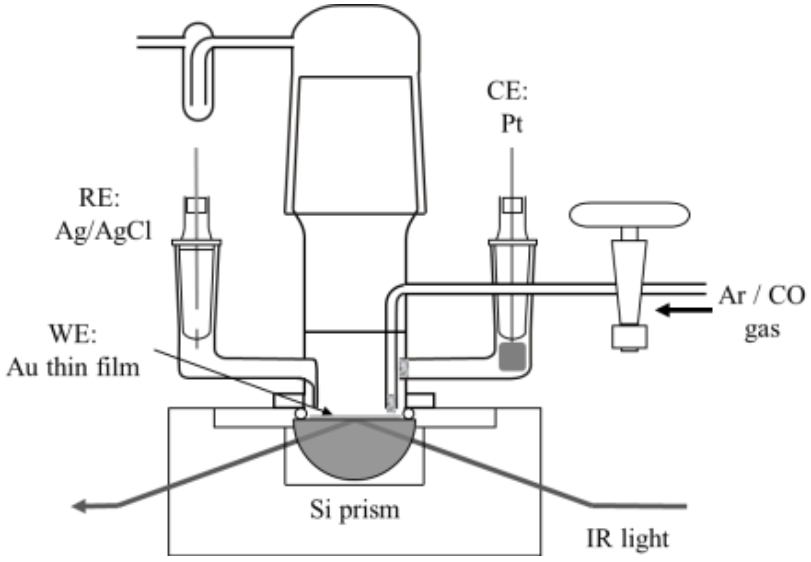

Fig. 5.1 Schematic diagram of surface-enhanced infrared absorption spectroscopy (SEIRAS) glass cell.

The single cell was connected to fuel cell test equipment (Chino Corp.). Pure H_2 (or H_2/CO mixture) and O_2 were supplied at flow rates of 80 mL/min to the anode and cathode, respectively, at ambient pressure. During the measurement, a single cell was operated at 75 °C, and the anode and cathode humidifiers were set at 75 °C and 70 °C, respectively.

5.3 Results and discussion

5.3.1 X-ray diffraction

XRD patterns of Pt-Ru/C and Pt-Ru/SnO_2/C catalysts are shown in Fig. 5.2. Both of the catalysts showed similar diffraction peaks. The broad peak at around 26 ° is assigned to C (002) plane as it can observed for both samples. The diffraction peak at around 40 ° and 69 ° are assigned to Pt (111) and (220) plane. If Ru and Pt with (Ru/Pt molar ratio of 1.5) make a merely complete alloy, peak at Pt (220) plane is expected to appear at 68.8 °, based on the following equation.[38, 39]

$$a = a_0 - 0.124\ \chi_{Ru} \qquad (\chi_{Ru}\text{: Ru atomic fraction}) \qquad (5.1)$$

Both of PtRu/C and PtRu/SnO_2/C catalyst showed a Pt (220) plane peak at 68.8 °, this indicates that alloying degrees of both PtRu/C and PtRu/SnO_2/C catalysts are identical and high enough. The possible SnO_2 (110) peak is at 25 °, which is interfered by C (002), then it cannot calculate the SnO_2 crystallite size.

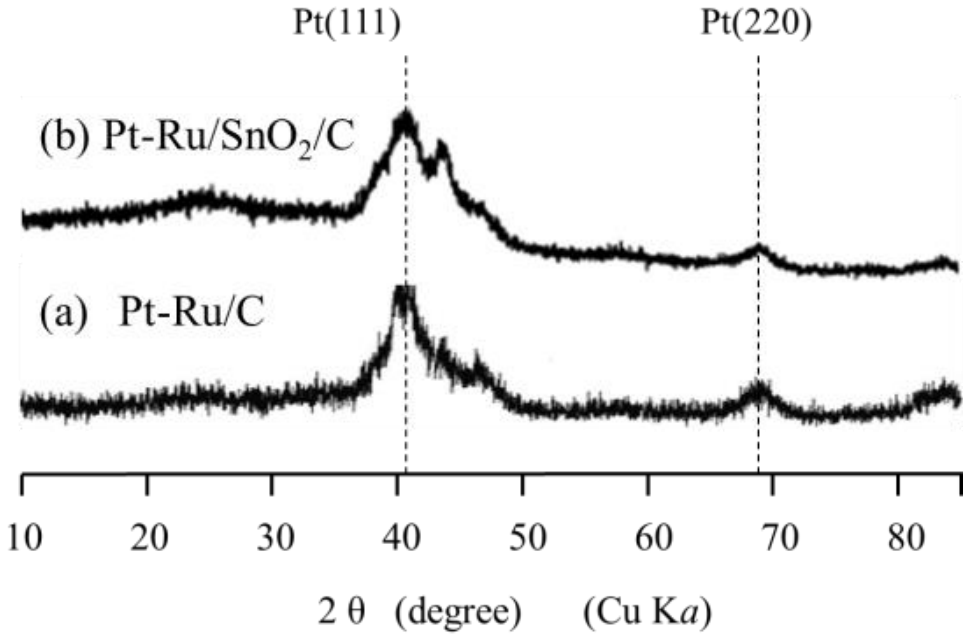

Fig. 5.2 XRD patterns of (a) PtRu/C and (b) PtRu/SnO_2/C.

5.3.2 STEM images

Fig. 5.3 shows STEM images of PtRu/C and PtRu/SnO_2/C catalysts. Both of the catalysts have similar morphologies with a uniform distribution on the carbon support and similar particle size distribution. Particle sizes of both catalysts ranging from 2 nm to 4 nm. These data suggested that the structure and morphology of PtRu particle of PtRu/SnO_2/C are the same as that of PtRu/C. The SnO_2 cannot recognize by STEM images due to the low content as 1.84 %.

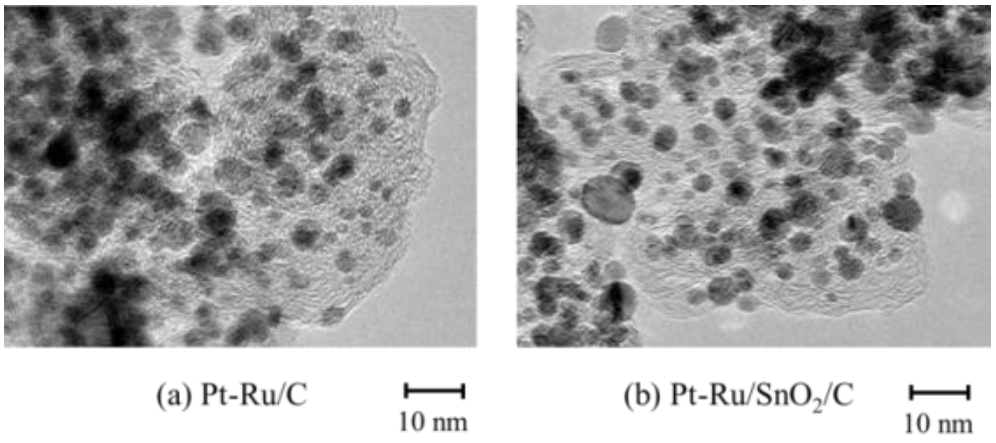

Fig. 5.3 STEM images of (a) PtRu/C and (b) PtRu/SnO_2/C.

5.3.3 CO stripping voltammetry

Fig. 5.4 shows the results of CO stripping voltammetry at 60 °C for of both PtRu/C and PtRu/SnO_2/C catalysts. For the PtRu/C catalyst, CO is electrochemically oxidized at 0.28 V. In case of PtRu/SnO_2/C, CO is electrochemically oxidized at 0.13 V. This result indicated that SnO_2 addition improved activity for electrochemical CO oxidation. Maillaerd et al.[40] reviewed the electrochemical CO oxidation on PtRu. Based on the bifunctional mechanism, CO is preferably adsorbed on Pt for PtRu/C, S(PtRu) is a surface site on the PtRu alloy, while CO-S(Pt) is CO adsorbed on the Pt. H_2O is oxidized to form OH group preferably on Ru surface.

$$CO + S(PtRu) \rightarrow CO\text{-}S(Pt) \quad (5.2)$$

$$H_2O + S(PtRu) \leftrightarrow OH\text{-}S(Ru) + H^+ + e^- \quad (5.3)$$

OH-S(Ru) is OH adsorbed on Ru. CO reacts with OH to form CO_2.

$$CO\text{-}S(Pt) + OH\text{-}S(Ru) \rightarrow CO_2 + H^+ + e^- + 2S(PtRu) \quad (5.4)$$

For PtRu/SnO_2/C catalyst, not only above reactions (5.3) and (5.4), but also following reactions (5.5) and (5.6) proceed

$$H_2O + S(SnO_2) \leftrightarrow OH\text{-}S(SnO_2) + H^+ + e^- \quad (5.5)$$

$$CO\text{-}S(Pt) + OH\text{-}S(SnO_2) \rightarrow CO_2 + H^+ + e^- + S(PtRu) + S(SnO_2) \quad (5.6)$$

$S(SnO_2)$ is surface site of SnO_2, while OH-$S(SnO_2)$ is OH adsorbed on SnO_2. It is obvious that the PtRu/SnO_2/C catalyst showed the lowest onset potential. By bifunctional mechanism, the enhancement of activity for electrochemical CO oxidation by the SnO_2 addition, was quantitatively evaluated by CO stripping voltammetry.

5.3.4 In situ IRRAS

By the FTIR results from our previous research showed that Pt/SnO_2, which has better CO oxidation, also has less CO tolerance than PtRu/C,[41] the ranking of CO stripping and tolerance of the catalysts are as follows:

CO oxidation by CO stripping: Pt/SnO_2 > PtRu > Pt

CO tolerance by MEA analysis: PtRu > Pt/SnO_2 > Pt

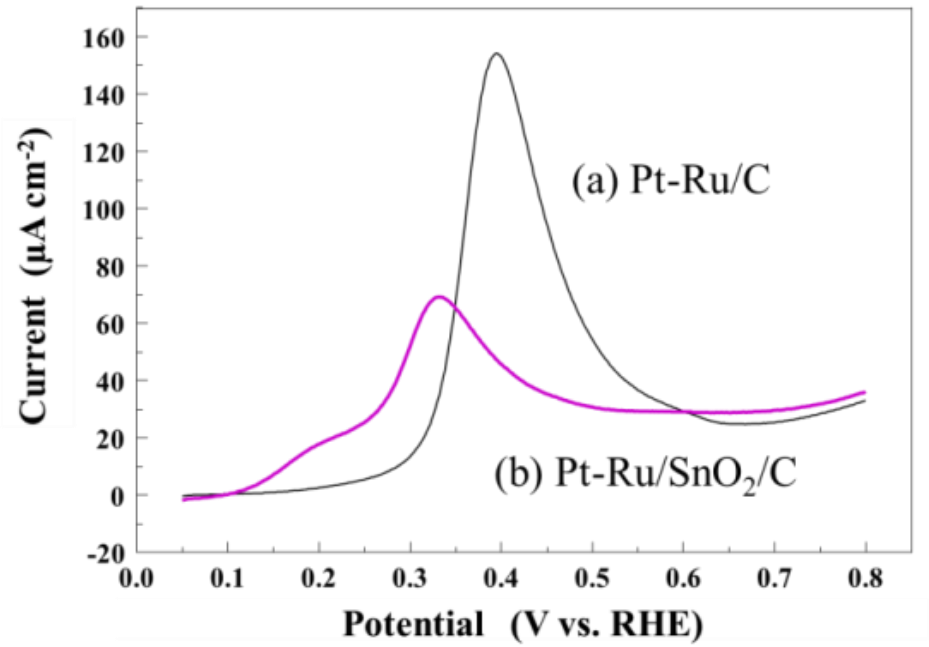

Fig. 5.4 CO stripping voltammetry at 60 °C for (a) PtRu/C and (b) $PtRu/SnO_2/C$. CO was (1) fed for 20 min at 0.05 V in 0.1 M $HClO_4$; (2) purged for 30 min; and (3) swept at 60 °C between 0.05 V and 0.8 V at 10 mV/s.

In situ IRRAS measurement was carried out to observe CO_2 formation on the catalyst surface during the electrochemical CO oxidation. Fig. 5.5 shows in situ IR spectra obtained from the PtRu/C and $PtRu/SnO_2/C$ surface in CO-dissolved 0.1 M $HClO_4$ solution, in the potential region between 0 V and 0.6 V. As shown in Fig. 5.5 (a), at 0.20 V, a new positive peak and a new negative peak appear at around 2,340 cm^{-1} and 2,030 cm^{-1}, which can be assigned to C-O stretching mode of CO_2 and Pt-adsorbed CO, respectively. Figs. 5.5 (a) and 5.5 (b) show the integrated IR intensities of generated CO_2 and the reacted CO for PtRu/C and $PtRu/SnO_2/C$ catalyst. Fig. 5.5 indicate that CO is oxidized over 0.2 V on PtRu/C, while CO is oxidized over 0.1 V on $PtRu/SnO_2/C$. Rate of CO_2 formation $PtRu/SnO_2/C$ over 0.2 V is higher than that on PtRu/C. Although CO oxidation peak cannot be observed by FTIR under 0.2 V, PtRu/C is well known as a high CO tolerance catalyst. Therefore, it can be considered that CO tolerance is not only depending on CO oxidation. The evaluation of bond strength is necessary to confirm the effect of adding SnO_2. Moreover, addition of metal oxide such as SnO_2

enhances electrochemical CO oxidation, but it might possibly reduce HOR activity.

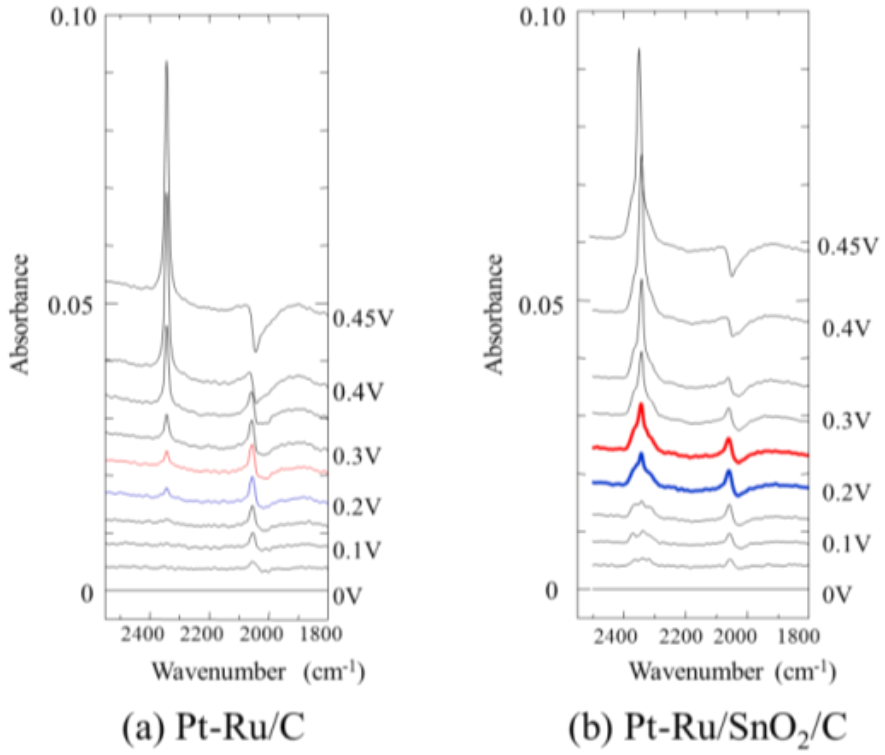

Fig. 5.5 IRRAS spectra of (a) PtRu/C and (b) PtRu/SnO_2/C deposited on a gold substrate surface CO was (1) fed for 20 min at 0 V in 0.1 M $HClO_4$; (2) purged for 35 min; (3) the electrode was pushed onto the CaF_2 prism window with the thin-layer geometry; the in situ IR spectra were recorded with a scan rate of 0.25 mV/s; 25 interferograms were co-added to each spectrum.

5.3.5 In situ SEIRAS

For the in situ SEIRAS measurements, CO was adsorbed at -150 mV, the potential was stepped to -200 mV and a series of spectra were taken at each potential in the range of -200 mV to 800 mV at 50 mV intervals. Fig. 5.6 shows the potential dependent FTIR spectra of CO adsorbed at saturation on PtRu/C catalyst (Fig. 5.6 (a)) and PtRu/SnO_2/C catalyst (Fig. 5.6 (b)). The spectrum observed at 800 mV was used as a reference. Linear bonded CO at Pt sites was observed at 2,009-2,020 cm^{-1} for PtRu/C and 2,014-2,025 cm^{-1} for PtRu/SnO_2/C.

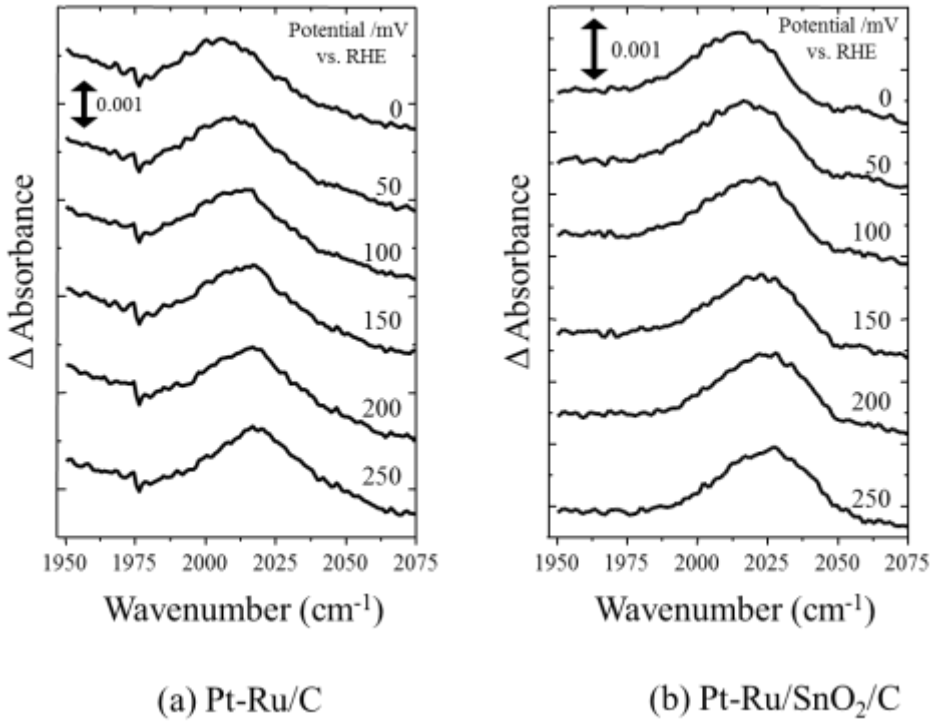

Fig. 5.6 SEIRAS spectra of adsorbed CO as a function of potential on (a) PtRu/C and (b) $PtRu/SnO_2/C$ in 0.5 M H_2SO_4.

Potential dependence of the peak wavenumber is plotted in Fig. 5.7 for PtRu/C and $PtRu/SnO_2/C$ catalyst. Linear frequency shift were observed for both PtRu/C and $PtRu/SnO_2/C$ catalysts with $d\bar{\upsilon}/dE$ = 42 cm^{-1}/V and 44 cm^{-1}/V, respectively, in the potential region where CO adsorbed on the surface. This peak shift to higher wavenumber with increasing potential can be explained as a lowering of the metal-CO binding due to the decreasing of back-donation from metal to CO.[42] The wavenumber of CO stretching band adsorbed on $PtRu/SnO_2/C$ always appeared ca. 5 cm^{-1} higher than the CO stretching band adsorbed on PtRu/C in the potential range between -200 mV to 50 mV. Since the coverage of CO decreases with an increase in the electrode potential, the peak wavenumber can shift by change of the dipole-dipole interactions as mentioned.[43, 44]

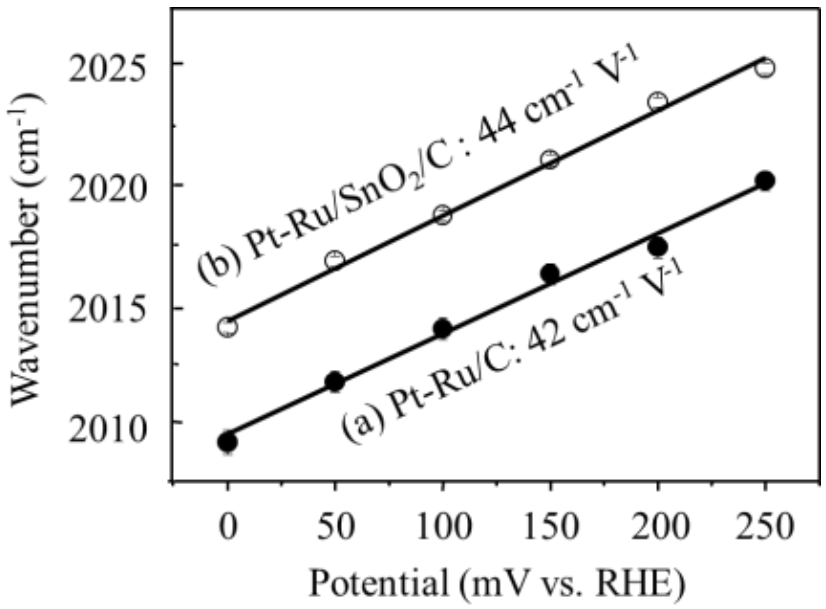

Fig. 5.7 The CO stretching peak frequency vs. potential for (a) PtRu/C and (b) PtRu/SnO_2/C.

Hoffman also reported that the peak could slightly shift to the higher wavenumber with an increase in CO coverage. In this potential range surface is fully covered with CO for PtRu/C, but not fully covered with CO in case of PtRu/SnO_2/C (as shown in Fig. 5.4). Thus, the peak shift to higher wave number observed in PtRu/SnO_2/C even with a small amount of desorbed CO can be explained by lowering of the metal-CO binding which result in adsorbed CO to be easily oxidized on PtRu/SnO_2/C compared to PtRu/C. Sato et al. also report the weaken of Pt-CO bond strength by sublayer of Pt-Ru alloy[45] and particle size by similar technic.[46] The CO-Pt bond strength was quantitatively evaluated by in situ SEIRAS measurements. Ligand effect of SnO_2 on PtRu catalyst was evaluated by this method. However, if addition of metal oxide reduces the HOR activity, ligand effect did not contribute to CO tolerance.

5.3.6 CO tolerance

The effect of CO concentration on cell voltage at 0.2 A cm^{-2} is shown in Fig. 5.8. PtRu/C catalyst and PtRu/SnO_2/C showed the same cell voltage as high as 0.78 V at 0.2 A cm^{-2} in the absence of CO. This means that HOR activity of PtRu/SnO_2/C is completely the same as PtRu/C catalyst, as is suggested by XRD measurement and STEM observation. In our previous study SnO_2-modified PtRu/C having high CO tolerance showed cell voltage of 0.76 V at 0.2 A cm^{-2} in the absence of CO, which is

0.02 V lowers than that of PtRu/C. While addition of SnO_2 reduce the HOR activity a little for SnO_2-modified PtRu/C in the previous study, addition of SnO_2 does not reduce the HOR activity at all for PtRu/SnO_2/C in the present study. PtRu/SnO_2/C catalysts showed higher cell voltage than PtRu/C catalyst in the presence of CO. PtRu/SnO_2/C shows the cell over 0.7 V at 0.2 A cm^{-2} in the presence of 500 ppm CO, and enhancement of CO tolerance is due to the SnO_2 addition.

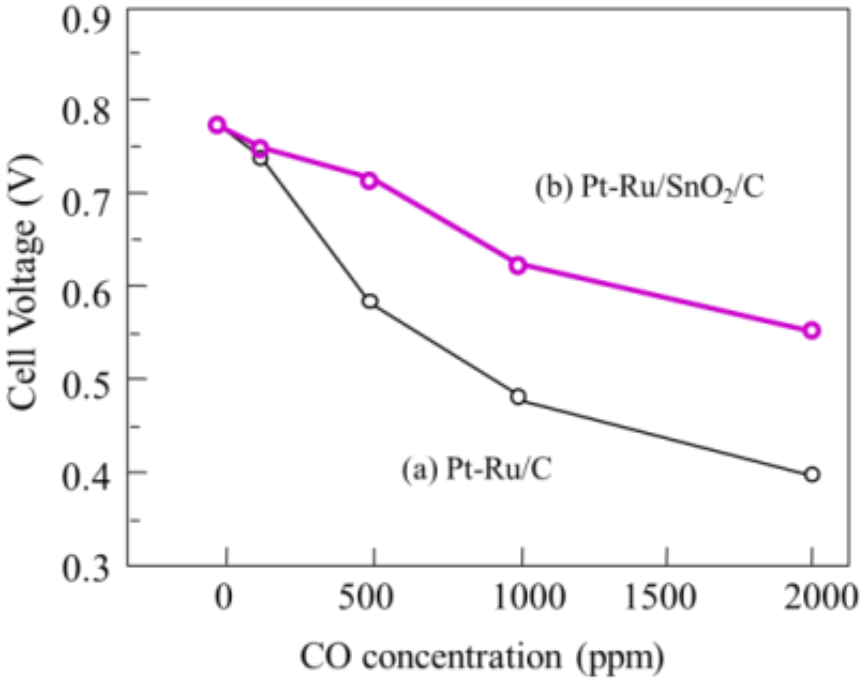

Fig. 5.8 Effect of CO concentration on cell voltage at 0.2 A cm^{-2}. Cell temp.: 70 °C; electrolyte: Nafion® NRE 212; cathode: Pt/C (0.5 mg cm^{-2}); O_2 humidified at 70 °C; flow rate: 80 mL/min; anode: (a) PtRu/C and (b) PtRu/SnO_2/C (0.5 mg PtRu cm^{-2}); H_2 containing 0-2,000 ppm CO humidified at 70 °C; and flow rate: 80 mL/min.

5.4 Conclusion

Electrochemical CO oxidation, Pt-CO bond strength, and HOR activity in MEA were quantitatively evaluated by CO stripping voltammetry, SEIRAS, and fuel cell test. Addition of SnO_2 does not reduce the HOR activity at all for PtRu/SnO_2/C. The weakening of Pt-CO bond strength contributes to CO tolerance, resulting in much higher activity in the presence of CO than commercial PtRu/C catalyst.

References

1. Watanabe, M.; Motoo, S. Electrocatalysis by Ad-Atoms: Part II. Enhancement of Oxidation of Methanol on Platinum by Ruthenium Ad-Atoms. *J. Electroanal. Chem.* **1975**, *60*, 267-273.
2. Watanabe, M.; Motoo, S. Electrocatalysis by Ad-Atoms: Part III. Enhancement of Oxidation of Carbon-Monoxide on Platinum by Ruthenium Ad-Atoms. *J. Electroanal. Chem.* **1975**, *60*, 275-283.
3. Igarashi, H.; Fujino, T.; Watanabe, M. Hydrogen Electro-Oxidation on Platinum Catalysts in the Presence of Trace Carbon Monoxide. *J. Electroanal. Chem.* **1995**, *391*, 119-123.
4. Gasteiger, H. A.; Markovic, N. M.; Ross, P. N., Electrooxidation of CO and H_2/CO Mixtures on a Well-Characterized Pt_3Sn Electrode Surface. *J. Phys. Chem.* **1995**, *99*, 8945-8949.
5. Watanabe, M.; Zhu, Y. M.; Uchida, H. Oxidation of CO on a Pt-Fe Alloy Electrode Studied by Surface Enhanced Infrared Reflection-Absorption Spectroscopy. *J. Phys. Chem. B* **2000**, *104*, 1762-1768.
6. Igarashi, H.; Fujino, T.; Zhu, Y.; Uchida, H.; Watanabe, M. CO Tolerance of Pt Alloy Electrocatalysts for Polymer Electrolyte Fuel Cells and the Detoxification Mechanism. *Phys. Chem. Chem. Phys.* **2001**, *3*, 306-314.
7. Lu, X.; Deng, Z.; Wei, S.; Zhu, Q.; Wang, W.; Guo, W.; Wu, C.-M. L. CO Tolerance of a Pt_3Sn (111) Catalyst in Ethanol Decomposition. *Catal. Sci. Technol.* **2015**, *5*, 3246-3258.
8. Mukerjee, S.; Urian, R. C.; Lee, S. J.; Ticianelli, E. A.; McBreen, J. Electrocatalysis of CO Tolerance by Carbon-Supported PtMo Electrocatalysts in PEMFCs. *J. Electrochem. Soc.* **2004**, *151*, A1094-A1103.
9. Shim, J.; Lee, C. R.; Lee, H. K.; Lee, J. S.; Cairns, E. J. Electrochemical Characteristics of Pt-WO_3/C and Pt-TiO_2/C Electrocatalysts in a Polymer Electrolyte Fuel Cell. *J. Power Sources* **2001**, *102*, 172-177.
10. Ueda, A.; Yamada, Y.; Ioroi, T.; Fujiwara, N.; Yasuda, K.; Miyazaki, Y.; Kobayashi, T. Electrochemical Oxidation of CO in Sulfuric Acid Solution over Pt and PtRu Catalysts Modified with TaO_x and NbO_x. *Catal. Today* **2003**, *84*, 223-229.
11. Takeguchi, T.; Anzai, Y.; Kikuchi, R.; Eguchi, K.; Ueda, W. Preparation and Characterization of CO-Tolerant Pt and Pd Anodes Modified with SnO_2 Nanoparticles for PEFC. *J. Electrochem. Soc.* **2007**, *154*, B1132-B1137.

12. Ioroi, T.; Yasuda, K.; Siroma, Z.; Fujiwara, N.; Miyazaki, Y. Enhanced CO-Tolerance of Carbon-Supported Platinum and Molybdenum Oxide Anode Catalyst. *J. Electrochem. Soc.* **2003**, *150*, A1225-A1230.
13. Koper, M. T. M.; Shubina, T. E.; van Santen, R. A. Periodic Density Functional Study of CO and OH Adsorption on PtRu Alloy Surfaces: Implications for CO Tolerant Fuel Cell Catalysts. *J. Phys. Chem. B* **2002**, *106*, 686-692.
14. Nakamura, J. The Effect of a Graphene Support on the Properties of Pt Electrode Catalysts in Fuel Cells. *Carbon* **2015**, *85*, 443-444.
15. Yoo, E.; Okada, T.; Kizuka, T.; Nakamura, J. Effect of Carbon Substrate Materials as a PtRu Catalyst Support on the Performance of Direct Methanol Fuel Cells. *J. Power Sources* **2008**, *180*, 221-226.
16. Oh, J.; Yoo, E.; Ono, C.; Kizuka, T.; Okada, T.; Nakamura, J. Support Effect of Anode Catalysts Using an Organic Metal Complex for Fuel Cells. *J. Power Sources* **2008**, *185*, 886-891.
17. Kondo, T.; Izumi, K.-i.; Watahiki, K.; Iwasaki, Y.; Suzuki, T.; Nakamura, J. Promoted Catalytic Activity of a Platinum Monolayer Cluster on Graphite. *J. Phys. Chem. C* **2008**, *112*, 15607-15610.
18. Russell, A. E.; Maniguet, S.; Mathew, R. J.; Yao, J.; Roberts, M. A.; Thompsett, D. In Situ X-Ray Absorption Spectroscopy and X-Ray Diffraction of Fuel Cell Electrocatalysts. *J. Power Sources* **2001**, *96*, 226-232.
19. Grgur, B. N.; Markovic, N. M.; Ross, P. N., Electrochemical Oxidation of Carbon Monoxide: From Platinum Single Crystals to Low Temperature Fuel Catalysts. Part II: Electrooxidation of H_2, CO and H_2/CO Mixtures on Well Characterized PtMo Alloy. *J. Serb. Chem. Soc.* **2003**, *68*, 191-205.
20. Grgur, B. N.; Markovic, N. M.; Ross, P. N., Electrooxidation of H_2, CO, and H_2/CO Mixtures on a Well-Characterized $Pt_{70}Mo_{30}$ Bulk Alloy Electrode. *J. Phys. Chem. B* **1998**, *102*, 2494-2501.
21. Wang, G. X.; Takeguchi, T.; Yamanaka, T.; Muhamad, E. N.; Mastuda, M.; Ueda, W. Effect of Preparation Atmosphere of Pt-SnO_x/C Catalysts on the Catalytic Activity for H_2/CO Electro-Oxidation. *Appl. Catal., B* **2010**, *98*, 86-93.
22. Axnanda, S.; Zhu, Z.; Zhou, W.; Mao, B.; Chang, R.; Rani, S.; Crumlin, E.; Somorjai, G.; Liu, Z. In Situ Characterizations of Nanostructured SnO_x/Pt (111) Surfaces Using Ambient-Pressure XPS (APXPS) and High-Pressure Scanning Tunneling Microscopy (HPSTM). *J. Phys. Chem. C* **2014**, *118*, 1935-1943.

23. Kamiuchi, N.; Matsui, T.; Kikuchi, R.; Eguchi, K. Nanoscopic Observation of Strong Chemical Interaction between Pt and Tin Oxide. *J. Phys. Chem. C* **2007**, *111*, 16470-16476.
24. Zhou, J. G.; Fang, H. T.; Maley, J. M.; Ko, J. Y. P.; Murphy, M.; Chu, Y.; Sammynaiken, R.; Sham, T. K. An X-Ray Absorption, Photoemission, and Raman Study of the Interaction between SnO_2 Nanoparticle and Carbon Nanotube. *J. Phys. Chem. C* **2009**, *113*, 6114-6117.
25. Marković, N. M.; Grgur, B. N.; Lucas, C. A.; Ross, P. N., Jr. Electrooxidation of CO and H_2/CO Mixtures on Pt (111) in Acid Solutions. *J. Phys. Chem. B* **1999**, *103*, 487-495.
26. Marković, N. M.; Lucas, C. A.; Grgur, B. N.; Ross, P. N., Surface Electrochemistry of CO and H_2/CO Mixtures at Pt (100) Interface: Electrode Kinetics and Interfacial Structures. *J. Phys. Chem. B* **1999**, *103*, 9616-9623.
27. Johnson, L.; Ejigu, A.; Licence, P.; Walsh, D. A. Hydrogen Oxidation and Oxygen Reduction at Platinum in Protic Ionic Liquids. *J. Phys. Chem. C* **2012**, *116*, 18048-18056.
28. Narischat, N.; Takeguchi, T.; Tsuchiya, T.; Mori, T.; Ogino, I.; Mukai, S. R.; Ueda, W. Effect of Activation Degree of Resorcinol-Formaldehyde Carbon Gels on Carbon Monoxide Tolerance of Platinum-Ruthenium Polymer Electrolyte Fuel Cell Anode Catalyst. *J. Phys. Chem. C* **2014**, *118*, 23003-23010.
29. Wakisaka, M.; Mitsui, S.; Hirose, Y.; Kawashima, K.; Uchida, H.; Watanabe, M. Electronic Structures of PtCo and PtRu Alloys for CO-Tolerant Anode Catalysts in Polymer Electrolyte Fuel Cells Studied by EC-XPS. *J. Phys. Chem. B* **2006**, *110*, 23489-23496.
30. Takeguchi, T.; Yamanaka, T.; Asakura, K.; Muhamad, E. N.; Uosaki, K.; Ueda, W. Evidence of Nonelectrochemical Shift Reaction on a CO-Tolerant High-Entropy State PtRu Anode Catalyst for Reliable and Efficient Residential Fuel Cell Systems. *J. Am. Chem. Soc.* **2012**, *134*, 14508-14512.
31. Yamanaka, T.; Takeguchi, T.; Wang, G. X.; Muhamad, E. N.; Ueda, W. Particle Size Dependence of CO Tolerance of Anode PtRu Catalysts for Polymer Electrolyte Fuel Cells. *J. Power Sources* **2010**, *195*, 6398-6404.
32. Wadayama, T.; Yoshida, H.; Ogawa, K.; Todoroki, N.; Yamada, Y. Carbon Monoxide Adsorption on Co Deposited Pt (100)-hex: IRRAS and LEED Investigations. *Appl. Surf. Sci.* **2010**, *256*, 4517-4521.

33. Quijada, C.; Rodes, A.; Huerta, F.; Vazquez, J. L. In Situ FT-IRRAS Study of SO_2 Adlayers Formed on Pt (111) Electrodes from Open-Circuit Adsorption in Acidic Media. *Electrochim. Acta* **1998**, *44*, 1091-1096.
34. Chu, D.; Gervasio, D.; Razaq, M.; Yeager, E. B. Infrared Reflectance Absorption-Spectroscopy (IRRAS) - Study of the Thermal-Stability of Perfluorinated Sulfonic-Acid Ionomers on Pt. *J. Appl. Electrochem.* **1990**, *20*, 157-162.
35. Osawa, M.; Ataka, K.-I.; Ikeda, M.; Uchihara, H.; Nanba, R. Surface Enhanced Infrared Absorption Spectroscopy Mechanism and Application to Trace Analysis. *Anal. Sci.* **1991**, *7*, 503-506.
36. Ye, S.; Haba, T.; Sato, Y.; Shimazu, K.; Uosaki, K. Coverage Dependent Behavior of Redox Reaction Induced Structure Change and Mass Transport at an 11-Ferrocenyl-1-Undecanethiol Self-Assembled Monolayer on a Gold Electrode Studied by an in Situ IRRAS-EQCM Combined System. *Phys. Chem. Chem. Phys.* **1999**, *1*, 3653-3659.
37. Miyake, H.; Ye, S.; Osawa, M. Electroless Deposition of Gold Thin Films on Silicon for Surface-Enhanced Infrared Spectroelectrochemistry. *Electrochem. Commun.* **2002**, *4*, 973-977.
38. Antolini, E.; Cardellini, F. Formation of Carbon Supported PtRu Alloys: An XRD Analysis. *J. Alloys Compd.* **2001**, *315*, 118-122.
39. Wang, D.; Zhuang, L.; Lu, J. T. An Alloying-Degree-Controlling Step in the Impregnation Synthesis of PtRu/C Catalysts. *J. Phys. Chem. C* **2007**, *111*, 16416-16422.
40. Maillard, F.; Lu, G. Q.; Wieckowski, A.; Stimming, U. Ru-Decorated Pt Surfaces as Model Fuel Cell Electrocatalysts for CO Electrooxidation. *J. Phys. Chem. B* **2005**, *109*, 16230-16243.
41. Takeguchi, T.; Anzai, Y.; Kikuchi, R.; Eguchi, K.; Ueda, W. Preparation and Characterization of CO-Tolerant Pt and Pd Anodes Modified with SnO_2 Nanoparticles for PEFC. *J. Electrochem. Soc.* **2007**, *154*, B1132-B1137.
42. Chang, S. C.; Weaver, M. J. Coverage-Dependent and Potential-Dependent Binding Geometries of Carbon Monoxide at Ordered Low Index Platinum Aqueous and Rhodium Aqueous Interfaces - Comparisons with Adsorption in Corresponding Metal Vacuum Environments. *Surf. Sci.* **1990**, *238*, 142-162.
43. Chang, S. C.; Weaver, M. J. Coverage-Dependent Dipole Coupling for Carbon Monoxide Adsorbed at Ordered Platinum (111)-Aqueous Interfaces: Structural and Electrochemical Implications. *J. Chem. Phys.* **1990**, *92*, 4582-4594.

44. Hoffmann, F. M. Infrared Reflection-Absorption Spectroscopy of Adsorbed Molecules. *Surf. Sci. Rep.* **1983**, *3*, 107-192.
45. Sato, T.; Kunimatsu, K.; Okaya, K.; Yano, H.; Watanabe, M.; Uchida, H. In Situ Atr-Ftir Analysis of the Co-Tolerance Mechanism on Pt_2Ru_3/C Catalysts Prepared by the Nanocapsule Method. *Energy Environ. Sci.* **2011**, *4*, 433-438.
46. Sato, T.; Okaya, K.; Kunimatsu, K.; Yano, H.; Watanabe, M.; Uchida, H. Effect of Particle Size and Composition on CO-Tolerance at PtRu/C Catalysts Analyzed by in Situ Attenuated Total Reflection FTIR Spectroscopy. *ACS Catal.* **2012**, *2*, 450-455.

Chapter 6

Effect of Nafion® Content on CO Tolerance of Pt_2Ru_3 PEFC Anode Catalyst: Pore Size Distribution Investigation.

6.1 Introduction

The term "CO tolerance" generally describes the performance of H_2 oxidation activity of anode catalysts under different intensity of CO contamination. In recent years, many researches have been aiming to develop a higher CO-tolerant electrocatalyst because of its necessity.[1-4] The utilization of ultra-pure hydrogen as fuels for Polymer Electrolyte Fuel Cells (PEFC) is limited due to the production cost and storage difficulties. Alternatively, hydrogen could be obtained from reformed fuels, such as steam-reformed methanol, ethanol or natural gas.[5-7] Especially, in case of residential PEFCs,[8, 9] steam-reformed natural gas can be utilized conveniently. A potential problem which arises from this system is the production of small amount of impurities, particularly carbon monoxide molecules, which strongly adsorb on the Pt catalyst usually employed in the anode and block the sites for hydrogen adsorption and oxidation.

Recently, from our previous studies about PtRu on resorcinol formaldehyde carbon gels (RFC), the cell performance can be operated under 2,000 ppm CO contamination and the cell voltage dropped only 16%. The result showed that carbon support could be a major factor for CO tolerance enhancement.[10-12] The high CO tolerance of the PtRu/RFC anode catalyst can be explained by triple-phase boundary theory. The tailored RFC support prepared using a proper amount of chemicals with a controlled degree of activation can improve the triple-phase boundary. The high activity of the catalyst itself is necessary but is not sufficient to be operated under CO contamination. The ionomer to carbon (I/C) weight ratio and the porosity have been identified as key structural parameters. The I/C ratio has a marked effect on the performance of the fuel cell and was reported to exhibit the best result at 25-30 wt%.[13-17] Several well-known techniques exist for determining the nano-scale and micro-scale porous structure. Scanning transmission electron microscopy (STEM) facilitates the visualization of two-dimensional porous structures. Nitrogen physisorption measurement is useful in determining pore-size distribution.[18, 19] Soboleva et al. determined the volumes of primary and secondary pores of two carbon support, using nitrogen physisorption measurements.[20] They found that the distribution

of ionomers among two supports with different pore structures and the codeposition of ionomers in the catalyst layer strongly influenced its porosity, covering pores smaller than 20 nm. They also modeled and validated the effect of ionomer content to the performance of the cell.[21]

The distribution of ion-conducting Nafion® should be good enough to extend the ion-conducting path in the catalyst layer. On the other hand, its amount should not be too much (more than 1.0 g cm^{-2}) to affect the efficiency of the electrocatalyst by blocking the active sites, restricting the certain channels in the three-phase interfaces for the transportation of reactants, as well as its electronic conductivity.[19] Uchida et al.[21] reported that Nafion® can cover the pores of carbon support which is 40 nm. Antolini et al.[22] reported that the proper thickness of Nafion® should be between 2-8 nm (approximately 20-30 wt%). Sasikumar et al., however, Sasikumar et al. found that the thickness of Nafion® was not relevant to the efficiency of the cell.[23, 24] Moreover, Kanninen et al. mentioned that the real optimum structure can only be determined after long-term testing under fuel cell conditions as the stability of the MEA is strongly dependent on the electrode structure.[25] To the best of our knowledge, although there are a number of studies for optimum amount of Nafion® content, the relation between Nafion® content and mesoporous structure of catalysts is still unclear. In this study, the effect of Nafion® content on the electrochemical performance of two anode catalysts was investigated and discussed.

6.2 Experimental

6.2.1. Resorcinol-formaldehyde carbon gel (RFC) preparation

A resorcinol-formaldehyde (RF) solution was prepared from resorcinol (R), formaldehyde (F), sodium carbonate (C), and distilled water (W). The molar ratios of resorcinol to formaldehyde (R/F) and the mass-to-volume ratio of resorcinol to water (R/W) were fixed at 0.5 mol/mol and 0.5 g/ml, respectively. The molar ratio of resorcinol to catalyst (R/C) was fixed at 1000. After carbon gel was prepared, carbonization and activation process were carried out under a 120 ccm N_2 flow at 1000 °C and 20 ccm CO_2 with 100 ccm N_2 flow at 1,000 °C, respectively. Activation degree (or burn-off ratio) was calculated as follows.

activation degree = weight loss after activation*100/weight before activation (6.1)

The resorcinol-formaldehyde carbon used in this work was RC1000ac58. Please be noted that RC1000ac58 indicates that the R/C ratio was 1,000 while the activation degree was 58.

6.2.2 Preparation of Pt_2Ru_3 anode catalysts

Firstly, Pt/RC1000ac58 (40 wt% Pt/C) was prepared by mixing RC1000ac58 with $Pt(NH_3)_2(NO_2)_2$ (4.554 wt% Pt, Tanaka Kikinzoku Kogyo K.K.), and distilled water in a three-neck flask and stirring vigorously at room temperature (20 °C) for 1 h. Pt was then reduced by ethanol and kept at 95 °C overnight. After that, the catalyst was filtered and washed with distilled water, followed by drying in N_2 at 80 °C for 10 h. Second, $RuCl_3 \cdot nH_2O$ (99.9 %, Wako) was dissolved in distilled water and RC1000ac58 supporting Pt was added. The Pt:Ru molar ratio was adjusted to 2:3. The mixture was kept at room temperature for 1 h. Then the Ru in the catalyst was reduced by keeping the catalyst overnight at 70 °C. After that, the obtained catalyst was, again, filtered and washed with distilled water. Then the catalyst was dried in N_2 at 80 °C for 10 h. At last, the catalyst was reduced in a H_2/Ar (5 % H_2) flow at room temperature for 1 h, followed by rapid heating to 880 °C within 12 min in He. The oven was turned off once the temperature reached 880 °C in order to allow the catalyst to be cooled down immediately. Then it was heated again at 150 °C for 2 h in H_2/Ar (5 % H_2) flow so that a Pt_2Ru_3/RC1000ac58 catalyst was obtained (RFC0). A commercial catalyst, Pt_2Ru_3/TKK TEC61E54 (Pt 29.6 %, Ru 23.0 %, Tanaka Kikinzoku Kogyo K.K.), was used as bought for comparison (TKK0).

6.2.3 Physical characterization

Nitrogen adsorption isotherms of all of the samples were measured at -196.15 °C using an adsorption apparatus (BELSORP-mini II surface area and pore size analyzer, BEL Japan). The specific surface areas were calculated from BET plots while pore size distribution and mesopore volume were calculated from Dollimore-Heal (DH) plots. Please be noted that mesopores were defined as the pores with diameters between 2 nm and 50 nm. Catalyst structure was investigated using a Hitachi HD-2000 scanning transmission electron microscope (STEM) instrument with electron energy of 200 kV and a beam current of 30 μA.

6.2.4 MEA preparation

In the membrane electrode assembly (MEA) preparation process, carbon paper (P50T) was used as the backing layers of the anode and the cathode. Anode catalyst inks were prepared by dispersing RFC0 catalyst in distilled water and ethanol mixed with different amounts of Nafion® solution (5 wt% dispersion, Aldrich). The weight ratio between the catalyst and Nafion® used were 9:1, 9:3, 9:5, and 9:9 and the obtained MEA were named as RFC1, RFC3, RFC5 and RFC9 in the order of increasing the amount of Nafion®. TKK1, TKK3, TKK5 and TKK9 were prepared in the same manner. For this reason, the prepared catalyst and the purchased catalyst mentioned in a section 2.3 will be referred to hereafter as RFC0 and TKK0, respectively. Cathode catalyst ink was prepared by dissolving a commercial Pt/C catalyst (46 wt%, TKK TEC10E50) in distilled water and ethanol including Nafion® (9:1). In each electrode, the corresponding catalyst ink was painted to achieve a metal loading of 0.5 mg cm^{-2} followed by a coating of 0.5 mg cm^{-2} Nafion®. Finally, the anode and cathode (22 mm × 22 mm) were placed onto the two sides of a Nafion® NRE-212 membrane (Aldrich) and hot-pressed at 135 °C and 10 MPa for 20 min to form the MEA.

6.2.5 Single cell performance testing and CO tolerance experiment

The MEA was assembled into a single cell (FC05-01SP, ElectroChem, Inc.) having flow field plates made of graphite and end plates made of copper. The end plates of the cell were attached to a heater. The single cell was connected to a fuel cell test apparatus (Chino Corp.). Pure H_2 (or H_2/CO mixture) and O_2 were supplied at flow rates of 80 mL min^{-1} to the anode and cathode, respectively, at ambient pressure. During measurements, the anode and cathode humidifiers were set at 70 °C and 68 °C, respectively, and the single cell was maintained at 70 °C.

The CO tolerance experiments were performed under the same conditions as single cell performance tests. The current density was set to 0.2 A cm^{-2}. First, starting with pure H_2 for 1 h and then 100 ppm of CO was mixed to H_2. The concentration of CO was increased every 2 h to 500 ppm, 1000 ppm, and finally 2,000 ppm.

6.3 Results and discussion

6.3.1 Surface area and pore distribution of the catalysts

Fig. 6.1 shows the surface area of RFC and TKK catalysts with various ratios of Nafion® content from 0 to 9. As the amount of Nafion® was increased, the surface area decreased. TKK0 has a surface area of 406 m^2 g^{-1}, which is smaller than that of

the RFC0 (1014 m^2 g^{-1}). Fig. 6.1 also shows the changes in surface areas of RFC and TKK catalysts after both catalysts had been mixed with various amounts of Nafion®. It can be seen that the surface areas per gram catalyst decreased with the increasing amount of Nafion®. In the case of TKK catalyst, when Nafion® was mixed to the catalyst (ratio of Nafion® to catalyst was 1:9, TKK1), surface area of TKK1 was smaller than TKK0 because the Nafion® had covered only some pores. When the amount of Nafion® was increased three times (ratio of Nafion® to catalyst was 3:9, TKK3), the surface areas of both TKK1 and TKK3 catalysts were almost not changed, which implies that Nafion® coated on the surface of catalysts without covering the pores. Unfortunately, when the amount of Nafion® was increased five times (ratio of Nafion® to catalyst was 5:9, TKK5), the surface area drastically decreased possibly because mesopores were fully covered by Nafion®. When the amount of Nafion® was increased nine times (ratio of Nafion® to catalyst was 9:9, TKK9), the surface area hardly increased. Therefore, these results imply that Nafion® in the case of TKK1 merely coated the surface of TKK catalyst, but Nafion® in the case of TKK5 fully covered the surface of TKK catalyst.

In the case of RFC catalyst, when Nafion® was mixed to the catalyst (ratio of Nafion® to catalyst was 1:9, RFC1), an increase in surface area of RFC1 from RFC0 was observed because of incomplete coating of Nafion®. When the amount of Nafion® was increased three times (ratio of Nafion® to catalyst was 3:9, RFC3) and five times (ratio of Nafion® to catalyst was 5:9, RFC5), the same trends of decrease of surface area due to gradual pore coverage were observed. The important result was when the amount of Nafion® was increased nine times (ratio of Nafion® to catalyst was 9:9, RFC9), the surface area did not change because the Nafion® coated some pores on the catalyst surface; similar to the case of the comparison between TKK1 and TKK3. However, the full coverage as in the case of TKK5 was not observed in the case of RFC catalyst.

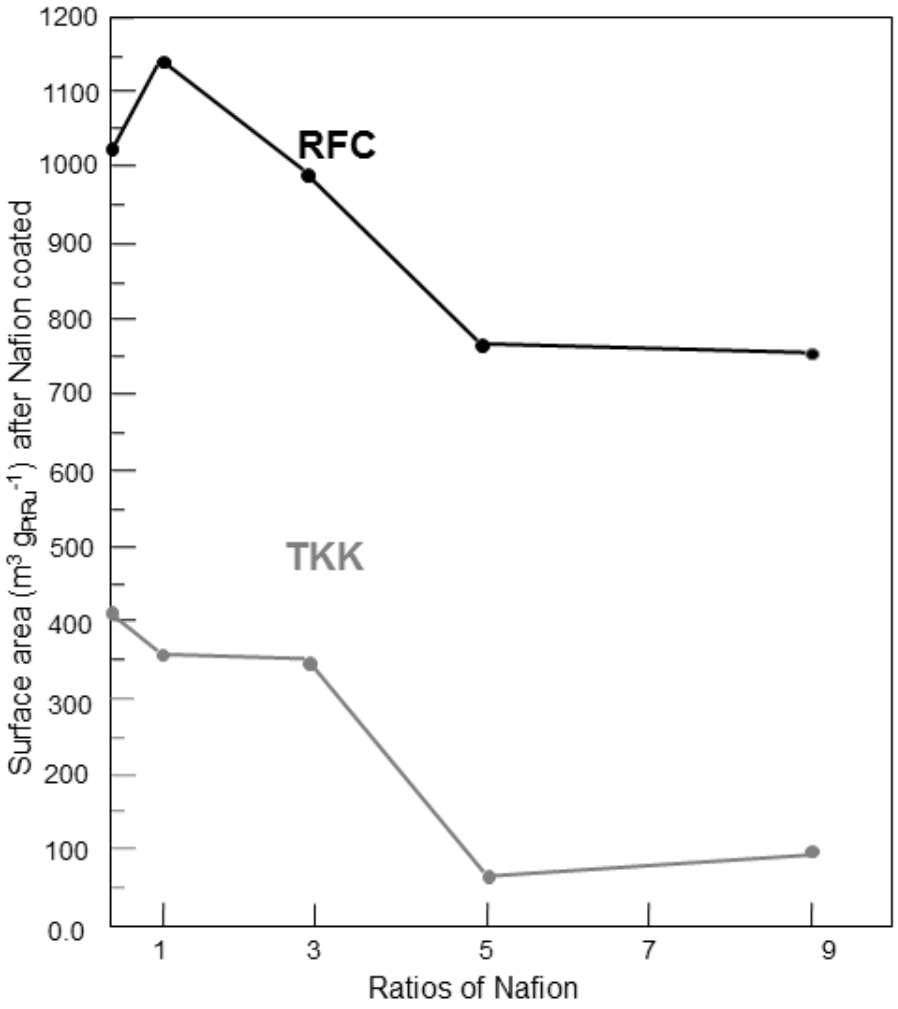

Fig. 6.1 The BET surface area of all catalysts.

6.3.2 TEM images of Nafion® mixed catalysts

Fig. 6.2 shows TEM images of some Nafion®-containing catalyst powder. It can be seen that the higher the Nafion® amount (the Nafion® ratio, to be exacted), the more easily Nafion® could be observed in the images. It is of note, however, that when comparing between two samples with the same amount of Nafion® content, Nafion® could be observed more easily in the images of the TKK samples than in the images of the RFC samples, due to the surface area and pore structure.

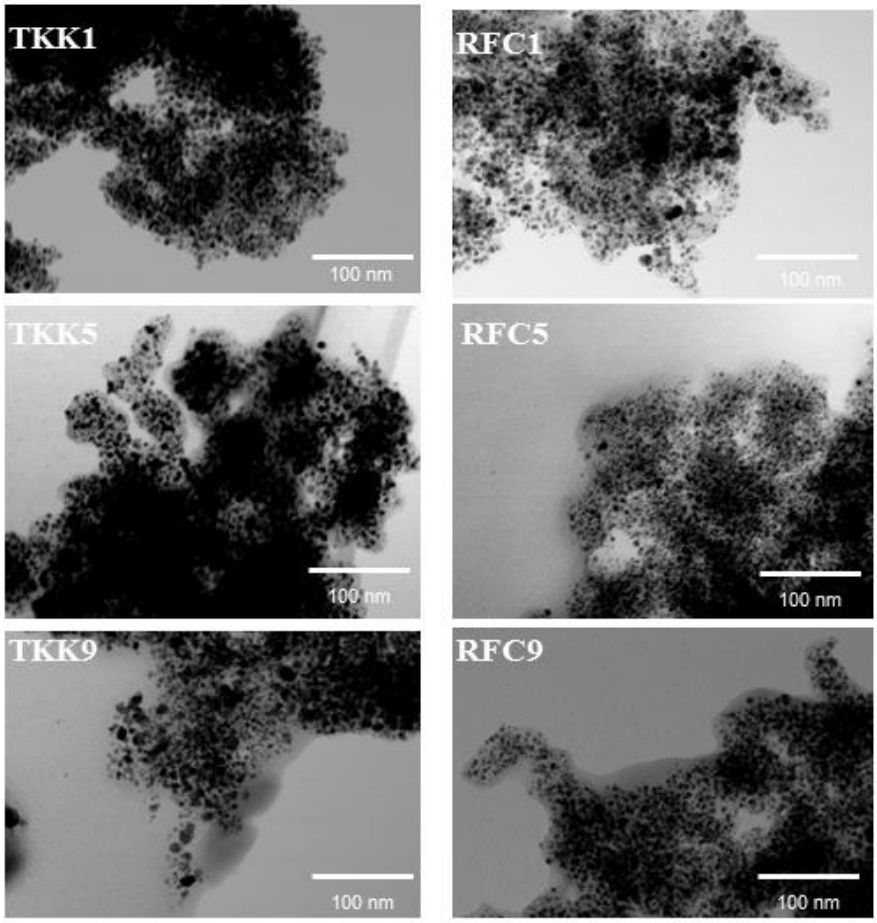

Fig. 6.2 TEM images of Nafion® mixed catalysts.

6.3.3 CO tolerance

The CO tolerance data of TKK and RFC catalysts with various Nafion® contents were summarized in Table 6.1. Fig. 6.3 (A) shows the efficiency of MEAs at various Nafion® contents without CO. In case of TKK series, the best performance is the MEA using TKK1 as anode catalyst (I/C ratio = 1:9). Higher Nafion® contents reduce not much MEA performace and remain the same MEA performance when using TKK3 to TKK9 as anode catalysts. Because all parameters are the same except the Nafion® content, it then can be concluded that TKK1 is at the optimum Nafion® content condition to operate without CO. On the other hand, RFC series revealed that RFC5 is at optimum condition. When 500 ppm CO, this level is practically found in real case, were introduced to these samples as shown in Fig. 6.3 (B), a trend of performance of MEAs using TKKs as anode catalysts did not change much. There was a significant

reduction of performance in case of RFCs with low Nafion® contents (RFC1 and RFC3). It shows the possibility that the necessary of Nafion® to enhance CO tolerance is more than that of pure H_2. Then, the results in Fig 6.3 (C), extreame condition of 2,000 ppm CO contamination, reassure that higher contents of Nafion® improve CO tolerance. Only when the I/C of MEAs were 5:9 and 9:9 that the anode catalysts were still able to operate at this point. Nafion® might have improved the transportation of ions (improve tripple-phase boundary (TPB)) and better TPB could enhance the CO tolerance.

Table 6.1 Cell voltages at 0.2 A cm^{-2} at different CO concentrations of TKK and RFC catalysts with various Nafion® contents

I : C Molar Ratio	Catalyst Name	CO Concentration (ppm)				
		0	100	500	1000	2000
1:9	TKK1	0.76	0.73	0.63	0.47	0
	RFC1	0.73	0	0	0	0
3:9	TKK3	0.74	0.67	0.47	0	0
	RFC3	0.73	0.38	0	0	0
5:9	TKK5	0.75	0.7	0.57	0.44	0.4
	RFC5	0.78	0.75	0.73	0.7	0.65
9:9	TKK9	0.75	0.67	0.44	0.38	0.34
	RFC9	0.76	0.7	0.62	0.52	0.36

TPB is a reasonable explaination of CO tolerance enhancement. In case of pure H_2, amount of Nafion® could manipulate an accessibility of ion. TKK1 presents the proper amount of Nafion® but too much Nafion® in the other TKKn retards the transport of ions. In contrast, RFC1 and RFC3 present situation that lacking of Nafion® could also reduce the performance and the reduction is more severe than in case of too much Nafion®. One question might arise; Is there no problems when the amount of Nafion® is really too much in the system? As the understanding is that large amount of Nafion® hinders transportation of ions and increase the resistance of the cell but the MEA preparation process can manage this problem. The hot-press process to bind cathode, anode and ionomer with pressure and heat could deminish the exess amount of Nafion®. Moreover, the pore which were blocked with Nafion® could be reproduced at this process.[26, 27]

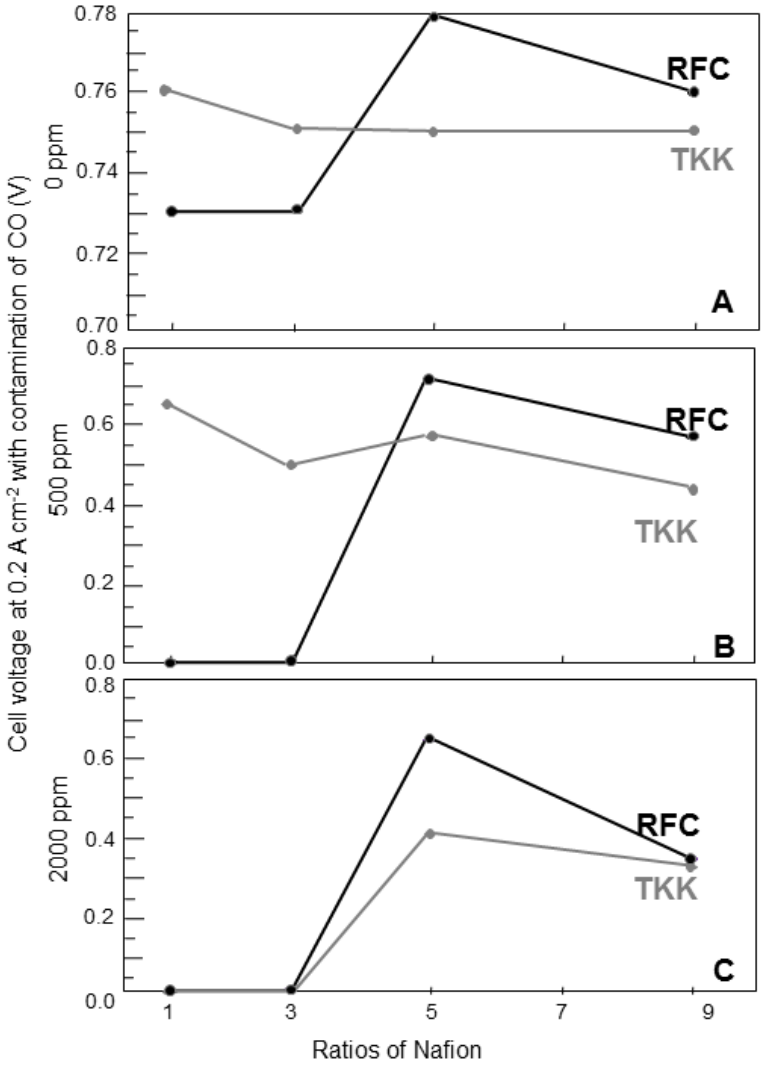

Fig. 6.3 The CO tolerence of Nafion® mixed catalysts: (A) Pure H_2, (B) 500 ppm CO/H_2, and (C) 2,000 ppm CO/H_2.

6.3.4 Effect of Nafion® mixing on pore volume

In order to understand the effect of Nafion® content, the pore volume and pore structure of each sample was measured. As shown in Table 6.2, the mesopore volumes of TKKs (calculated by DH plot) show critical decreased at 81.2 % when the Nafion® content was increased 5 times. In case of RFCs, the decrease in mesorepore volume of RFC9 at 51.9 % should be considered as a critical decrease.

Table 6.2 The mesopore volumes and average pore diameters calculation by DH plots.

Catalyst	Surface area of catalysts ($m^2 g^{-1}$)	Volume of mesopores ($cm^3 g^{-1}$)	Reduction of mesopore volume (%)	Average pore diameter by DH plots (nm)
TKK0	406	0.77	-	108.6
TKK1	318	0.74	4.4	79.9
TKK3	276	0.61	17.1	94.6
TKK5	45	0.11	81.2	146.9
TKK9	51	0.01	94.7	125.1
RFC0	1014	1.23	-	44.5
RFC1	1060	1.08	-	51.6
RFC3	741	0.75	30.6	59.7
RFC5	501	0.51	31.5	44.5
RFC9	389	0.25	51.9	197.3

The results of average pore diameters revealed important information about the difference in pore structures of TKKs and RFCs. This information agrees well with the changing of surface are after increase the ratios of Nafion®. In the case of TKKs, when Nafion® was mixed to pure carbon (changing from TKK0 to TKK1) the average pore diameter decreased by 27.7 nm and the thickness of Nafion® coating was 13.8 nm. After that, increasing the Nafion® amount (change from TKK1 to TKK3) reduced pore diameter. The reduction of pore diameter might imply that thickness of coated Nafion® on mesopores became thicker. After this point (changing from TKK5 and TKK9) the pore diameter increased drastically which might imply that all mesopores had been covered. On the other hand, in the case of RFCs, when Nafion® was first introduced to pure carbon (changing from RFC0 to RFC1), the pore diameter increased, possibly due to the fill-up of micropores. Even when the Nafion® amount was increased from RFC1 to RFC3, the pore diameter still increased. This micropore filled-up phenomenon did not appear in case of TKK. Until RFC5, the average pore diameter started to decrease to 44.5 nm, which represented the Nafion® coating thickness of 7.6 nm. After this point, RFC9, the pore diameter increased again by the same reason with TKK5 and TKK9. Therefore, the important point of both series was the step that Nafion® coated on the catalyst surface before the pore diameter growing up again as TKK1 and RFC5. This corresponds well with the CO tolerance data that the MEAs using TKK1 and RFC5 as anode catalysts showed the highest performance in its series.

Fig. 6.4 confirms the change in pore diameter. From TKK0 to TKK1, the peak of pore distribution shifts from about 100 nm to 60 nm which means that Nafion® coating thickness is about 20 nm. For RFCs cases, the peaks of pore distribution show almost no change until RFC5. Therefore, it can confirm by pore size distribution that in case of

TKK catalysts, the optimize I:C ratio is less than 5:9 but in the case of RFC catalysts, the optimize I:C ratio is less than 9:9.

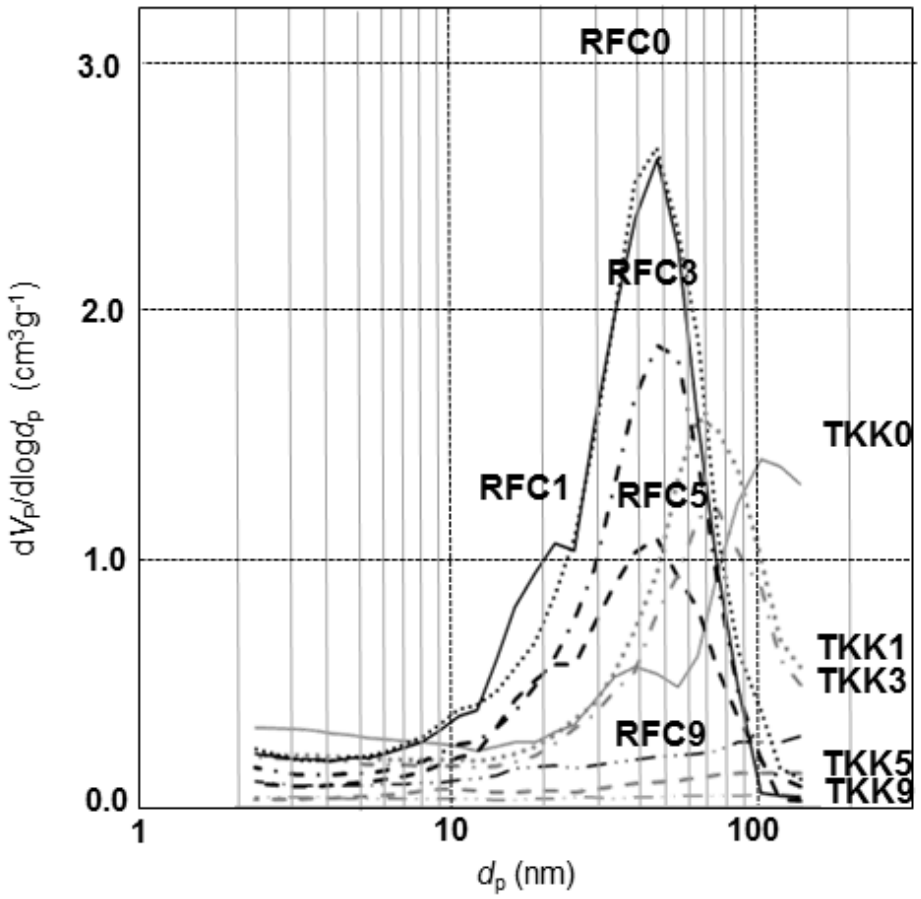

Fig. 6.4 Pore distribution of all catalysts.

6.4 Conclusion

The optimized amount of Nafion® is very important, precise, and has a significant effect on the CO tolerance of MEA. Inadequate loading of Nafion® leads to an unstable electricity genaration of MEA under CO environment. On the other hand, overloading of Nafion® leads to the decrease of cell efficiency even though it still be able to tolerate high contamination of CO. The triple phase boundary theory explains that the transportation of protons through Nafion® can enhance or inhibit the efficiency of fuel cells. Moreover, the result form this research shows that the optimized amount of Nafion® greatly depends on the surface area and the average pore diamter.

References

1. Pedersen, C. M.; Escudero-Escribano, M.; Velázquez-Palenzuela, A.; Christensen, L. H.; Chorkendorff, I.; Stephens, I. E. L. Benchmarking Pt-Based Electrocatalysts for Low Temperature Fuel Cell Reactions with the Rotating Disk Electrode: Oxygen Reduction and Hydrogen Oxidation in the Presence of CO (Review Article). *Electrochim. Acta* **2015**, *179*, 647-657.
2. Cheng, X.; Shi, Z.; Glass, N.; Zhang, L.; Zhang, J.; Song, D.; Liu, Z.-S.; Wang, H.; Shen, J. A Review of PEM Hydrogen Fuel Cell Contamination: Impacts, Mechanisms, and Mitigation. *J. Power Sources* **2007**, *165*, 739-756.
3. Antolini, E.; Gonzalez, E. R. The Electro-Oxidation of Carbon Monoxide, Hydrogen/Carbon Monoxide and Methanol in Acid Medium on PtSn Catalysts for Low-Temperature Fuel Cells: A Comparative Review of the Effect of PtSn Structural Characteristics. *Electrochim. Acta* **2010**, *56*, 1-14.
4. Ehteshami, S. M. M.; Chan, S. H. A Review of Electrocatalysts with Enhanced CO Tolerance and Stability for Polymer Electrolyte Membarane Fuel Cells. *Electrochim. Acta* **2013**, *93*, 334-345.
5. Amphlett, J. C.; Mann, R. F.; Peppley, B. A. On Board Hydrogen Purification for Steam Reformation/PEM Fuel Cell Vehicle Power Plants. *Int. J. Hydrogen Energy* **1996**, *21*, 673-678.
6. Ogden, J. M.; Steinbugler, M. M.; Kreutz, T. G. A Comparison of Hydrogen, Methanol and Gasoline as Fuels for Fuel Cell Vehicles: Implications for Vehicle Design and Infrastructure Development. *J. Power Sources* **1999**, *79*, 143-168.
7. Brown, L. F. A Comparative Study of Fuels for on-Board Hydrogen Production for Fuel-Cell-Powered Automobiles. *Int. J. Hydrogen Energy* **2001**, *26*, 381-397.
8. Echigo, M.; Shinke, N.; Takami, S.; Tabata, T. Performance of a Natural Gas Fuel Processor for Residential PEFC System Using a Novel CO Preferential Oxidation Catalyst. *J. Power Sources* **2004**, *132*, 29-35.
9. Inaka, H.; Sumi, S.; Nishizaki, K.; Tabata, T.; Kataoka, A.; Shinkai, H. The Development of Effective Heat and Power Use Technology for Residential in a PEFC Co-Generation System. *J. Power Sources* **2002**, *106*, 60-67.
10. Takeguchi, T.; Yamanaka, T.; Asakura, K.; Muhamad, E. N.; Uosaki, K.; Ueda, W. Evidence of Nonelectrochemical Shift Reaction on a CO-Tolerant High-Entropy State PtRu Anode Catalyst for Reliable and Efficient Residential Fuel Cell Systems. *J. Am. Chem. Soc.* **2012**, *134*, 14508-14512.
11. Narischat, N.; Takeguchi, T.; Mori, T.; Ogino, I.; Mukai, S. R.; Ueda, W. Enhanced

CO Tolerance of PEFC Anode Catalyst by Optimized Degree of Activation of Resorcinol-Formaldehyde Carbon Support. *ECS Trans.* **2014**, *64*, 145-150.

12. Narischat, N.; Takeguchi, T.; Tsuchiya, T.; Mori, T.; Ogino, I.; Mukai, S. R.; Ueda, W. Effect of Activation Degree of Resorcinol-Formaldehyde Carbon Gels on Carbon Monoxide Tolerance of Platinum-Ruthenium Polymer Electrolyte Fuel Cell Anode Catalyst. *J. Phys. Chem. C* **2014**, *118*, 23003-23010.
13. Lee, S. J.; Mukerjee, S.; McBreen, J.; Rho, Y. W.; Kho, Y. T.; Lee, T. H. Effects of Nafion® Impregnation on Performances of PEMFC Electrodes. *Electrochim. Acta* **1998**, *43*, 3693-3701.
14. Lee, D.; Hwang, S. Effect of Loading and Distributions of Nafion® Ionomer in the Catalyst Layer for PEMFCs. *Int. J. Hydrogen Energy* **2008**, *33*, 2790-2794.
15. Lai, C.-M.; Lin, J.-C.; Ting, F.-P.; Chyou, S.-D.; Hsueh, K.-L. Contribution of Nafion® Loading to the Activity of Catalysts and the Performance of PEMFC. *Int. J. Hydrogen Energy* **2008**, *33*, 4132-4137.
16. Kim, K.-H.; Lee, K.-Y.; Kim, H.-J.; Cho, E.; Lee, S.-Y.; Lim, T.-H.; Yoon, S. P.; Hwang, I. C.; Jang, J. H. The Effects of Nafion® Ionomer Content in PEMFC MEAs Prepared by a Catalyst-Coated Membrane (CCM) Spraying Method. *Int. J. Hydrogen Energy* **2010**, *35*, 2119-2126.
17. Morgan, R. D.; Haan, J. L.; Masel, R. I. Effects of Nafion® Loading in Anode Catalyst Inks on the Miniature Direct Formic Acid Fuel Cell. *J. Power Sources* **2010**, *195*, 6405-6410.
18. Lange, K. J.; Carlsson, H.; Stewart, I.; Sui, P.-C.; Herring, R.; Djilali, N. PEM Fuel Cell CL Characterization Using a Standalone FIB and SEM: Experiments and Simulation. *Electrochim. Acta* **2012**, *85*, 322-331.
19. Hannach, E., M.; Soboleva, T.; Malek, K.; Franco, A. A.; Prat, M.; Pauchet, J.; Holdcroft, S. Characterization of Pore Network Structure in Catalyst Layers of Polymer Electrolyte Fuel Cells. *J. Power Sources* **2014**, *247*, 322-326.
20. Soboleva, T.; Zhao, X.; Malek, K.; Xie, Z.; Navessin, T.; Holdcroft, S. On the Micro-, Meso-, and Macroporous Structures of Polymer Electrolyte Membrane Fuel Cell Catalyst Layers. *ACS Appl. Mater. Interfaces* **2010**, *2*, 375-384.
21. Uchida, M.; Aoyama, Y.; Eda, N.; Ohta, A. Investigation of the Microstructure in the Catalyst Layer and Effects of Both Perfluorosulfonate Ionomer and PTFE-Loaded Carbon on the Catalyst Layer of Polymer Electrolyte Fuel Cells. *J. Electrochem. Soc.* **1995**, *142*, 4143-4149.
22. Antolini, E. Graphene as a New Carbon Support for Low-Temperature Fuel Cell Catalysts. *Appl. Catal., B* **2012**, *123–124*, 52-68.

23. Sasikumar, G.; Ihm, J. W.; Ryu, H. Dependence of Optimum Nafion® Content in Catalyst Layer on Platinum Loading. *J. Power Sources* **2004**, *132*, 11-17.
24. Sasikumar, G.; Ihm, J. W.; Ryu, H. Optimum Nafion® Content in PEM Fuel Cell Electrodes. *Electrochim. Acta* **2004**, *50*, 601-605.
25. Kanninen, P.; Borghei, M.; Ruiz, V.; Kauppinen, E. I.; Kallio, T. The Effect of Nafion® Content in a Graphitized Carbon Nanofiber-Based Anode for the Direct Methanol Fuel Cell. *Int. J. Hydrogen Energy* **2012**, *37*, 19082-19091.
26. Jeong S. Y.; Han O. H. Influence of Hot Pressing on the Pore Structure of Nafion® Electrolyte Membrane Investigated by ^{1}H NMR. *Bull. Korean Chem. Soc.* **2009**, *30*, 1559 - 1562.
27. Zhang, J.; Yin, G.-P.; Wang, Z.-B.; Lai, Q.-Z.; Cai, K.-D. Effects of Hot Pressing Conditions on the Performances of MEAs for Direct Methanol Fuel Cells. *J. Power Sources* **2007**, *165*, 73-81.

Chapter 7

General Conclusion

In this thesis, the effects of PtRu anode catalyst supports in polymer electrolyte fuel cells (PEFCs) are described. The decoration of the support to obtain state-of-the-art CO-tolerant anode catalyst is also described. The content of each chapter can be summarized as follows.

In Chapter 1, a general introduction of fuel cells and detailed information on residential fuel cells (which are based on a PEFC) were given. The major problem with a hydrogen fuel source, CO contamination, was also stated. Information from a literature review about the role of platinum and how it can be improved was provided. One factor affecting CO tolerance that would be interesting to investigate for enhancement of CO tolerance is the carbon support. Resorcinol-formaldehyde carbon (RFCs) gels were selected to be used as supports because their pore structure is adjustable.

In Chapter 2, the preparation of resorcinol-formaldehyde carbon gels with degrees of CO_2 activation from 0 to 88 % was described. Pt and Ru nanoparticles were dispersed on these carbons by a rapid quenching method. The crystallite sizes of the PtRu particles in the prepared catalysts were smaller than those in a typical commercial catalyst. STEM pictures showed that increasing the degree of activation led to a better distribution of PtRu particles on the surface of the carbon. TEM images also showed the same trend of a higher degree of activation leading to the formation of smaller PtRu particles. However, when the degree became too large (Pt_2Ru_3/RC1000ac88), large particles tended to be formed inside the carbon. Micorpores stabilized PtRu particles on the support surface, but an excessively high volume of micropores increased the electrical resistance of the cell. Finally, CO tolerance tests by single cell experiments were performed. Pt_2Ru_3/RC1000ac58, prepared with a carbon support having the optimum degree of activation, showed the best performance due to its appropriate carbon micropore structure that allowed uniform dispersion of PtRu particles. The results of this study showed that adjustment of the degree of activation of the carbon support leads to efficient deposition of PtRu particles both in terms of particle size and size distribution. The resultant catalyst has better catalytic performance and higher CO tolerance.

In experiments for which results are shown in chapter 3, two different commercial carbon supports (ECP and ECP600JD carbons) were used with Ru:Pt ratios of 1.0, 1.3,

1.5 and 2.0. The PtRu/C catalysts using carbon ECP had a higher Ru atomic fraction in PtRu, but those using carbon ECP600JD had a larger charge coverage due to their larger surface area and provide smaller PtRu particles. Only Ru-Pt bonding contributes to CO oxidation but Ru-Ru bonding does not. We thus proposed a new parameter, the Pt-Ru surface relative bonding ratio. This ratio is the multiplication of Ru atomic fraction in PtRu and charge coverage, which can indicates of CO tolerance enhancement. Moreover, the Pt-Ru surface relative bonding ratio could be optimized by selection of carbon supports.

In Chapter 4, the preparation of Pt_2Ru_3 anode catalysts using RFCs prepared at various R/C ratios (i.e., 200, 800 and 1,000) was described. The catalysts that were prepared had similar physical properties such as alloying degree, PtRu particle size and BET surface area. However, they exhibited significantly different degree of CO tolerance. In addition, catalysts having larger volumes of mesopores with modal sizes after Nafion® mixing as large as 50 nm exhibited higher CO tolerance. These results suggested the importance of large mesopore volume for CO tolerance. Effective CO removal due to the high diffusivity in large mesopores enhanced the CO tolerance of the MEA.

In experiments for which results are shown in chapter 5, tin oxide decoration was deposited on the carbon support before PtRu deposition to synthesize PtRu/SnO_2/C. In the absence of CO, the PtRu/C catalyst and PtRu/SnO_2/C showed cell voltages that were not greatly different. After CO was fed together with H_2, the difference in cell voltages was quite clear. With greater CO contamination, the difference in cell voltages became more significant. Furthermore, both the activity of electrochemical CO oxidation and the Pt-CO bond strength were quantitatively evaluated. The addition of SnO_2 decreased Pt-CO bond strength while maintaining HOR activity to enhance CO tolerance.

Finally, in Chapter 6, the importance of the triple-phase boundary theory is shown by the effect of Nafion® contents. It was found that too little loading of Nafion® greatly reduced the MEA efficiency, while too much loading of Nafion® might block the accessibility of gases through the pore structure, which can be reproduced by a hot-pressing process. CO tolerance was also affected by the amount of Nafion® loading. The optimum amount of Nafion® did not directly depend on either the I/C ratio or the surface area of a support. It was also found, however, that an appropriate pore diameter and appropriate pore volume of mesopores of the support in the catalyst are critical factors for enhancing CO tolerance by broadening the TPB region.

All of the experiments provided new information about the contribution of the support to CO tolerance of PtRu anode catalysts for polymer electrolyte fuel cells

(PEFCs). Micropores could assist the formation of small and uniformly dispersed PtRu particles. Mesopores could affect not only the diffusivity of the reactant and product gases but also the distribution of Nafion®. Moreover, the addition of tin oxide promoted the ligand effect of a PtRu catalyst; thus, the electrooxidation activity was improved.

List of Publications

Published papers

1) Napan Narischat, Tatsuya Takeguchi, Takeshi Mori, Shinichiroh Iwamura, Isao Ogino, Shin R. Mukai, and Wataru Ueda, Effect of the Mesopores of Carbon Supports on the CO Tolerance of Pt_2Ru_3 Polymer Electrolyte Fuel Cell Anode Catalyst. *International Journal of Hydrogen Energy*, **2016**, in press.
2) Takeguchi, T., Kunifuji, A., Narischat, N., Ito, M., Noguchi, H., Uosaki, K., and Mukai, S. R. Ligand Effect of SnO_2 on Pt-Ru Catalyst and Relation between Bond Strength and CO Tolerance. *Catalysis Science and Technology*, **2016**, 6 (9), pp. 3214.
3) Napan Narischat, Tatsuya Takeguchi, Takanori Tsuchiya, Takeshi Mori, Isao Ogino, Shin R. Mukai, and Wataru Ueda, Effect of Activation Degree of Resorcinol–Formaldehyde Carbon Gels on Carbon monoxide Tolerance of Platinum–Ruthenium Polymer Electrolyte Fuel Cell Anode Catalyst. *Journal of Physical Chemistry C*, **2014**, 118(40), pp. 23003.
4) Napan Narischat, Tatsuya Takeguchi, Takeshi Mori, Isao Ogino, Shin R. Mukai, and Wataru Ueda, Enhanced CO Tolerance of PEFC Anode Catalyst by Optimized Degree of Activation of Resorcinol-Formaldehyde Carbon Support. *Electrochemistry Society Transaction*, **2014**, 64(3), pp, 145.

Presentations

1) Napan Narischat, Tatsuya Takeguchi, and Wataru Ueda, Effect Nafion loading to CO Tolernace in the PtRu/C Catalyst for PEFC, CSE Summer School 2012, Jozankei , Japan, 20 July 2012.
2) Tatsuya Takeguchi and Napan Narischat, Hightly CO Tolerant Multifunctional Pt_2Ru_3/C Catalyst Modify by Tin Oxide, International Fuel Cell Workshop (IFCW) 2012, Yamanachi, Japan, 3 August 2012.
3) Napan Narischat, Tatsuya Takeguchi, Takanori Tsuchiya, Shin R. Mukai, and Wataru Ueda, Effect of Micropore Structure of Carbon Support on CO Tolerance of Pt_2Ru_3 Anode Catalyst for PEFC, Electrochemistry Society (ECS) 223, Toronto, Canada, 14 May 2013.
4) Napan Narischat, Tatsuya Takeguchi, Takanori Tsuchiya, Takeshi Mori, Isao Ogino, Shin R. Mukai, and Wataru Ueda, Effect of Carbon Support Structure on CO Tolerance of Pt_2Ru_3 Anode Catalyst for PEFC, CSE Summer School 2013 with post-conference of ISHHC-16, Jozankei , Japan, 20 July 2012.

5) Napan Narischat, Tatsuya Takeguchi, Takeshi Mori, Isao Ogino, Shin R. Mukai, and Wataru Ueda, TEM and SEM study of Pt-Ru Particles Formation Mechanism on Rc1000 Carbons, FCC 2nd International Symposium, Hokkaido University, Sapporo, Japan, 9 December 2013.

6) Napan Narischat, Tatsuya Takeguchi, Takeshi Mori, Isao Ogino, Shin R. Mukai, and Wataru Ueda, Enhance CO Tolerance of PEFC Anode Catalyst by Optimized Degree of Activation of Resorcinol-Formaldehyde Carbon Support, ECS226 with SMEQ Joint International Meeting and Polymer Electrolyte Fuel Cells 14, Cancun, Mexico, 14 October 2014.

7) Napan Narischat, Tatsuya Takeguchi, Takeshi Mori, Shinichiroh Iwamura, Isao Ogino, and Shin R. Mukai, Function of porosity of carbon support on CO tolerance of PtRu anode catalyst for PEFC, CSE Summer School 2014, Jozankei, Japan, 20 July 2014

8) Napan Narischat, Tatsuya Takeguchi, Takeshi Mori, Shinichiroh Iwamura, Isao Ogino, and Shin R. Mukai, The Distribution of Nafion over PtRu/RFC for High CO Tolerance PEFC Anode Catalyst, the 28 meeting of Japan Society on Adsorption, Hokkaido University, Sapporo, Japan, 24 Oct 2014.

Acknowledgements

Foremost, I would like to express my deepest gratitude to my advisor Prof. Tatsuya Takeguchi for continuous support of my Ph.D study for his very patience, motivation, kindness, and warm encouragement. His suggestions helped me in all the time of research and writing of this thesis. I also would like to thank members of CREST project; Mr. Hideyoshi Arikawa, Ms. Keiko Ukita and Ms. Akane Kunifuji for their warm welcome and encouragement since I started living in Japan by myself.

I would like to express my sincere thanks to Prof. Ueda for his invaluable suggestions, constructive questions and encouragement for the first 2 years of my Ph.D. study. I also would like to thanks all other Prof. Ueda's lab members; Prof. Hideshi Hattori, Prof. Ken-ichi Shimizu, Assist. Prof. Toru Maruyama, Dr. Nicholas Dummer, and other students in the class of 2012 – 2013, for their warm participation, helpful guidance and sincere support.

Sincere gratitude to Prof. Shin R. Mukai, for his patience, kindness, encouragement, and immense knowledge. It is my honor to be his advisee for the last two years of my Ph.D. study. I would like to thank Assoc. Prof. Isao Okino and Assist. Prof. Shinichiroh Iwamura for their guidance, collaboration and support throughout the completion of this work. I also would like to thanks to all other Prof. Mukai's lab member, especially to Mr.Takeshi Mori for his continuous collaboration and support throughout the completion of my research.

I would like to thank Assoc.Prof. Koichi UI, Assist. Prof. Yoshihiro Kadoma, Ms. Miyuki Kojima, and all other Prof. Takeguchi's lab members at Iwate university for their warm welcome, support and encouragement.

I would like to thank Prof. Marc Koper, Prof. Kiyataka Asakura, Prof. Kohei Uosaki, Prof. Hidenori Noguchi, and Assist. Prof. Mikio Ito for an inspiring and invaluable discussion.

I would like to thank Assist. Prof. Pongtorn Dhupatemiya, Assist. Prof. Bunpot Sirinutsomboon and Dr. Thidarat Wongsawa for their helpful comments on this thesis.

I would like to thank the Graduate School of Chemical Sciences and Engineering at Hokkaido University for the "Advanced Graduate School of Chemistry and Materials Science (AGS)" scholarship.

Last but not least, I would like to thank all of my friends and my family for their support and encouragement.

Napan Narischat

2016